Lehrstuhl für Steuerungs- und Regelungstechnik
Technische Universität München
Univ.-Prof. Dr.-Ing./Univ. Tokio Martin Buss

Design and Control Aspects of Humanoid Walking Robots

Dirk Wollherr

Vollständiger Abdruck der von der Fakultät für Elektrotechnik und Informationstechnik der Technischen Universität München zur Erlangung des akademischen Grades eines

Doktor-Ingenieurs (Dr.-Ing.)

genehmigten Dissertation.

Vorsitzender: Univ.-Prof. Dr.-Ing. Klaus Diepold

Prüfer der Dissertation:

1. Univ.-Prof. Dr.-Ing./Univ. Tokio Martin Buss

2. Univ.-Prof. Dr.-Ing., Dr.-Ing. habil. Heinz Ulbrich

Die Dissertation wurde am 31.3.2005 bei der Technischen Universität München eingereicht und durch die Fakultät für Elektrotechnik und Infromationstechnik 23.6.2005 angenommen

Foreword

This thesis has emerged from four years of work at three different Labs. Both, the intellectual, and the physical journey left a significant imprint on my personality; all through the wide range of emotional experiences, ranging from the joyfull kick of success through anger and the crestfallen thought of giving up in times where nothing seems to work – in the retrospective, I do not want to miss any of it.

The fundaments of this work have been laid at the Control Systems Group, Technische Universität Berlin, where the main task of assembling knowledge has been accomplished and many practical experiences could be gained. With this know-how, I was given the chance to spend seven months at the Nakamura-Yamane-Lab, Department of Mechano-Informatics, University of Tokyo, where the humanoid robot UT-Theta has been developed[1]. This robot provided a relyable platform to experiment with walking control algorithms. The end of my journey is the Institute of Automatic Control Engineering, Technische Universität München, where I found ease and comfort to structure my mind and write down the results of my research.

First of all, I would like to thank my doctoral advisor Prof. Martin Buss, who lead me on my way whenever I was in need of a guiding hand, and let me walk freely, where I found the road ahead myself.

Furthermore I found an invaluable help in the cooperation with the Simulation and Systems Optimization Group, Technische Universität Darmstadt. With their experience in generating gait trajectories, Prof. Oskar von Stryk, Dr. Michael Hardt, Max Stelzer and Jutta Kiener greatly supported the construction of a first humanoid prototype.

Prof. Yoshihiko Nakamura finally gave me the opportunity to work on a great hardware platform in a productive environment and broadened my view in the world of robotics – *domo arigatou Nakamura-sensei*.

I am also indebted to Marion Sobotka (TU Berlin/TU München), Dr. Fabio Zonfrilli (Università di Roma "La Sapienza"), and Dr. Tomomichi Sugihara (University of Tokyo) who supported me as collegues and encouraged me as friends. To all my students, Karsten Gänger, Steffen Schostan, and Thorsten Hinzmann, I thank you very much for the efforts you took. Last but not least, I would like to mention Uwe Weidauer, who was always happy to implement my ideas and realized the impossible.

And of course, my deepest and unconditional gratitude for my parents for their continual and unconditioned support and patience with me – I am very lucky to have them.

Munich, 2005. Dirk Wollherr

[1]The reseach stay in Tokyo was generously supported by the Japanese Society for the Promotion of Science (JSPS).

to my parents

...

Design and Control Aspects of Humanoid Walking Robots

The research presented in this dissertation discusses the development of a humanoid biped robot from the planning stage to biped walking focusing on low level control. Concepts in hardware design, posture manipulation, and hybrid joint control, that are novel in humanoid robotics, are presented and entirely verified in hardware experiments. Decisive for the future performance of the robot is a careful selection of an appropriate motor-gear-combination during hardware design, as oversized actuators increase the total weight of the robot, thus deteriorating the walking performance. A systematic procedure for actuator selection based on optimal control is discussed. When replaying precalculated trajectories with a humanoid robot, it is often desirable to modify the posture of the robot thus compensating for control errors or adapting the trajectory for new situations. This task can be accomplished by a method termed *Jacobi Compensation*. A walking controller based on the inverted pendulum method is implemented on the humanoid UT-Theta. This robot is equipped with an innovative knee joint allowing to switch between actuated motion and free swinging. To ensure smooth and reliable operation with this joint, a hybrid, nonlinear, time optimal knee controller has been implemented.

Betrachtungen über Design und Regelung humanoider Laufroboter

Die Dissertation beschreibt die Entwicklung eines humanoiden Laufroboters von der Planungsphase bis zum zweibeinigen Gehen, wobei der Schwerpunkt bei elementaren Regelungsaufgaben liegt. Es werden Konzepte der Hardwaregestaltung, der Anpassung der Körperhaltung und der Regelung hybrider Gelenke vorgestellt, deren Einsatz auf dem Gebiet humanoider Laufroboter neu ist. Während der Entwicklung der Hardware ist eine sorgfältige Auswahl einer geeigneten Motor-Getriebe-Kombination entscheidend für die zukünftige Leistungsfähigkeit des Roboters, da überdimensionierte Antriebe das Gesamtgewicht des Roboters erhöhen und somit die Laufeigenschaften verschlechtern. Ein systematischer Ansatz, Antriebe auszuwählen, wird vorgestellt, bei dem eine geeignete Motor-Getriebe-Kombination durch Lösen eines Optimalsteuerungsproblems ermittelt wird. Wenn im Voraus berechnete Trajektorien auf einen Humanoiden angewendet werden, ist es nützlich, wenn seine Haltung modifiziert werden kann, um Regelfehler zu kompensieren oder die Trajektorien neuen Gegebenheiten anzupassen. Hierzu wird ein Verfahren mit dem Namen *Jacobi Compensation* vorgestellt. Ein Gangregler, der auf der Methode des invertierten Pendels beruht, wird an dem Humanoiden UT-Theta implementiert. Dieser Roboter verfügt über eine innovative Kniekonstruktion, die ein Umschalten zwischen aktivem Antrieb und passivem Schwingen des Unterschenkels ermöglicht. Gleichmäßiger und zuverlässiger Betrieb dieses Gelenks wird durch einen speziellen hybriden, nichtlinearen und zeitoptimalen Regler sichergestellt. Die Konzepte, die in dieser Dissertation vorgestellt werden, wurden sämtlich in Hardwareexperimenten validiert.

Contents

Notations

Abbreviations

CoM	Center of Mass
CoP	Center of Pressure
DoF	Degrees of Freedom
GCoM	Ground Projection of Center of Mass
NPCM	Normal Projection of Center of Mass
PWM	Pulse Width Modulation
ZMP	Zero Moment Point

Conventions

Scalars, Vectors, and Matrices

Scalars are denoted by upper and lower case letters in italic type. *Vectors* are denoted by lower case letters in boldface type, as the vector $\boldsymbol{x}$ is composed of elements x_i. *Matrices* are denoted by upper case letters in boldface type, as the matrix $\boldsymbol{M}$ is composed of elements M_{ij} (i-th row, j-th column).

x	scalar
$\boldsymbol{x}$	vector
$\boldsymbol{X}$	matrix
$f(\cdot)$	scalar function
$\boldsymbol{f}(\cdot)$	vector function
$\dot{\boldsymbol{x}}$, $\ddot{\boldsymbol{x}}$	equivalent to $\frac{\mathrm{d}}{\mathrm{d}t}\boldsymbol{x}$ and $\frac{\mathrm{d}^2}{\mathrm{d}t^2}\boldsymbol{x}$
$\overline{x}$	upper bound for $\boldsymbol{x}$
$\underline{x}$	lower bound for $\boldsymbol{x}$
$\boldsymbol{X}^T$	transposed of matrix $\boldsymbol{X}$
$\boldsymbol{X}^{-1}$	inverse of matrix $\boldsymbol{X}$
$\boldsymbol{X}^{\#}$	pseudoinverse of matrix $\boldsymbol{X}$
$\boldsymbol{X}^{*}$	singularity robust (SR-) inverse of matrix $\boldsymbol{X}$

Subscripts and Superscripts

$\boldsymbol{x}_R$, $\boldsymbol{x}_L$	referring to right or left
d_x, d_y, d_z	component of vector $\boldsymbol{d}$ in x-, y-, z-direction
d_h, d_v	horizontal or vertical component of vector $\boldsymbol{d}$
d_N, d_T	normal or tangential component of vector $\boldsymbol{d}$
q_k, q_{k-1}, q_{k+1}	angle q at sampling time k, $k-1$ or $k+1$

Symbols and Abbreviations

a	acceleration
$a_{\text{max,brake}}$	maximum acceleration during braking
$a_{\text{max,accel}}$	maximum acceleration during acceleration
c_t	cost of transportation
$c_e t$	total energy consumed by system
$c_m t$	mechanical energy consumed by system
d_x, d_y, d_z	length, width and height of a body
$\Delta\theta(t)$	position error
η	efficiency of gearbox
$\boldsymbol{F}_G$	gravitation force
$\boldsymbol{F}_I$	inertia force
$\boldsymbol{F}_R$	ground reaction force
$\boldsymbol{g}$	earth acceleration
Γ	error measure
$\boldsymbol{\Gamma}_D$	derivative gain matrix
$\boldsymbol{\Gamma}_P$	proportional gain matrix
$\boldsymbol{I}$	identity matrix
$\boldsymbol{J}$	Jacobian matrix
$\boldsymbol{J}_{\text{foot}}$	Jacobian matrix for foot position
$\boldsymbol{J}_{\text{foot,hip}}$	Jacobian matrix for foot and hip position
$\boldsymbol{J}_{\text{hip}}$	Jacobian matrix for hip position
k	weighting factor
$\boldsymbol{K}_D$	derivative gain matrix
$\boldsymbol{K}_P$	proportional gain matrix
κ	condition number
l	length of rod
m	mass
$\boldsymbol{M}$	mass matrix
$\boldsymbol{M}_I$	inertia moment
n	number of revolutions per time
N	gear ratio
μ_R, μ_T	friction coefficient
$\boldsymbol{p}$	position vector
$\boldsymbol{p}_{\text{CoM}}$	location of center of mass (CoM)
$\boldsymbol{p}_{\text{CoP}}$	location of center of pressure (CoP)
$\boldsymbol{p}_{\text{GCoM}}$	location of ground projection of CoM (GCoM)
$\boldsymbol{p}_{SF}$	location of support foot
$\boldsymbol{p}_{\text{ZMP}}$	location of zero moment point (ZMP)
P_W	power consumption

$\boldsymbol{q}(t)$	joint angles
$\boldsymbol{q}_a(t)$	actual joint angles
$\boldsymbol{q}_c(t)$	correction joint angles
$\boldsymbol{q}_d(t)$	desired joint angles
$\boldsymbol{q}_e(t)$	control error
$\boldsymbol{q}_t(t)$	trajectory joint angles (reference)
$\boldsymbol{\Sigma}(t)$	component of singular value decomposition (SVD)
t	time
T	sampling rate
t^*	arbitrary, fixed time
τ	motor torque
θ_{1-17}	joint angles
θ_{cmd}	commanded angle
θ_{comp}	compensation angle
θ_{drive}	angle of the driven part
θ_{gap}	angle of the backlash gap
θ_{cmd}	reference angle
θ_{shank}	angle of the shank/fixed part
$\boldsymbol{u}(t)$	control input
$\boldsymbol{U}(t)$	component of singular value decomposition (SVD)
$\boldsymbol{V}(t)$	component of singular value decomposition (SVD)
$V(\boldsymbol{x}, t)$	Lyapunov function
$\boldsymbol{W}$	weighting matrix
$\boldsymbol{x}_c(t)$	Carthesian correction term

List of Figures

List of Tables

1 Introduction

All through the written history of mankind testimony of the human desire for an artificial helper assuming the burden of unpleasant or hard labor can be found. Already Greek mythology gives account of Talos, a bronze automaton forged by Hephaestus and the Cyclopes. Confided to Europa by Zeus, the goddess sent Talos to Crete where he guards the island throwing stones at any approaching ship.

In the early modern times, people started to make significant effort to construct mechanical automata that could apply their skills to a specific design example. Representatives are the figure of a girl playing a lute (1540, Gianello della Tore, Kunsthistorisches Museum, Vienna) or the steam man (1893, George Moore) shown in Fig. 1.1, a walker powered by a gas-fired boiler.

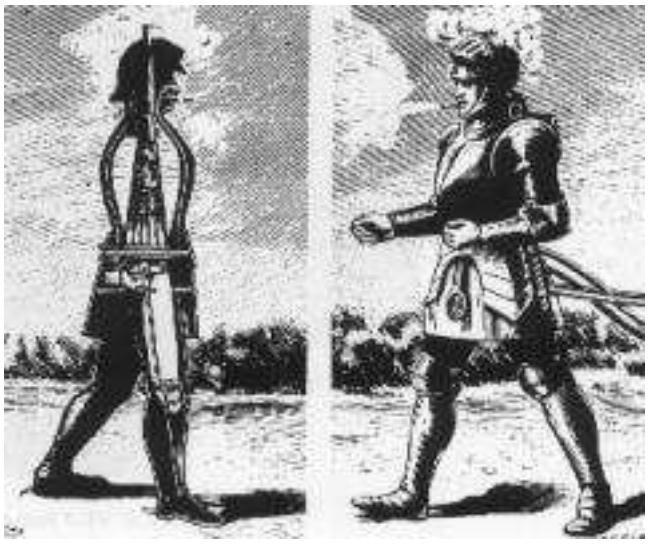

Figure 1.1: Steam man by George Moore, 1893.

During the emerging industrialization in the beginning of the 20th century, people were taken by the technological advances that had revolutionized the society within a couple of years and believed in an almighty power of technology without limits. In this spirit the Czech Karel Čapek (1890–1938) wrote the play "R.U.R. – Rossum's Universal Robots" (Prague 1921, New York 1922, [115]) thus creating the basis for modern Science Fiction literature. He coined the term "robot", which is derived from the Czech words "robota", meaning compulsory labor, and "robotnik", a term for a peasant owing such work. Furthermore, R.U.R. ties the term robot to the vision of an intelligent artificial being with a mind of its own.

This vision is entailed by the fear of men being suppressed by machines with superior physical and intellectual powers. Danger is suspected either from a rebellion of the robots striving to free themselves from human slavery as in R.U.R. or from evil meaning men

availing themselves of the robots superior powers as in the movie "Metropolis" by Fritz Lang.

In 1950 Isaac Asimov (1920–1992) published the book "I, Robot" [4] telling the story of a fictive evolution of robotics starting with the first robot built in 1996 until 2057. Asimov establishes the "Three Laws of Robotics", that ensure robots to be no danger for humans, and arrange coexistence of humans and robots within the limits of society:

Law 1: A robot may not injure a human being, or, through inaction, allow a human being to come to harm.

Law 2: A robot must obey the orders given it by human beings except where such orders would conflict with the first law.

Law 3: A robot must protect its own existence as long as such protection does not conflict with the first or second law.

The book of Asimov gives a detailed discussion of these laws and a comprehensive debate on the dangers for mankind arising from intelligent robots and how to treat these potential threats or even integrate robots into society.

Contrary to Western literature, the subject of robots being a threat to people is replaced in Japan by the notion of a robot hero protecting mankind: Osamu Tezuka created in 1951 the character "Tetsuwan Atom", who soon became famous world wide by the name "Astro Boy" [106] and can be considered the first robot pop star.

In a retrospective analysis it is interesting that most Science Fiction authors assessed the development to be quicker than it turned out to be. It is commonly assumed that first intelligent humanoid robots exist by the turn of the century. Descriptions of robot evolution focus on the development of the brain, motion issues such as walking are neglected and taken for granted.

In recent publications, the term "robot" has generally been replaced by "biped humanoid", as "robot" today usually describes a wide range of actuated mechanical machines. Often, the terms "biped" and "humanoid" are used synonymously, although they are not necessarily interchangeable: the term "biped" only refers to the fact that the robot has two legs, while "humanoid" expresses the similarity to a human with some respect. An example for a non-humanoid biped is the animal-type biped presented in [136], the counter example of a humanoid without legs is Waseda Eye WE-4 [73], a human-like head which emulates the human senses and even is capable to express emotions.

Still guided by the idea of creating an universal helper and partner in any situation, a worldwide competition is intended to push development of biped humanoids today: the RoboCup Federation [16] organizes the annual Robot Soccer World Championship. The goal of this federation is to boost robotics research and, – according to their website – "by the year 2050, develop a team of fully autonomous humanoid robots that can win against the human world soccer champion team."

Apart from this sporting challenge, question comes up of the usefulness of humanoid robots. Areas of application for humanoid robots are plentiful and humanoids are likely to influence many domains of human daily life [39]. In Japan, efforts are made to establish humanoid robots as helpers in the household or in hospitals. Due to the inverted age pyramid, sorrows arise how to care for elderly and needy people, if by the year 2035 in Japan more than 30% of the population are older than 65 years and 18% passed their 75th

anniversary [7]. This is a significant increase compared to the year 2000, where only 19% of the Japanese were aged 65 or older, backed by 67% of the population being in their working age (15–64). These figures document that elderly care by humans alone cannot be guaranteed. Support by robots can help to relieve nurses from monotonous obligations providing more time to see to the social needs of the patients. Hence, efficient, safe, and reliable machines must be developed fulfilling the high requirements on skillfulness and universality necessary for such job. The envisioned humanoid shape and locomotion is supposed to facilitate acting in environments designed for humans. Existing commercial service robots for performing simple tasks like lawn mowing or vacuuming so far are only applicable to single, very specialized tasks. A humanoid robot on the other hand should be able to utilize devices developed for humans like conventional lawn mowers or vacuum cleaners. Such robots could even be capable of performing complex tasks like fetching and bringing, dusting, cleaning dishes or assisting.

Unacceptable or dangerous tasks in environments not accessible to humans due to lack of space, extreme climatic conditions or contamination could be assumed by walking robots. Thus it could be imagined in case of a hazardous incident in a nuclear power plant to have leakages sealed by robots. Due to the high motility, a walking robot could move through obstructed terrain. For this scenario, the robot needs not necessarily be controled autonomously: using single autonomous subsystems, e. g. balanced gait and quick reactions on external events can be assured while the manipulation systems are tele operated by a human. Decisions on the order of executing different tasks hence remain at the discretion of the operator thus deploying the expert's invaluable experience base without putting him or her at risk.

Another economically very important field of application for humanoid robots is the entertainment sector. An increasing number of enterprises – inspired by the great success of the Sony AIBO, a dog-like toy with four legs and some cognitive abilities – develop humanoid robots targeted as playfellows able to communicated similar to humans. Recent toys already show emotion based conduct and resemble small children. Such robots are considered to evolve towards a standard entertainment platform.

In the following, previous research at the Institute of Automatic Control Engineering (LSR), Technische Universität München, is discussed, being the fundament for results presented in this thesis.

1.1 Spade- and Groundwork in Autonomous Walking

In the scope of the German Research Foundation (DFG) Priority Program "Autonomous Walking", considerable research for the coordination of image processing and motion planning has been conducted.

A system capable of recognizing obstacles in its environment from images of a stereo camera has been developed [59]. Those obstacles are classified into the three groups "surmountable", "unsurmountable" and "step" and registered in a self maintained map. This system has been evaluated using the ViGWaM (**Vi**sion **G**uided **Wa**lking **M**achine) emulation environment. Based on those visual information, the robot is capable to plan a suitable path from his current position to a desired destination with respect to the obstacles. From a precalculated database with many step trajectories, an appropriate sequence of step primitives is selected such that the robot does not collide with obstacles. En-

hancements for an improved scene reconstruction and extraction of precise obstacle data is presented in [11].

This autonomous navigation of a vision-guided robot requires close coordination of perception and locomotion. Consequently, perception must be controlled to assure that the humanoid is always provided the highest possible amount of task-relevant information about the walking scenario. Therefore a task-specific and situation-dependent intelligent gaze control scheme that selects the optimal view direction has been developed, that allows the acquisition of information required for collision-free and goal-oriented locomotion [89].

Originating from this research on vision guided walking, a new project has been launched evaluating enhancements for the orientation capabilities of the robot. Key idea is to mimic the human field of sight consisting of a foveal and a peripheral area by installing cameras with different zooms on one camera head. Precise classification of objects can be achieved by focusing the object with zoom cameras while the wide angle cameras observe the environment e. g. for approaching humans. This technique can also be combined with high speed cameras for quick interaction e. g. in robot soccer.

The reference trajectories are obtained by a situation dependent online selection and concatenation of single walking primitives, which are stored in an offline computed database [13]. Optimal control techniques are employed for the systematic synthesis of walking primitives. Unilaterality conditions between the feet and the ground, friction conditions, restrictions of the joint drives as well as further restrictions of the task space are taken into account by constraints to the optimization problem. The gait generation method developed at the LSR optimizes the whole body posture resulting in very smooth motions.

As an experimental platform, the humanoid robot Johnnie has been developed at the partner Institute for Applied Mechanics [21]. This highly sophisticated 1.8 m tall robot weighing 40 kg marks state-of-the-art technology. With its 17 Degrees of Freedom (DoF) it shows an impressive walking performance with a top speed of 2.0 km/h and a maximum step length of 45 cm.

However, due to its mechanical complexity and high cost, Johnnie – like most current sophisticated robots – is not easily available for research experiments. As operation of the robot requires the attendance of qualified experts, researchers cannot implement and test new algorithms by themselves. Furthermore, the size and weight the robot even demands for a team of operators, as emergency measures in case of instable behavior cannot be handled by a single person.

High expenses for the mechanical construction prohibit building of a larger number of robots, which complicates research, especially if experiments require modifications in the hardware.

Motivated by those experiences a request was formulated for a cheap, modular and small-size humanoid platform to evaluate novel control methods and approaches in artificial intelligence. The development of such a plaform is discussed in this work.

1.2 Main Contributions and Outline of Dissertation

A legged robot has to fulfill many tasks that are not directly linked to its primary purpose, to provide some kind of service. These tasks can be categorized into low-level tasks – such as joint, balance, and walking control – and high-level tasks comprising e. g. orientation, navigation, path planning or cooperation. While low-level tasks are very time critical

resulting in immediate visible malfunction upon failure, these tasks only ensure elementary functioning and by themselves cannot cause any useful action of the robot. Useful activity, however, i. e. motions suitable to solve a given task, are commanded by high-level processes.

The work presented here focuses on the design and the low-level control aspect of humanoid robots. In the course of the thesis the development cycle of a prototype humanoid robot from the design phase to the implementation of a walking control algorithm is discussed. At each step – design, posture adaptation, and control – new ideas and concepts are introduced and validated in hardware experiments. Supplementary information, especially videos and publications, can be found on the author's web page[1].

Robot Design

An autonomous walking robot for fast, dynamic walking is designed that allows testing and evaluation of new ideas and concepts in hard and software. Contrary to many current – highly developed and technically very advanced – humanoid robots such as Honda ASIMO [32], Johnnie [58] or HRP-2 [48], the new robot is conceived as a comparatively cheap platform. A modular design from off-the-shelf components is stipulated to ensures easy maintenance and quick reproducibility. These characteristics target at providing a convenient platform for IT research. The robot designed and built in the scope of this thesis is considered a proof-of-concept prototype towards this research platform, details on the construction are given in App. A.

As the weight-to-power ratio of a humanoid is decisive for its performance, joint actuators must be selected to closely match the requirements thus avoiding oversized motor-gear-combinations incorporating extra weight to the robot. In order to provide a methodic approach to this problem, a systematic design process – described in Chapter 3 – based on optimal control has been developed in close cooperation with the "Simulation and Systems Optimization Group", Technische Universität Darmstadt. Using a detailed dynamic model of the robot, gait trajectories are computed by solving an optimal control problem, minimizing e. g. the energy consumption during the step. From these gait trajectories, the requirements on the actuators for maximum torque and velocity are obtained and used for further actuator selection. Formulating the actuator selection task as an optimal control problem is considered novel; although in this dissertation described for humanoid walking robots, the method can be equally applied to any type of robot.

Walking Control

A core task for humanoid walking robots is the actual walking controller, generally consisting of a gait pattern generator and the balance control. For this problem, there exist two fundamental approaches: one possibility to set about this matter is to rely on a very accurate model of the walker and to compute gait trajectories trusting in sufficient accordance of the model with reality. The other direction relies an on approximating the robot dynamics by a simple model with reduced system states, e. g. an inverted pendulum. Accordance of the simplified model with the real dynamics is ensured by feedback control.

In the first approach, the trajectories are generally computed offline incorporating many constraints like balanced or energy efficient walking. As the trajectories are inherently balanced, only little control is required to compensate disturbances.

Besides the accurate model of the robot dynamics, this method also assumes that commanded gait trajectories are closely matched by the real motion. Robots equipped with

[1] `http://www.lsr.ei.tum.de/~dw`

planetary gears however often exhibit a significant divergence between the commanded and the real posture due to gear backlash.

Another difficulty arising from the approach with precalculated walking patterns is the size of the necessary database with gait trajectories, as variations in step length, walking direction, speed or ground inclination generally require recalculated dedicated walking patterns.

Therefore it is useful to have a means of correcting the posture of the robot by superposing the precalculated pattern with a correction term thus correcting posture errors or adapting trajectories to new situations, e. g. adjusting flat ground trajectories to walking on slopes. A method allowing such modifications termed *Jacobi Compensation* is presented in Chapter 4. The method uses Jacobian matrices to translate desired Cartesian motions of selected parts of the body into corresponding joint space motions. The use of Jacobi matrices to generally adapt the posture of humanoids to new situations has not been reported yet. Stability properties of Jacobi Compensation are discussed and applicability is documented in hardware experiments.

The inverted pendulum method is a walking control strategy that classes as a simplified model approach. The robot dynamics are described by an inverted pendulum where the pendulum base coincides with the robot support foot and the pendulum mass represents robot center of mass. Chapter 5 describes the implementation of this control method on the humanoid UT-Theta developed at the Nakamura & Yamane Lab. of the University of Tokyo. This robot features some mechanical innovations like a special knee joint with a backlash clutch allowing to switch between actuated and free swinging mode; the goal is to bridge between actuated humanoid robots and passive walkers to achieve more natural looking walking patterns. Handling the hybrid character and the nonlinear dynamics of the joint imposes strong demands on the knee joint controller to ensure quick reaction on commanded trajectories and smooth operation not disturbing the delicate dynamics of the humanoid. Hence, a hybrid, nonlinear, time optimal controller for the knee joint is proposed and implemented.

2 State of the Art

This chapter introduces the fundamentals of humanoid walking by defining common terms and concepts. As a basis for understanding humanoid gait its properties are analyzed and physical criteria for balanced locomotion are derived. In order to give a brief overview of the state of the art in biped control, the most successful control strategies and some humanoid biped projects are presented.

2.1 Introduction

The basis for current humanoid walking research has been laid by Vukobratović in 1969 [119] who was one of the first to analyze biped walking [121] and establish criteria for balanced gait [120]. Since then, most research on biped walking is rooted in these fundamental investigations.

Trying to implement human-like locomotion capabilities for robots, researchers have always been torn between a technological approach and a biological approach. The former relies on concepts and techniques known from robotics, where abilities are realized departing deliberately from the solution chosen by the natural archetype. This approach can either be motivated by the attempt to find a better solution or a lack of comprehension of nature.

The biological approach on the other hand starts by thoroughly analyzing the functioning of animals or humans. These mechanisms are then adapted and translated into algorithms understandable to machines. Information processing in animal and human brains is rather complex and an analysis is often not possible with current technology; therefore assumptions on the functioning of natural signal processing can be validated by implementing the concept in a robot and observing its effect. Hence, there is a mutual benefit of a collaboration for engineering, biology and neuroscience.

This chapter gives a condensed summary of the state of the art in humanoid biped walking after more than three decades of research. Starting with an analysis of human gait, Sec. 2.2 introduces some notions commonly used in humanoid walking and criteria for balanced gait. An overview of the most important control strategies is given in Sec. 2.3. A major issue for feedback controllers is to determine reliably the system state. The problem of state measurement is discussed in Sec. 2.4, including an overview of sensor systems. A number of the most successful biped robots is presented in Sec. 2.5.

2.2 Fundamentals

2.2.1 Biped Gait

From the technical point of view, humanoid gait is often divided into different phases. This discrimination is made, as bipeds show very different dynamical properties depending on the number of ground contact points and the contact type.

As shown in Fig. 2.1, humanoid walking can generally be split into the *double support phase*, where both feet have ground contact, and the *single support phase* with one foot being flat on the ground, while the other swings through the air. Especially for fast walking, the swing phase is further classified into a *pre-swing* and a *post-swing phase*, see [13]. During the pre-swing phase the swing foot rolls about the toes, and the post-swing phase is characterized by the swing foot landing on its heel and rolling about it.

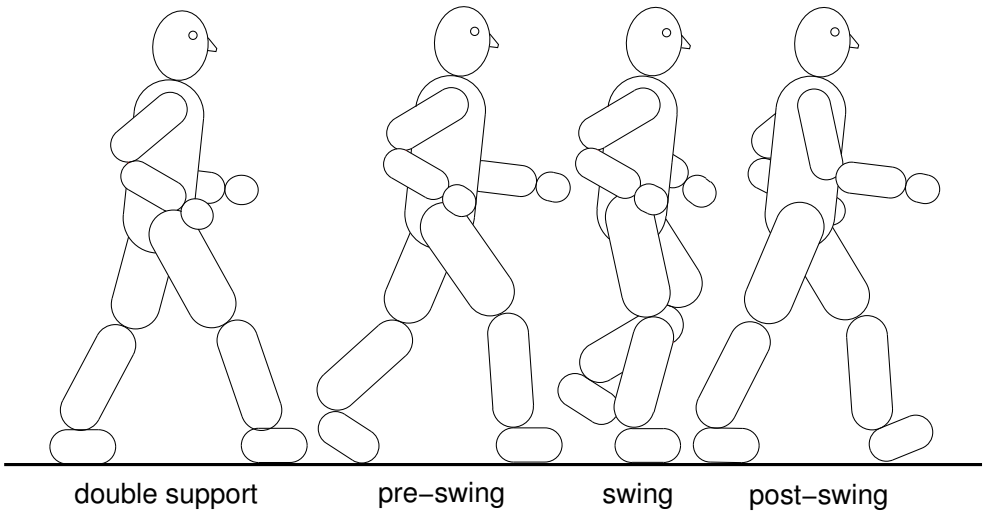

Figure 2.1: Phases of dynamic biped gait.

Depending on the type of gait, not all phases can be observed. When robots are walking very slowly, the pre- and post-swing phase are generally omitted, thus always keeping the sole of the feet parallel to the ground. In very fast and dynamic motion on the other hand, the double support phase, with both feet flat on the ground, often is not distinguishable; running is even characterized by a complete lack of a double support phase, the single support phases are separated by a flight phase.

The ground contact being the supporting basis has a substantial influence on the ability to balance the robot in an upright position. The great variety of ground contact situations however constitutes the necessity for a more generic description of the foot contact situation. Therefore the term *supporting area* has been introduced:

Definition 2.1: *Supporting area.*
The *supporting area* is formed by the convex hull about the ground support points. ■

Fig. 2.2 illustrates this definition in the case of single and double support.

During the single support phase with only one foot having ground contact, the supporting area is the convex hull about the foot contact area. The supporting area in double support

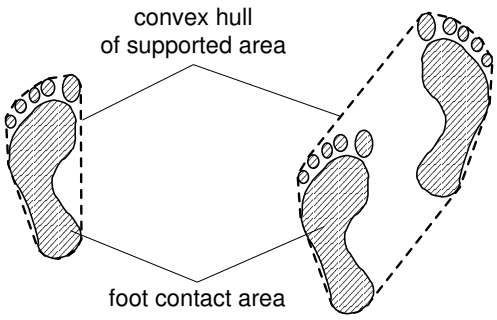

Figure 2.2: Supporting area during single and double support phase.

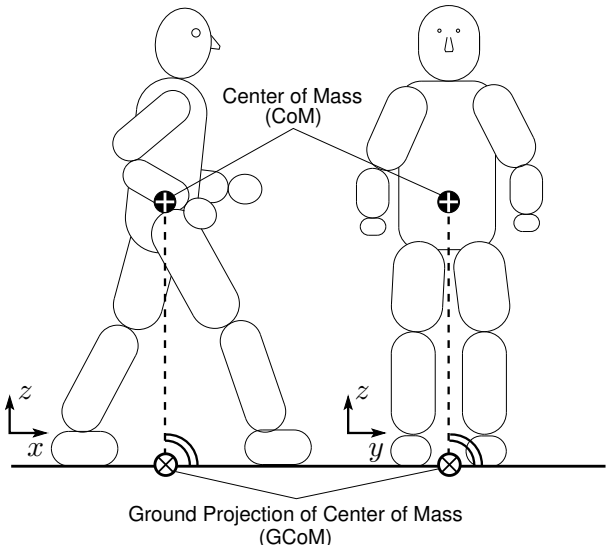

Figure 2.3: Ground Projection of Center of Mass (GCoM).

phase, however, comprises the contact area of both feet as well as the domain between them.

The feet of walking robots are not attached to the ground and can slip or lift off. Hence, forces can only be tranmitted in one direction and friction forces and the gravitational force alone ensure, that the support foot remains at a fixed position on the ground. Therefore, the weight of the robot limits the applicable force and the lever arm becomes decisive for the achievable torque. The lever arm being essentially determined by the contact area, the supporting area becomes specially important for balanced walking. Therefore the supporting area is a central part of all commonly used equilibrium criteria.

2.2.2 Equilibrium Criteria

To implement biped walking controllers it is essential to determine whether the robot is in danger of tilting. Therefore, mathematical criteria for this property are discussed in the following.

Ground Projection of Center of Mass

A motionless robot only experiences gravitational forces, which are exerted on all parts of the robot. These forces can be replaced by a virtual force acting at the center of mass (CoM)

$$\boldsymbol{p}_{CoM} = \frac{\sum_i m_i \boldsymbol{p}_i}{\sum_i m_i}, \tag{2.1}$$

of the robot, where m_i denotes the mass of the ith link of the robot and $\boldsymbol{p}_i$ the position of its center of mass.

The location of the center of mass is decisive for the equilibrium of the robot. Its orthogonal projection to the ground is commonly referred to as the *Ground Projection of Center of Mass* (GCoM) [24] or the *Normal Projection of the Center of Mass* (NPCM) [53], see Fig. 2.3.

The location $\boldsymbol{p}_{GCoM}$ of the GCoM is the point that fulfills the relation

$$\sum_i ((\boldsymbol{p}_{GCoM} - \boldsymbol{p}_i) \times m_i \boldsymbol{g}) = \boldsymbol{0}, \tag{2.2}$$

i. e. the GCoM is the point on the ground, where the sum of all moments exerted on the motionless robot is zero. If the GCoM resides within the supporting area, the gravitation force does not generate a tilting moment and the robot remains standing.

However, during fast locomotion, dynamic forces dominate static forces. As the GCoM does not take these dynamic forces into account, it becomes meaningless and bipeds may fall over although the GCoM resides within the supporting area. Hence other criteria must be applied.

Zero Moment Point and Foot Rotation Index

Rotation of an object about a given axis requires the presence of a torsional moment. Therefore, if the robot does not encounter a moment about the horizontal axes x and y, i. e.

$$\boldsymbol{M}_x = 0 \quad \text{and} \quad \boldsymbol{M}_y = 0, \tag{2.3}$$

the robot is balanced.

From (2.3) follows the Definition of the Zero Moment Point:

Definition 2.2: *Zero Moment Point (ZMP).*

The *Zero Moment Point* $\boldsymbol{x}_{ZMP}$ is the point, where the ground reaction force $\boldsymbol{F}_R$ has to act to compensate all horizontal moments $\boldsymbol{M}_x$, $\boldsymbol{M}_y$, see Fig. 2.4 [118, 119]. ■

Hence, the robot is equilibrated, if the ZMP is within the supporting area.

During locomotion the robot experiences – besides the gravitation force $\boldsymbol{F}_{G,i}$ acting at the center of mass $\boldsymbol{p}_i$ of the ith link – dynamic forces: Accelerating masses entails an inertial force $\boldsymbol{F}_{I,i}$ and the corresponding moment $\boldsymbol{M}_{I,i}$, which also acts at $\boldsymbol{p}_i$. Furthermore there is a resultant ground reaction force $\boldsymbol{F}_R$, which can be decomposed into a vertical component $\boldsymbol{F}_{R,v}$ and a horizontal component $\boldsymbol{F}_{R,h}$, i. e. $\boldsymbol{F}_R = \boldsymbol{F}_{R,v} + \boldsymbol{F}_{R,h}$. Accordingly the moment can be broken up into $\boldsymbol{M} = \boldsymbol{M}_h + \boldsymbol{M}_v$. Thus, the dynamic equilibrium during motion is expressed by the equilibrium of forces and moments:

$$\boldsymbol{F}_{R,v} + \boldsymbol{F}_{R,h} + \sum_i (\boldsymbol{F}_{I,i} + \boldsymbol{F}_{G,i}) = 0 \tag{2.4}$$

$$\boldsymbol{p}_{ZMP} \times \boldsymbol{F}_R + \sum_i \boldsymbol{p}_i \times (\boldsymbol{F}_{I,i} + \boldsymbol{F}_{G,i}) + \sum_i \boldsymbol{M}_{I,i} + \boldsymbol{M}_{ZMP,h} + \boldsymbol{M}_{ZMP,v} = 0. \tag{2.5}$$

According to (2.3), the horizontal component of the moment is zero, $\boldsymbol{M}_{ZMP,h} = \boldsymbol{0}$. Substituting $\boldsymbol{p}_i = \boldsymbol{p}_{ZMP} + (\boldsymbol{p}_i - \boldsymbol{p}_{ZMP})$ in (2.5), solving (2.4) for $\boldsymbol{F}_R$ and inserting into (2.5) yields

$$\sum_i (\boldsymbol{p}_i - \boldsymbol{p}_{ZMP}) \times (\boldsymbol{F}_{I,i} + \boldsymbol{F}_{G,i}) + \sum_i \boldsymbol{M}_{I,i} = \boldsymbol{0}. \tag{2.6}$$

Equation (2.6) allows another interpretation of the ZMP according to [12]:

The *Zero Moment Point* (ZMP) is the point on the walking ground surface at which the horizontal components of the resultant moment generated by active forces and moments acting on human/humanoid links are equal to zero. [118]

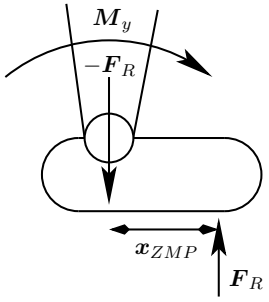

Figure 2.4: Forces and moments during single support phase.

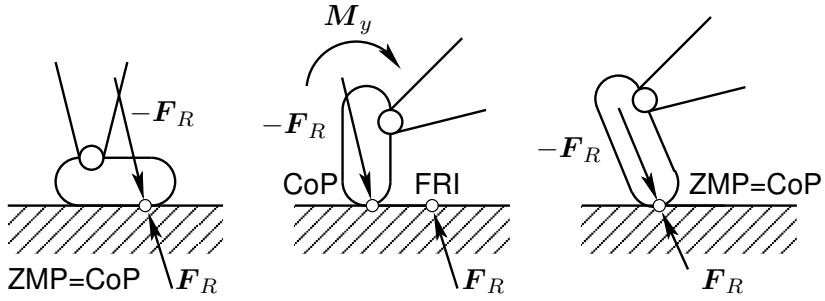

Figure 2.5: The possible relative position of ZMP and CoP: dynamically balanced gait (left), unbalanced gait (the system as a whole rotates about the foot edge and overturns) (middle), and intentional foot-edge equilibrium ("balletic locomotion")(right).

In 1999, Goswami [23, 24] introduced the notion of *foot rotation indicator* (FRI), also known as *imaginary ZMP* (iZMP) [118]. The FRI is physically identical to the ZMP and both points coincide as long as ZMP/FRI remain inside the supporting area. But unlike the ZMP, the FRI is allowed to leave the supporting area, see Fig. 2.5. Although the gait is not balanced anymore (unbalanced gait), the FRI still has a useful interpretation: the distance of the FRI to the supporting area is a measure for the "degree" of instability of the gait and hence can give some invaluable information when controlling a stumbling biped. Technical feasibility of such motion is not clear and has not been proven yet.

The concept of the ZMP being a physical approach, is very useful in numerical simulations, as it can easily be calculated from the system state. In hardware experiments however, this information is not necessarily known and measurement often is subject to considerable noise. Hence, another another criterion, that can be evaluated more easily, is desirable.

Center of Pressure

Most humanoid robots are equipped with force-torque-sensors at the feet of the robot. Therefore the Center of Pressure criterion results directly from evaluating those sensors.

Definition 2.3: *Center of Pressure.*

The *Center of Pressure* (CoP) is defined as the point on the ground where the resultant of the ground reaction forces acts [24]. ■

There are two types of interaction of the foot with the ground: the normal forces $\boldsymbol{F}_{N,i}$ and the frictional tangential forces $\boldsymbol{F}_{T,i}$. The CoP is the point

$$\boldsymbol{p}_{\mathrm{CoP}} = \frac{\sum_i \boldsymbol{p}_i F_{N,i}}{\sum_i F_{N,i}}, \tag{2.7}$$

where the resultant $\boldsymbol{F}_R = \sum_i \boldsymbol{F}_{N,i}$ acts; $\boldsymbol{p}_i$ is the vector from the origin to the point of action of force $\boldsymbol{F}_{N,i}$ and $F_{N,i} = |\boldsymbol{F}_{N,i}|$. As the interaction between foot and ground is always unilateral, $F_{N,i} \geq 0$ holds. Hence, $\boldsymbol{p}_{\mathrm{CoP}}$ always lies within the supporting area.

In [24], Goswami proved that ZMP and CoP are identical during single support phase for balanced walking. This identity implies that definitions referring to the ZMP can be applied accordingly using the CoP. The ZMP is easy to compute and therefore well suited

for gait generation, while the CoP can easily be measured and hence is more suitable for control of a walking robot. Due to their identity, these criteria can be used interchangeably thus facilitating computation.

Besides criteria for a balanced robot, there are restrictions on the ground reaction forces to avoid slipping or lifting off.

Ground Reaction Forces

As already mentioned, the ground reaction forces determine fixed contact of the support foot with the ground. Therefore, to maintain ground contact, the vertical component

$$F_{R,v} > 0$$

of the ground reaction force $\boldsymbol{F}_R$ as defined in Fig. 2.4, must always be positive. Otherwise the foot lifts off the ground and the robot cannot be controlled anymore.

Slipping of the support foot is avoided by restricting the horizontal component $F_{R,h}$ to remain within the so-called *friction cone*

$$\sqrt{F_{R,x}^2 + F_{R,y}^2} = F_{R,h} \leq \mu_R F_{R,z},$$

where μ_R is the friction coefficient.

The equilibrium criteria introduced in this chapter are evaluated in most walking control algorithms. Furthermore, they help to determine the difference between slow, static motion and fast, dynamic walking.

2.2.3 Statically and Dynamically Balanced Gait

As already mentioned, dynamic forces like Coriolis, centrifugal and inertial forces, dominate the static gravity forces with increasing walking velocity. The dynamic forces can usually be neglected in slow motion, hence a common classification of walking gait distinguishes between statically and dynamically balanced gait.

Definition 2.4: *Statically balanced motion.*
The movement of a robot is called *statically balanced*, if the GCoM and the ZMP always remain within the supporting area during the entire motion [17, 91]. ■

Accordingly, fast motion taking into account dynamic forces is referred to as dynamically balanced motion.

Definition 2.5: *Dynamically balanced motion.*
If the ZMP resides within the supporting area during the motion of a human/humanoid while the GCoM leaves the supporting area, then this motion is called *dynamically stable*. ■

Note that Def. 2.4 is a special case of Def. 2.5, as GCoM and ZMP are identical for a motionless robot. Obviously, the maximum achievable step length for statically balanced gait is limited compared to dynamically balanced gait [91].

The terms and criteria explained in Sec. 2.2 are the fundament for humanoid walking control. The following section gives an overview of the most commonly used control strategies.

2.3 Overview of Control Strategies

For humanoid biped robots, the problem of equilibrated robust walking is most fundamental and current solutions yet remain unsatisfactory for real world application.

There are three fundamentally different approaches to humanoid walking control: One strategy assumes very accurate models of the real robot and its environment. Using this model for physically consistent motion generation, the approach relies on close accordance of the calculated dynamics with the real hardware behavior. Another starting point is to use a rather simple and abstract model of the dynamic behavior and achieve accordance with reality by feedback control. The third research direction can be subsumed as nature inspired control techniques. These include methods based on neural networks, fuzzy logic or genetic algorithms and are generally inspired by the idea to enable robots to act in unknown environments and to react on unforeseen events.

One of the most popular approaches based on a simplified model is the inverted pendulum method belonging to the category of strategies relying on feedback control.

2.3.1 Inverted Pendulum Method

Miura and Shimoyama [72] studied the inverse pendulum approximation for the control of the Biper-3 robot. Later on, Kajita et al. [43–46] extended the inverse pendulum approach and tested its validity on various robots.

In this approach, the dynamics of the robot are approximated by those of an inverted pendulum linearized about the upper equilibrium point. The mass is concentrated at the center of mass (CoM) of the robot, and the base of the pendulum coincides with the support foot of the robot, as illustrated in Fig. 2.6. Based on this dynamic model, an appropriate location for the foot placement can be computed in order to counterbalance the tilting motion.

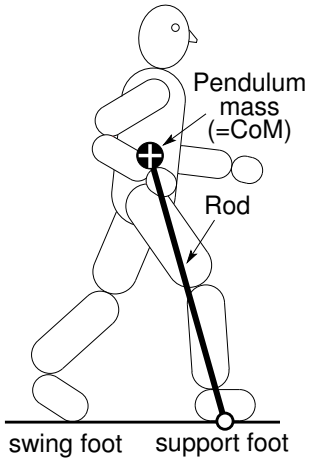

Figure 2.6: Inverted Pendulum Method.

Errors between the computed motion of the inverted pendulum and the real motion of the robot must be compensated by feedback control. One solution is to use the actuated ankle joint and apply a small correction torque. However, the single mass inverted pendulum is a non-minimum phase system, which imposes problems for controlling the ZMP. Therefore Napoleon et al. [77] proposed an extension towards a two mass inverted pendulum to overcome this deficiency.

Sugihara [100] proposed a method to manipulate the location of the center of mass using the whole body motion, and to control the evolution of the inverted pendulum through ZMP manipulation [102].

As the Inverted Pendulum Method is very flexible and gait patterns can be computed online, it is used in many humanoids. A more detailed description of this approach can be found in Sec. 5.4.

Used in robots: Honda Asimo [34], Johnnie [105], HRP-2 [1], UT-Theta [111].

2.3.2 Dynamics Filter

A very interesting and promising approach referred to as "Dynamics Filter" has been formulated by Yamane and Nakamura [133], who presented a nonlinear filter-like method that transforms a given motion trajectory – motion captured, hand drawn, numerically generated, etc. – into a motion that is physically consistent for the target platform.

The approach requires the availability of accurate equations of motion of the robot with environmental constraint forces. Applying any given motion trajectory, that has not specifically been designed for the robot, to this model generally results in a violation of physical constraints. The basic concept is to only specify joint trajectories for some joints and compute Cartesian trajectories for single, arbitrarily selected, fixed points of the robot from the given trajectory. These Cartesian motions are then mapped back to a joint motion.

As humanoid robots are redundant systems, this inverse mapping generally allows an infinite number of solutions. Candidate solutions for a robot motion are those that satisfy the robot equations of motion, thus a set of physically consistent motions is obtained. Among these physically valid motions the one matching the desired motion most closely is chosen.

This method can be implemented in a computationally efficient way thus allowing online trajectory generation. As the optimization is local, knowledge of the total trajectory during the filtering process is not necessary, hence the trajectory can even be modified while it is being executed. Another advantage is its generality allowing to apply this strategy to any motion without restrictions.

Used in robots: Sony QRio [95].

2.3.3 Passive-Dynamic Walkers

Contrary to the previous active control methods, where joint angles and ground reaction forces are measured and precisely controlled, passive dynamic walkers achieve biped walking without electronic support.

Passive dynamic walkers [9] are mechanical devices designed specifically for walking down shallow slopes. They have no motors or controllers, yet they can exhibit humanlike motions. This is achieved by exploiting their natural dynamics, i. e. passive walkers have been mechanically designed such that a machine of this class will settle into a steady, periodic gait without active control or energy input. Energy loss due to friction or impact is compensated by utilizing the potential energy of the slope converting it into kinetic energy. This idea was first introduced and examined by McGeer [67–70] in 1989.

One very interesting observation with passive walking are very smooth trajectories giving the impression of human-like gait. This reinforces the observation of high energy efficiency of human gait.

In 2001, Ruina et al. [10] succeeded in building the first three-dimensional, kneed, two-legged, passive-dynamic walking machine, the Cornell Passive Walker, see Fig. 2.7. Thus they proved the theoretic considerations to be valid. In this experiment, the two-dimensional model by McGeer is extended by adding specially curved feet, a compliant heel and mechanically constrained arms thus achieving a harmonious and stable gait.

However, passive walkers are very sensitive to initial conditions and can only walk at a dedicated speed imposed by the mechanical construction. Thus transferring the idea of

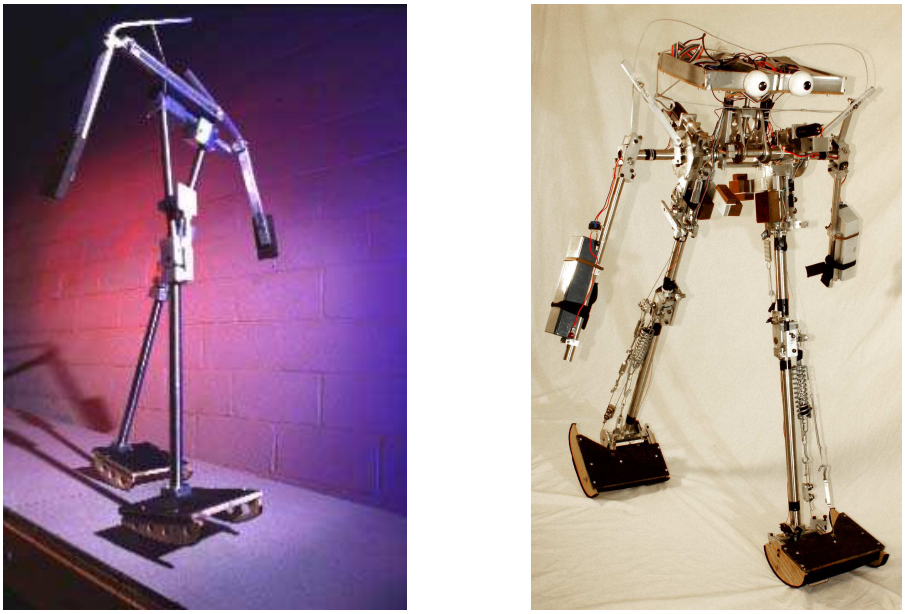

Figure 2.7: The Cornell Passive Walker with arms (left) and the Cornell Biped (right). ©Cornell University

passivity to actuated humanoids is an interesting challenge addressed by many researchers [123]. An intermediate mixture between passive walkers and actuated humanoids has been introduced by Spong [96–98], who showed that by adding a single actuator to a passive walker, energy loss can be compensated. It is even possible to add energy to the system such that the robot can climb up slopes.

Various energy efficient biped walkers have been built [9], e. g. the Cornell Biped shown in Fig. 2.7, the Delft biped, or the MIT learning biped. An established measure to compare efficiency between humans and bipeds of different size is the cost of transportation

$$c_t = (\text{energy used})/(\text{weight} \times \text{distance traveled}). \tag{2.8}$$

It is useful to distinguish between the specific energetic cost c_{et} of transportation and the specific mechanical cost c_{mt} of transport, where c_{et} reflects the total energy consumed by the system and c_{mt} only considers the mechanical work of the actuators.

The 13-kg Cornell Biped, for example, walking at 0.4 m/s has $c_{et} \approx 0.2$ and $c_{mt} \approx 0.055$. Humans are similarly energy effective, walking with $c_{et} \approx 0.2$, as estimated by the volume of oxygen they consume, and $c_{mt} \approx 0.05$. By contrast, the Honda humanoid Asimo is estimated to have $c_{et} \approx 3.2$ and $c_{mt} \approx 1.6$. Thus Asimo uses at least 10 times the energy (scaled) of a typical human.

These data confirm that adopting concepts from passive walkers to humanoid robots constitutes an important aspect towards autonomous and energy efficient walking.

2.3.4 Other Control Strategies

There are various other methods to achieve balanced humanoid walking. Yamaguchi et al. [131, 132] solved the problem to obtain trajectories inversely from a desired ZMP movement; the upper body motion is used to compensate the moment about the desired ZMP. This strategy has been implemented in the Waseda Leg and Wabian series.

Miura and Shimoyama [72], who developed the Biper robots, as well as Raibert et al. [82, 83] controlled their robots by foot placement feedforward control. This method yields an asymptotically stable periodic gait.

A method to manipulate the ZMP has been presented by Sugihara [99–101]. Based on an inverted pendulum model, the CoM is controlled through a Jacobian such that the ZMP shows the desired behavior.

Apart from these classical control approaches, there are approaches to mimic the human neuro-system by employing neural networks [15] or to emulate the central pattern generator [65, 103] as it can be found in human beings.

Another direction employs genetic algorithms or neural networks to acquire and improve gait trajectories on an evolutionary basis [3, 8].

A thorough survey of these methods can be found in [49].

2.3.5 Lowlevel Joint Control

A very crucial part of humanoid robot control is the accuracy of the low level joint controllers following commanded trajectories.

In many robotics applications the joint position is controlled by a simple PID controller. However, their performance is unsatisfactory in dynamic environments with fast changing reference positions and varying reaction forces, since nonlinear and coupling terms of the joint dynamics are subsumed into a disturbance term. If these dynamic forces become larger, the controller cannot compensate.

Significant improvement [57] – especially for high joint velocities – can be achieved by adopting computed torque controllers [88]. This controller compensates the effect of nonlinearities by a feedback system, hence the remaining dynamics ideally correspond to a pure double integrating system.

Raibert [84] compared PID, computed torque and sliding mode controllers with respect to their performance. His experiments show the sliding mode controller superior to the other systems, especially for large parametric uncertainty. However, realizing high sampling rates as required by sliding mode controllers usually comes at the cost of heavy hardware solutions that deteriorate the overall system performance and thus are not suitable for biped walking machines at present state of technology.

When implementing feedback controllers mentioned in Sec. 2.3, special importance comes to installed sensing system, as they close the feedback loop.

2.4 Sensors for Humanoid Robots

One important difficulty in humanoid robotics lies in the development of a powerful sensing system. Apart from measuring the state of each joint, the overall body posture must be determined, as humanoids are not fixed to the ground and hence lack a fixed reference frame.

In general for all sensor systems it must be distinguished between analog and digital sensors. Analog sensors represent the measured quantity as a voltage, which has to be digitized by an AD converter for further processing. Digital sensors directly produce a digital representation thus superseding the AD converter.

Besides sensor noise and and electromagnetic disturbances, the AD conversion process itself add extra noise to the signal, as AD converters rely on an accurate reference voltage. Such accurate sources however are difficult to realize on autonomous platforms. Hence, as a rule of thumb, the accuracy of digitized analog signals ranges around 0.5 %; further reduction of the noise requires high efforts.

Digital sensors on the other hand generally are much more robust and require less evaluation electronics; therefore such sensors generally are preferable for mobile, autonomous application.

2.4.1 Joint Position and Velocity Measurement

Pulse encoders [66] allow a very accurate measurement of the relative joint position. These digital sensors work on an optical basis counting the number of slots in a disk passing a light barrier. Using two channels with an offset of a quarter of the slot distance, it is possible to determine the direction of rotation. In robotics application, a resolution of approx. 2^{16} bit, including the reduction gear is feasible; with higher resolutions the detection of slots often becomes too slow to register fast motions, i. e. fast joint motion is not detected. High resolutions are on the other hand necessary for computing a low noise velocity signal by difference quotient at high sampling rates.

However, if pulse encoders with two tracks, i. e. relative encoders, are installed on the motor side before a reduction gear, the absolute joint position cannot be initialized as the initial joint position is unknown. This can be bypassed by installing microswitches that can be detected by automatic initialization routines. Pulse encoders with Gray-code encoded tracks deliver absolute position information. However, these absolute encoders require n tracks to produce a resolution of $1/2^n$ per circle - thus they are substantially more expensive, larger and heavier than relative encoders [88].

A possibility to directly measure the joint velocity, rather than computing it from position signals, is available through dc tachometers. These are small dc generators whose magnetic field is provided by a permanent magnet.

The output voltage is proportional to the angular velocity and shows a residual ripple due to the presence of a commutator. This ripple cannot be eliminated by filtering, as its frequency depends on the rotation velocity. The general disadvantages of analog sensors apply.

A method to digitally measure rotatory velocity is to measure the time between two consecutive rising edges in the pulse encoder signal. This yields less quantization noise than differentiating the position signal, yet it requires additional evaluation electronics.

2.4.2 Force and Torque Measurement

It is particularly important to know the interaction forces of the robot with its environment. Therefore most humanoids dispose of a force-torque-sensor between the foot and the ankle joint in order to measure the ground reaction forces.

Force-torque-sensors are usually based on strain gauges measuring the deformation of dedicated beams in the sensor construction [71]. Hence, these sensors show a very high bandwidth and are well suited for measuring ground contact forces. However, they can be mechanically destroyed by overload.

Another approach is to measure the motor currents and compare the measured current with the required force computed from a system model. The advantage of this method is that any environmental contact can be detected, dedicated sensors are not required. Unfortunately the dynamics of the electronic circuit are very fast, hence very high sampling rates are required. The necessary processing capabilities are generally not available on autonomous robots.

2.4.3 Body Orientation Measurement

A major and yet unsolved problem is to measure the absolute orientation of the humanoid body with respect to a fixed world coordinate system. This is necessary as bipeds are not fixed to the ground and hence lack a known reference. Balance control requires high bandwidth signals to allow fast reaction to slight deviations from the desired orientation. The maximum achievable walking speed currently is limited by the bandwidth of available orientation sensors [57].

Although magnetic field sensors generally meet the requirements, they are very sensitive to EMF disturbances from mobile phones or brush fire in the motors. Furthermore metal housings can deflect or even shield the magnetic earth field.

Accelerometers produce a voltage output proportional to the acceleration of the sensor with a high bandwidth. Unfortunately, the signal of inexpensive sensors developed for automobile applications are very noisy and not suitable to detect slight accelerations. Integration of the signal is not possible due to a temperature dependent bias.

Another candidate type of sensors are Gyroscopes producing a rotational velocity signal. Their bandwidth of approximately 85 Hz is rather low for humanoid balance control and the signal shows a significant drift.

Efforts have been made to fuse signals from different types of sensors and construct an accurate, fast, and reliable signal [57]. Although interesting solutions have been presented, the problem of determining the body orientation still remains an open issue.

In spite of all difficulties and unsolved problems, many quite successful humanoid biped projects have succeeded in building robots.

2.5 Humanoid Biped Projects

This chapter sketches a brief overview of the most important research projects in humanoid biped robots, see Tab. 2.1, a more detailed overview can be found in [21]. As the group of humanoid robots is rather large and covers a huge variety of very different disciplines – ranging from walking control to emotional mimicking and human-machine-interaction – this chapter focuses on humanoid walking robots.

2.5.1 Waseda

The Humanoid Robotics Institute of the Waseda University is the first group to build hardware humanoid robots. Their current Wabian series, see Fig. 2.8 stands in the long tradition of the Wabot Project that started in 1968 and produced the first humanoid in 1970. A multitude of different versions of the Wabot- and Wabian series have been released

since then examining different kinds of actuators, especially various types of artificial muscles, and novel control methods. The humanoid research has since the beginning been accompanied by research in intelligent prothesis. By joining these related research fields, synergies have been exploited by exchanging biological and robotics know-how.

The latest model Wabian-RV with 43 actuated and 8 passive joints is currently amongst the most complex humanoids. It disposes of advanced visual and auditory senses to mimic the capabilities of the human sensory systems. Based on the sensing information, the whole body motion of Wabian-RV is generated online. For this purpose the dynamics of the robot are reduced by just describing the knee trajectory. This method allows robot gait with stretched knees which is not possible with most other methods due to the configuration singularity. Stable walking is realized by a stiffness/compliance control.

For memorizing and performing complex walking patterns systematically and effectively, a method for online teach-in of low-level and high-level has been developed using a speech recognition system. The robot can emotionally interact with humans by showing feelings like happiness, sadness and anger.

2.5.2 Honda Asimo

Started in 1986, the success of the Honda humanoid series P2, P3 and Asimo, see Fig. 2.9, aroused a widespread interest both in public and in the research community. Conceived as a human size universal helper, the latest model Asimo shows one of the most advanced walking technologies; unfortunately little information on the technology is published. Asimo disposes of a set of precalculated trajectories. If these trajectories do not match the requirements, new motions are generated online by interpolating between two closely matching patterns. The resulting motion is further refined adapting the dynamic properties based on estimating future behavior. The walking controller shows very fast and dynamic walking performance.

Asimo also sets standards in human-robot-interaction. It can recognize individual people by their faces and thus react specifically to the person. Hence, the Honda robot has successfully performed reception or guiding tasks on trade fairs or presentations.

2.5.3 Sony QRio

Another robot developed by industry is the Sony QRio [40, 95], see Fig. 2.10. As opposed to Asimo, the concept of this small size robot does not follow the idea of a universal helper, but is rather designed as an entertainment platform. With this perspective, development focuses on one side on creating an inexpensive platform suitable for the mass market and on the other side on implementing entertaining performances like gymnastics shows, dancing synchronized between several robots or singing. QRio has a highly advanced equilibrium system allowing it to balance on a moving surf board or skating on roller skates.

A special tool [54] has been created that allows people with little technical background knowledge to graphically teach-in new motion patterns. Based on the Dynamics Filter [133] method, balanced motion patterns are generated from the teach in specifications that can be transfered to the robot. This system even accounts for external reaction forces, thus QRio can be tought to grab a ball and throw it away.

2.5.4 HRP-2

The humanoid HRP-2 [48], see Fig. 2.11 is a joint development of several Japanese research institutes and Kawada Industries Inc., financed by the Japanese Ministry of Economy, Trade and Industry (METI). The project goal is to provide a high quality research platform which can be turned into an industrial product towards the end of the project.

Due to the large number of researchers working on this robot, it has shown remarkable performances in a multitude of research problems, e. g. stepping over obstacles [26], running [74] or safe falling over [19]. Other directions of research include walking on uneven surfaces, tipping-over control or getting up if the robot has fallen down. Furthermore research in human-machine interaction are envisioned.

2.5.5 Johnnie

In the scope of a project supporting by the German Research Foundation (DFG), the humanoid Johnnie [22, 57, 58] shown in Fig. 2.12 has been developed with the goal to enhance abilities in autonomous walking. Johnnie possesses a highly developed visual guidance system [61, 90] based on a stereo camera system. Obstacles are classified into e. g. "possible to step on", "possible to step over" or "not negotiatable". According to the distribution and type of obstacles Johnnie plans a suitable trajectory towards the target and selects an appropriate gait pattern allowing smooth locomotion. Thus, the robot is able to show a very smooth walking performance; once a suitable walking path is found, obstacles can be handled without stopping and adjusting position in front of it. Gait patterns are already adapted several steps in advance in order to reach the obstacle at a distance apt for negotiating it.

2.5.6 UT-Theta

The humanoid UT-Theta [76, 79] shown in Fig. 2.13 developed at the University of Tokyo excels by some innovative design ideas: in order to maximize the motility of the robot, a double spherical hip joint has been developed where all 6 rotation axes of the two hip joints intersect in a single point thus allowing motion of the upper body without effect on the leg motion.

Another innovation is the knee joint with backlash clutch that can be switched between a passive and an actuated mode. The key idea was to transfer the concept of passive walkers to actuated humanoids thus mimicking human walking properties and obtaining a more natural looking gait.

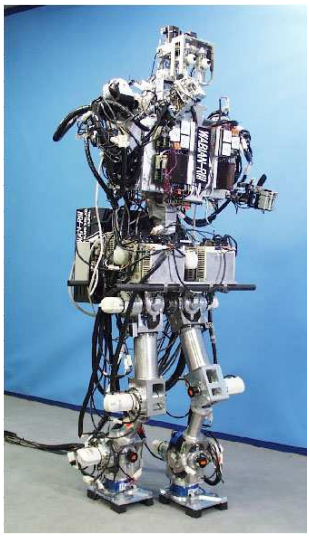

Figure 2.8: Wabian RIII.
©Waseda University

Figure 2.9: Honda Asimo.
©Honda Motor Co.

Figure 2.10: Sony QRio.
©Sony Corp.

Figure 2.11: HRP-2.
©Kawada Industries

Figure 2.12: Johnnie.
©TU München

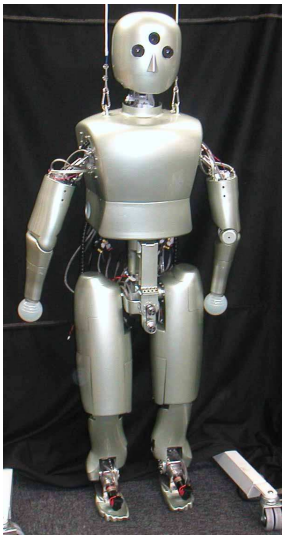

Figure 2.13: UT-Theta.
©University of Tokyo

Robot	*Developer*	*Height* [cm]	*Weight* [kg]	*DoF act./pass.*	*Speed* [m/s]	*Devel. time*	*Effort* [Prs-yrs]	*Specialties*
Wabian	Waseda University [122]	166	107	43/8	0.21	1992-2000	⊙	one of the first humanoid projects
HRP-2	AIST [1]	154	58	30/0	0.7	1998–2002	⊙	
Asimo	Honda Corp. [34]	120	52	24/0	0.4	1986–	⊙	
SDR-4X/QRIO	Sony Corp. [95]	58	7	38/0	⊙	2000–	⊙	running, gymnastics
Partner Robots	Toyota Motor Corp. [113]	120	35	⊙	⊙	⊙	⊙	
H6	University of Tokyo [109]	137	55	35/0	⊙	2000–	⊙	25 cm step height
Hoap	Fujitsu Automation [18]	50	7	25/0	⊙	⊙	⊙	
Pino	Kitano Symbiotic Systems Project [51]	70	4.5	26/0	0.05	1999–	4.5	
UT-θ	University of Tokyo [111]	150	45	21/2	⊙	2001–2004	12	innovative mechanical design
UT-μ:mighty	University of Tokyo [110]	58	7	20/0	⊙	2002–	3	high motility
Guroo	University of Queensland [108]	120	38	12/0	⊙	2001–	⊙	
BARt-UH	University of Hanover [114]	100	25	6/0	0.3	1999	2	stair climbing
Johnnie	Technische Universität München [105]	180	40	17/4	0.55	1998–2004	12	perception based walking

⊙: data not published or not found by the author.

Table 2.1: Overview of humanoid robot projects.

2.6 Summary

In spite of more than three decades of research in humanoid robotics, there still remain many challenges. Although there exist a variety of approaches for controlling balanced gait, the walking performance of todays humanoids is still at the level of a toddler. However, even if motions from current humanoids still look somewhat "robotish" and little natural, their performances are quite impressive and exert a fascination on the spectator.

Improvements are required on both, the hardware side by employing advanced sensing systems and the control side. From the current point of view, joint strategies combining the advantages of different control methods seem to be most promising.

Another important issue is generalization and abstraction of sensor data. Information of a variety of sensing devices must be fused by assessing the reliability of each signal in a given situation and extracting accurate information on the current system state.

3 Humanoid Robot Design Based on Optimal Control

The first step towards humanoid biped walking is a thorough hardware design with respect to the specific requirements of the robot. Special attention must be turned to the selection of appropriate actuators as oversized motors increase the total weight of the robot, thus deteriorating the walking performance. Here, a procedure for actuator selection based on optimal control is discussed.

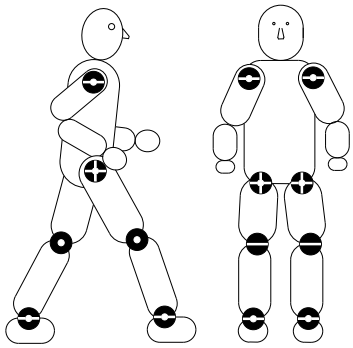

3.1 Problem Description

The design of a humanoid walking robot is very important for the achievable performance of the robot, especially the weight of the system imposes physical limits. Additional weight deteriorates the walking performance, as a higher mass has to be accelerated; the maximum achievable joint acceleration decreases with rising weight. Hence motor-gear-combinations should be chosen as light as possible, thus just about fulfilling the requirements on possible torque, acceleration and velocity.

Besides the increased weight of more powerful motors, they usually also consume more power and therefore require larger and more batteries. Furthermore, the electronics to handle higher currents become heavier and bulkier. Oversized motors not only increase the total weight of the robot by their own excess weight, but also entail further gains.

This chapter presents a systematic way to accurately determine the actuation requirements of a robot during planning phase and select an appropriate motor-gear-combination from the manufacturers offerings [129]; the method has been developed in a joined effort with the Simulation and Systems Optimization Group, Technische Universität Darmstadt.

Many research groups investigate biped walking machines and put a lot of effort into hardware design [3, 37, 56]. The actual development and production can be so expensive and time consuming that university research labs have difficulty competing with larger companies [32, 33, 40], where even dedicated actuators are developed exclusively for use in humanoids [20].

In contrast to the just mentioned projects, the method presented here is used exemplarily to design a small-size and fast, autonomous humanoid walking machine using off-the-shelf components wherever possible, especially commercially available high performance DC motors.

The biped is intended for fast, dynamic walking; thus, its dynamic behavior is extremely important. Numerical simulation and optimization of full nonlinear dynamic models are used throughout the entire design process. Efficient recursive multibody dynamic algorithms [31] are particularly well-suited for modeling legged systems. These are combined with powerful nonlinear optimization programs [117] to generate gait trajectories [28, 29] or to optimize kinematic and dynamic model parameters. Using this data, a choice for the motors and gears is made, which delivers the desired performance. The robot design, i. e. trade-off between motor weight and power, are further optimized with respect to a target walking speed of approximately 0.5 m/s.

The organization of this chapter is as follows: Sec. 3.2 describes the preliminary kinematic structure of the humanoid based on the desired size and rough estimations of body masses. Using this model, the actuator requirements for walking at a desired velocity are computed in Sec. 3.3. The torque and velocity ratings are evaluated in the motor selection process discussed in Sec. 3.4.

3.2 Initial Assumptions for the Kinematic Structure

The first step when designing humanoid robots is to decide on some fundamental parameters of the humanoid such as size and kinematic structure.

Current human-sized walking machines have a typical weight of 40–60 kg at a height of 160–180 cm. This size and weight makes them difficult to operate, as elaborate safeguard systems have to be installed to prevent the robot from damage in case of a system failure. These safeguard systems usually require additional operators, hence handling the robot demands a team to deal with the complex system. Small size robots on the other hand usually lack a significant payload, thus only limited sensory extensions can be installed. Otherwise few high quality sensors exist in a miniaturized, lightweight version.

Hence, opting for the dimensions means pondering between a size and weight manageable by a single operator and an over-miniaturization resulting in expensive micro-components and a cramped – thus hard to maintain – design. As a compromise, a target height of 70 cm is chosen. Assuming human-like proportions [116] yields the dimensions given in Tab. 3.1.

Table 3.1: Link dimensions in local coordinates and mass distribution.

		Torso	Thigh	Shank
Dimensions	d_x [m]	0.1	0.14	0.15
	d_y [m]	0.25	0.1	0.1
	d_z [m]	0.385	0.1	0.1
Masses	12 kg-Model [kg]	7.355	1.161	1.161
	18 kg-Model [kg]	11.03	1.742	1.742

With the human structure in mind, each leg is chosen to dispose of 6 degrees of freedom (DoF), where 2 DoF are located in the ankle allowing for forward and lateral motion, 1 DoF is placed in the knee and the hips dispose of a full range of motility with 3 DoF. The robot furthermore possesses arms with 2 DoF in each shoulder intended for compensating leg momenta by swinging, thus providing lateral stability. The preliminary kinematic model thus has 16 DoF as shown in Fig. 3.1, the head is considered immobile for simplicity reasons.

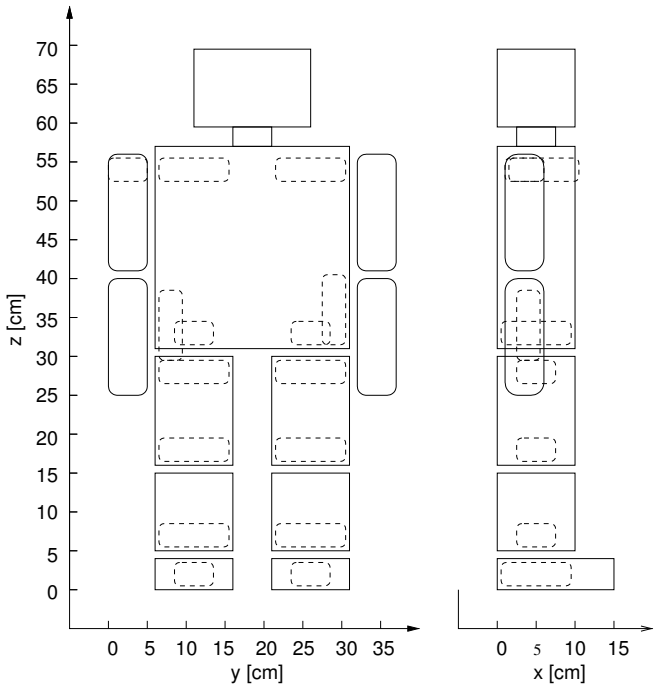

Figure 3.1: Preliminary model.

Two different weight classes are considered for the robot: a heavier 18 kg version and a lightweight 12 kg one. From rough approximations taking into account the location and weight of motors, link masses are assigned as listed in Tab. 3.1; the mass within each link is assumed to be uniformly distributed.

With these assumptions on the kinematic structure and parameters, a dynamical model is computed approximating the system dynamics of the designated humanoid prototype. This model is used for computing the actuator requirements.

3.3 Determining of Joint Torque Requirements

The demands on the joint torques when performing a target task are calculated by solving an optimal control problem. This process is similar to generating gait trajectories as described in App. B.

An optimal control problem is formulated, where a cost function assessing the "performance" of the gait is minimized subject to various constraints. These constraints ensure the physical feasibility of the step and contain information on initial and final positions and velocities.

For the motor selection process, the biped motion is optimized over one step, where the movement is constrained to the sagittal plane. Each leg instantaneously lifts off from the ground when the other collides with the ground representing the most efficient form of walking without feet [27]. The leg collision with the ground is modeled as perfectly inelastic, i. e. the leg tip velocity is instantaneously zero after collision.

With the goal of an autonomous, fast-moving biped, a performance measure is chosen that minimizes energy loss. It is known that the principal form of energy loss for these systems is Joule thermal loss [50]. As identical motors are sought for all joints for ease

Table 3.2: Numerical investigative modeling frameworks.

Experimental Model	Weight	Average Forward Speed
Model 1	12 kg	0.417 m/s (1.5 km/h)
Model 2	12 kg	0.555 m/s (2.0 km/h)
Model 3	18 kg	0.417 m/s (1.5 km/h)
Model 4	18 kg	0.555 m/s (2.0 km/h)

of maintenance and repair, this measure can be expressed as the integral of the squared applied generalized forces. An additional constraint is imposed on the maximum power consumption P_W for each motor. The optimal control problem

$$\min_{\boldsymbol{u}(t)} \left\{ \int_0^{t_f} \boldsymbol{u}(t)^T \boldsymbol{u}(t)\, \mathrm{d}t \right\} \quad \text{subject to} \quad \max_{t\in[0,t_f],i\in\{1,\dots,n\}} |\dot{q}_i(t) u_i(t)| \leq P_W \tag{3.1}$$

is formulated, where $\dot{q}_i$ is the joint i angle velocity and n the total number of links. The optimization (3.1) is also subject to the robot dynamics

$$\begin{aligned} \ddot{\boldsymbol{q}} &= \boldsymbol{M}(\boldsymbol{q})^{-1}\Big(\boldsymbol{B}\,\boldsymbol{u} - \boldsymbol{C}(\boldsymbol{q},\dot{\boldsymbol{q}}) - \boldsymbol{G}(\boldsymbol{q}) + \boldsymbol{J}_c(\boldsymbol{q})^T \boldsymbol{f}_c\Big) \\ \boldsymbol{0} &= \boldsymbol{g}_c(\boldsymbol{q}) \end{aligned} \tag{3.2}$$

where $\boldsymbol{M}$ is the positive-definite mass-inertia matrix, $\boldsymbol{C}$ is the Coriolis and centrifugal force vector, $\boldsymbol{G}$ the gravitational force vector, $\boldsymbol{q}$ the generalized coordinates, and $\boldsymbol{u}(t)$ are the control inputs mapped with the constant matrix $\boldsymbol{B}$ to the actively controlled joints. The constraint Jacobian $\boldsymbol{J}_c = \frac{\partial \boldsymbol{g}_c}{\partial \boldsymbol{q}}$ is obtained from the holonomic ground contact constraints $\boldsymbol{g}_c$, and $\boldsymbol{f}_c$ is the ground contact force.

The optimal control problem (3.1) is solved numerically using the method of direct collocation based on a parameterization of state and control variables using piecewise polynomials and its solution with sparse, large-scale sequential quadratic programming [29, 117].

Four different models, as shown in Table 3.2, are used to investigate the torque and power requirements for dynamic walking. In spite of the wide range of power, torque, and speed output characteristics present in commercial high performance motors, a significant void generally exists between motors with a 20–25 W maximum power output and those with a 70 W maximum power output, the latter having a much increased weight. For this reason, Models 1 and 2 are both optimized with a joint maximum power output of $P_W = 20\,\mathrm{W}$ as in (3.1). The problem is not solvable in this form for Models 3 and 4 most likely due to the fact that the forward velocity constraints could not be met with the increased weight and limited power availability. Thus, P_W is set higher for the heavier models: $P_W = 25\,\mathrm{W}$ for Model 3, $P_W = 40\,\mathrm{W}$ for Model 4.

An optimal control problem for one walking step is solved numerically for each model resulting in solution trajectories of joint velocities, accelerations, applied torques, and required power. The results for Models 2 and 4 are displayed in Tables 3.3 and 3.4. The power maxima indicated in these tables may be slightly above the upper bound due to polynomial approximations between calculated grid points. The most important conclusion that the data provides is that required power increases at a rate faster than linear with respect to the overall system weight. The larger motors with greater power outputs in turn

Table 3.3: Simulation results for Model 2 (0.555 m/s, 12 kg): Maximum torque = 187 Nm due to vertical contact force.

		Hip support leg	Knee support leg	Hip swing leg	Knee swing leg
Velocities	Aver. (rpm)	19.7	14.4	53.8	62.0
	Max. (rpm)	81.7	102	99.8	127
Accelerations	Max. (rad/s^2)	409	515	318	323
Torques	Aver. (Nm)	1.54	1.95	0.947	0.299
	Max. (Nm)	5.67	4.21	1.71	0.993
Power	Aver. (W)	3.50	3.51	5.80	2.13
	Max. (W)	15.4	23.1	13.9	6.02

Table 3.4: Simulation results for Model 4 (0.555 m/s, 18 kg): Max. torque = 269 Nm due to vertical contact force.

		Hip support leg	Knee support leg	Hip swing leg	Knee swing leg
Velocities	Aver. (rpm)	19.8	14.4	54.6	62.8
	Max. (rpm)	83.8	105	101	126
Accelerations	Max. (rad/s^2)	731	815	485	538
Torques	Aver. (Nm)	2.29	2.95	1.36	0.42
	Max. (Nm)	8.05	6.16	2.38	1.40
Power	Aver. (W)	5.32	5.60	8.47	3.07
	Max. (W)	27.3	41.9	20.2	9.05

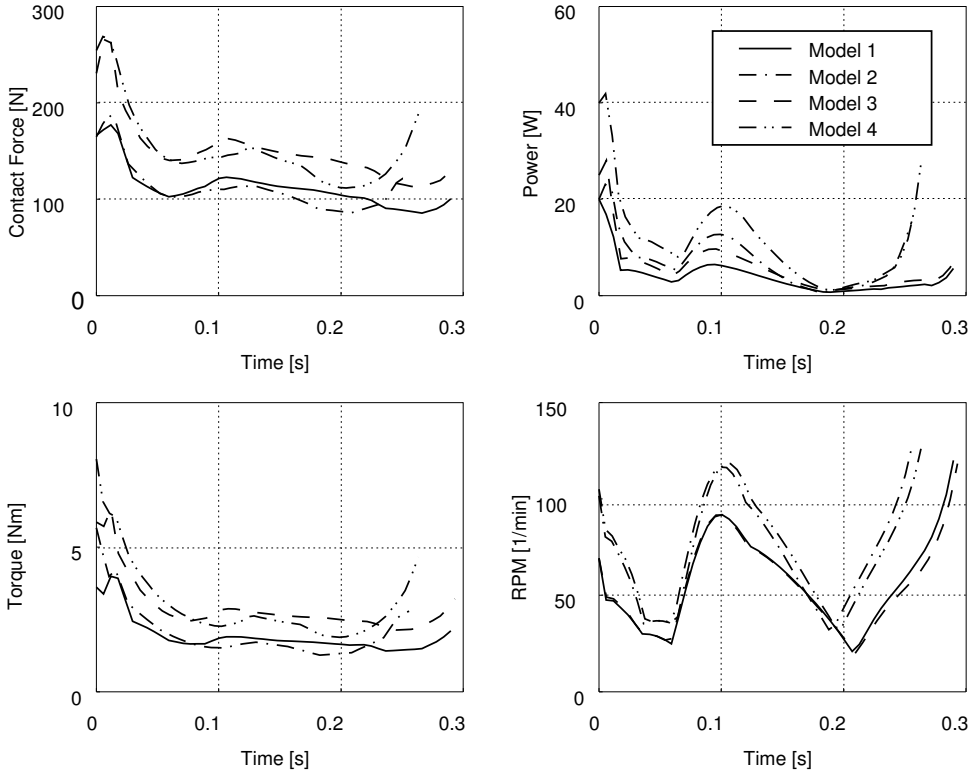

Figure 3.2: Simulation results for four models. The upper left plot shows the contact force between the support foot and the ground. The other characteristics have been taken from the knee joint, as it shows highest actuation requirements of all joints.

Table 3.5: Motor characteristics for the 12 and 18 kg models.

	12 kg model	18 kg model
Operational torque	1.5–2.5 Nm	2.5–3.5 Nm
Maximum torque	3.0 Nm	4.0 Nm
Operational RPM	50–75 rpm	65–90 rpm
Maximum RPM	90 rpm	100 rpm
Maximum Power	15 W	20 W

weigh much more so that system weight quickly spirals upward making the construction of a system capable of fast movements increasingly difficult. Thus, a strong effort is made to keep the total biped weight small.

Figures 3.2 and 3.3 display various trajectories for the four models. Spikes in the torque and speed trajectories are a consequence of the model and the high average forward velocity. These occur near the time of collision of the leg with the ground. A well-designed foot construction including damping elements should avoid these peaks; therefore, they are neglected in the motor selection process. A foot will permit the biped to make larger and fewer steps thus reducing the predicted high values for the joint velocities. The relationship between the maximum required motor torque and its turning speed is also shown in Fig. 3.3. The data of interest is summarized in Table 3.5 to be used for motor selection.

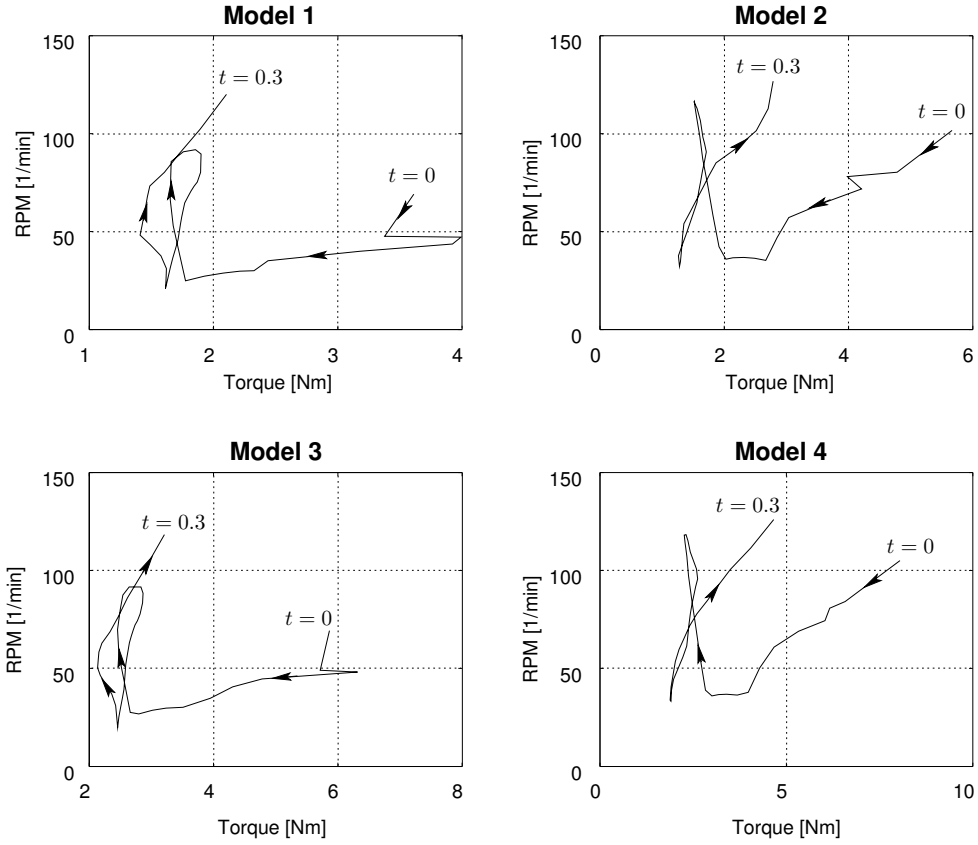

Figure 3.3: Torque-RPM-workspace of the knee joint from simulation data for four models.

3.4 Motor Selection

The actuator selection task is to find a drive train satisfying the desired characteristics in Table 3.5. This is done by selecting a number of candidate motor-gear-combinations and determining their torque-RPM-workspaces. These achievable workspaces are then mapped on the required workspaces shown in Fig. 3.3. If the required workspace is a subset of the achievable workspace, the motor-gear-combination is suitable for the examined task. From all suitable drive trains, the lightest is chosen to minimize the total weight of the robot.

The workspace of a motor-gear-combination is largely determined by its no-load speed and the stall torque. The stall torque

$$\tau_{\text{stall}} = \frac{\tau_{\text{motor}}}{N\,\eta} \tag{3.3}$$

of a motor-gear-combination is calculated from the chosen gear ratio N, the efficiency η of the gearbox and the motor stall torque τ_{motor}, while the no-load speed

$$n_r = n_o\,N \tag{3.4}$$

is obtained from the gear output speed n_o and gear ratio N.

Figures 3.4 and 3.5 show some motor workspaces mapped on the workspace of Models 2 and 4 respectively. The robot workspaces have been scaled by the gear ratio, i. e. the plotted robot workspaces show the requirements on the motor for a given gear ratio. This allows to investigate the applicability of motors with different voltage ratings $V_m \in \{30\,\text{V}, 42\,\text{V}, 48\,\text{V}\}$, as a lower system voltage reduces the number of required batteries.

In Fig. 3.5, the desired workspace is not covered as well by the motor characteristic lines as with the 12 kg robot. The heavier robot will not be able to be driven nearly as fast as the lighter one; a traveling speed of 0.417 m/s though is still achievable.

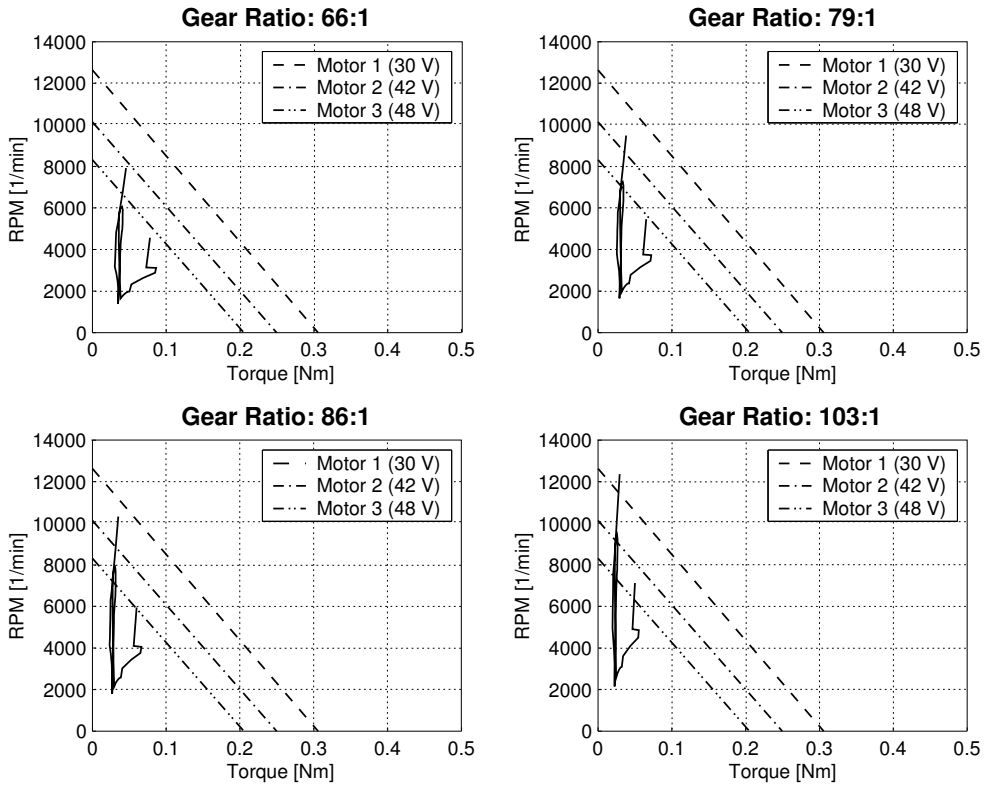

Figure 3.4: Model 2: Motor workspaces for three voltage ratings mapped onto robot workspace for different gear ratios.

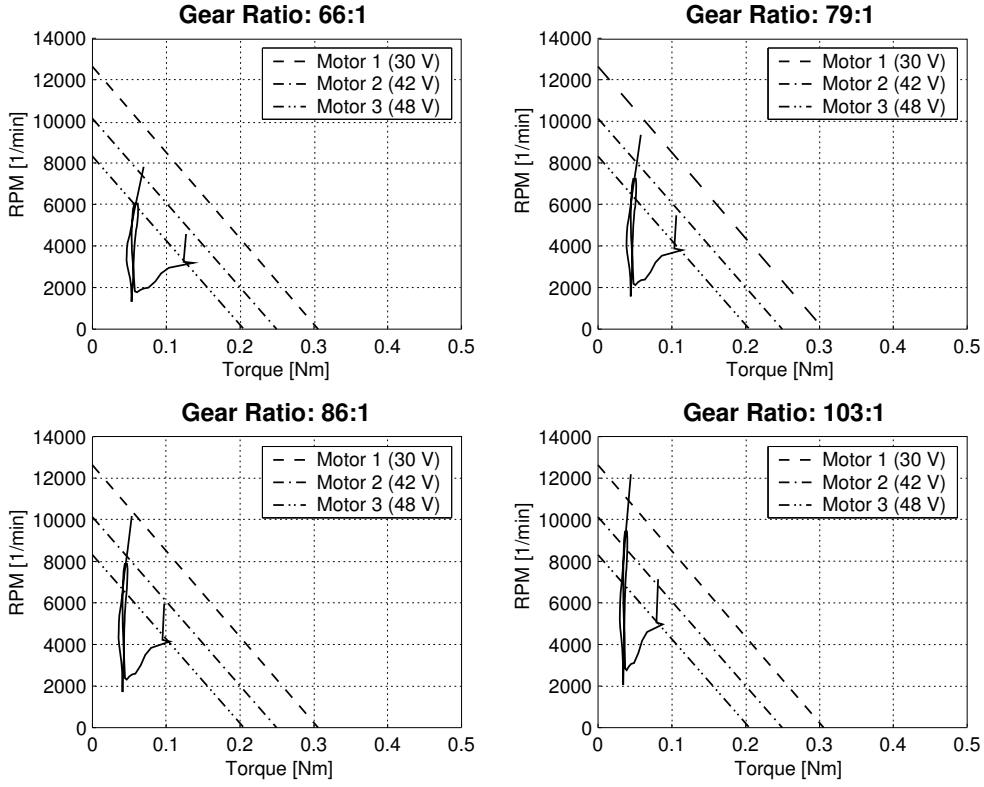

Figure 3.5: Model 4: Motor workspaces for three voltage ratings mapped onto robot workspace for different gear ratios.

3.5 Summary

As the weight-to-power ratio of a humanoid is decisive for its performance, joint actuators must be selected to closely match the requirements. On the one hand, the joint actuator must be capable to deliver the torque required to achieve a commanded acceleration and the desired maximum velocity. On the other hand, the actuator should be as lightweight as possible to keep the total weight of the robot low.

The strategy presented in this chapter, which has been developed in close cooperation with the "Simulation and Systems Optimization Group", Technische Universität Darmstadt, provides a methodic approach to this problem.

By solving an optimal control problem, motion trajectories for a given task are calculated, that minimize e. g. the energy consumption during the step. Contrary to most other gait generation methods, the optimization considers the entire step cycle rather than optimizing single snap shots. From these gait trajectories, the requirements on the actuators for maximum torque and velocity, i. e. the required workspace, are obtained. The reachable workspace of a motor-gear-combination is mapped onto the required workspace. The drive train is apt, if the required workspace is a subset of the reachable workspace. Thus a graphical criterion to decide on the suitability of the drive train for the desired task.

Formulating the actuator selection task as an optimal control problem is considered novel; although in this dissertation described for humanoid walking robots, the method can be equally applied to any type of robot. Application of this method in a practical design process of the humanoid prototype described in App. A proved the method useful and capable to harmonize with common engineering development methods.

4 Online Posture Correction

One way to achieve humanoid biped locomotion is to offline generate gait trajectories and to replay them on the robot. However, it is sometimes desirable to modify these trajectories in order to correct postural errors or to slightly adapt the motion if environmental constraints do not match the anticipated conditions.

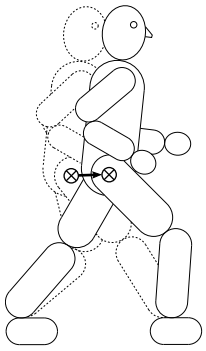

4.1 Problem Description

Current research to achieve biped locomotion can largely be classified into two different approaches: Gait trajectories are either computed online according to the actual intention and perception data of the robot [38, 47, 104, 134], or a large set of trajectories is computed offline [5, 14, 30, 128] and the robot selects the trajectory best fitting for the situation on hand [60].

While in situ generation of trajectories – at least potentially – enables the robot to react to any encountered situation, it is currently not possible to consider special "aesthetic" criteria [35] like smoothness and energy efficiency with this approach. Incorporating such constraints requires optimization of the complete gait cycle. However, such problems are not apt to realtime implementation, as convergence of the problem is sensitive to initial values which generally have to be tuned manually, solutions cannot be found within guaranteed time limits. Many research groups, hence, focus on offline generation of trajectories.

In recent work [14, 30, 128] it has been shown that such optimal control problems considering a variety of constraints such as dynamic stability, joint actuator torque limitations, contact force constraints at the feet and others can be solved to generate step and stride trajectories offline using advanced numerical optimal control algorithm.

One disadvantage of precalculated trajectories is that the robot is unable to accomplish motions for which trajectories are not available, thus a huge database of step primitives generally is necessary. In an effort to reduce the size of the required database and to increase the possible field of application of the robot it is therefore desirable to modify trajectories online such that they can be applied to slightly different situations than they have originally been computed for. One of the key challenges – which is the main focus in this chapter – is sensor-based online modification of computed trajectories to improve walking stability and performance.

Here, a novel *Jacobi Compensation* method is proposed that permits to move parts of the body in selected task coordinate directions and thus alters the posture of the robot.

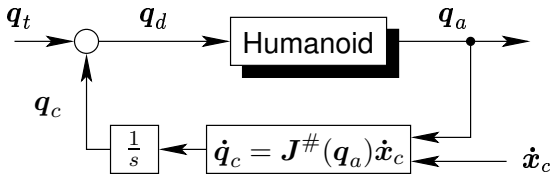

Figure 4.2: Jacobi Compensation. The precalculated trajectory $\boldsymbol{q}_t$ is modified by addition of an online and task-dependent calculated correction term $\boldsymbol{q}_c$. The necessary correction $\dot{\boldsymbol{x}}_c$ is determined in Cartesian space and transformed into joint space via the Jacobian.

Efforts to modify precalculated trajectories online followed by other research groups focus on ensuring gait stability by controlling the Zero Moment Point (ZMP) [36] or adapting existing trajectories for walking in the plane to ones that are suitable to walking on slopes [137]. The online use of Jacobians for posture control of biped robots is considered novel.

The chapter is structured as follows: The Jacobi Compensation method presented in Sec. 4.2 is illustrated more descriptively in simulations in Sec. 4.3. Sec. 4.4 gives an analysis of the stability properties, followed by Sec. 4.5 suggesting a more robust implementation. In Sec. 4.6, the method is applied to a hardware walking experiment with the humanoid robot, that is presented in App. A.

4.2 Online Compensation

When precalculated optimal control trajectories are replayed in practice by humanoid robots, the joint angles often differ from the intended ones. These deviations in the posture can result in violation of stability criteria or motion constraints and are caused by modeling errors, link flexibilities, gear loss, backlash, joint control errors and external disturbances inflicted on the robot by the environment. The result is a degraded walking performance. Commonly, a sensor-based control strategy is applied to cope with such errors.

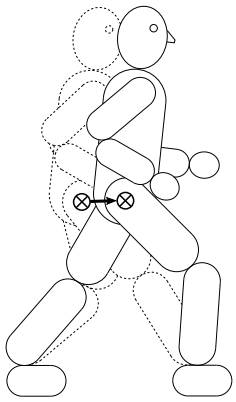

Figure 4.1: Moving selected points on the robot by Jacobi Compensation.

In this section a novel method termed *Jacobi Compensation* is proposed, which modifies precalculated trajectories by shifting dedicated point on the robot in task coordinate directions. Task coordinates are selected Cartesian directions of fixed points on the robot, e. g. the hip coordinate, the CoM and others, see Fig. 4.1. Appropriately applied, stability criteria deviation can be reduced thereby improving the walking performance.

The a priori selected task coordinates shall be moved by $\dot{\boldsymbol{x}}_c \in \mathbb{R}^m$ in Cartesian space. The vector $\dot{\boldsymbol{x}}_c$ has one entry for each direction of each point that can be modified, hence the dimension m is the influenceable degree of freedom. The commanded joint angles $\boldsymbol{q}_t$, obtained from a precalculated trajectory, are modified by adding $\boldsymbol{q}_c = \boldsymbol{f}(\dot{\boldsymbol{x}}_c)$, where $\boldsymbol{f}(\cdot)$ transforms the Cartesian motion $\dot{\boldsymbol{x}}_c$ into a joint space motion $\boldsymbol{q}_c \in \mathbb{R}^n$, n is the number of joints of the robot. As shown in Fig. 4.2, this correction $\boldsymbol{q}_c$ is linearly superimposed with the joint configuration $\boldsymbol{q}_t$ resulting in a new desired posture $\boldsymbol{q}_d = \boldsymbol{q}_t + \boldsymbol{q}_c$ of the robot.

The relation $\boldsymbol{f}(\cdot)$ between Cartesian task coordinate motion and joint space motion is described by the Jacobian

$$\boldsymbol{J}(\boldsymbol{q_a}) = \left[\frac{\partial \boldsymbol{x_c}}{\partial q_1} \quad \cdots \quad \frac{\partial \boldsymbol{x_c}}{\partial q_n}\right]\Big|_{\boldsymbol{q}=\boldsymbol{q}_a} \in \mathbb{R}^{m\times n}, \tag{4.1}$$

a function of the actual joint angles $\boldsymbol{q}_a \in \mathbb{R}^n$, which maps the velocity $\dot{\boldsymbol{q}}_c$ in joint space to the velocity $\dot{\boldsymbol{x}}_c$ in Cartesian space according to

$$\dot{\boldsymbol{x}}_c = \boldsymbol{J}(\boldsymbol{q_a})\,\dot{\boldsymbol{q}}_c. \tag{4.2}$$

The inverse mapping of (4.2) is not unique as the system generally is redundant. Therefore the pseudoinverse

$$\boldsymbol{J}^{\#}(\boldsymbol{q}_a) := \boldsymbol{J}^T(\boldsymbol{J}\boldsymbol{J}^T)^{-1} \tag{4.3}$$

is used, which solves the ambiguity by minimizing the Euclidean norm $||\dot{\boldsymbol{q}}_c||_2$; here, $m \leq n$ and $\mathrm{rk}\,(\boldsymbol{J}(\boldsymbol{q}_a)) = m$ is assumed for existence of a solution, i. e. the motion is modified along less or equal task coordinates $\boldsymbol{x}_c$ than degrees-of-freedom n of the system. The correction velocity thus computes to

$$\dot{\boldsymbol{q}}_c = \boldsymbol{J}^{\#}(\boldsymbol{q_a})\,\dot{\boldsymbol{x}}_c\ , \tag{4.4}$$

which is integrated to obtain the position modification $\boldsymbol{q}_c$ in joint space. Superimposing it with the precalculated trajectory $\boldsymbol{q}_t$ as shown in Fig. 4.2 adapts the trajectory to the actual requirements.

Applications of this method are plentiful: In the hardware experiments in Sec. 4.6 the Jacobi Compensation is used to alter the posture of the robot and thus modify precalculated trajectories to improve walking stability and performance. Other applications include the possibility to adapt precalculated gait trajectories to fit for walking on slopes by shifting the center of mass uphill, i. e. in the direction of the negative gradient of the slope; this involves not only walking straight uphill, but also across the slope.

In the following, the Jacobi Compensation is illustrated more descriptively with the help of simulation results.

4.3 Simulation Results

The Jacobi Compensation described in Sec. 4.2 is now demonstrated in a simulation experiment using a mechanically simple, but illustrative example of a planar 4 DoF Scara robot depicted in Fig. 4.3. Stressing its kinematic similarity with a planar walker and with the desired target platform in mind, the ends of the Scara will be referred to as the "feet" and the middle joint is termed "hip".

The properties of the Jacobi Compensation are illustrated by simulating the tasks "move swing foot outwards" and "move hip over the supporting area". These tasks are also relevant in hardware experiments, as they correspond to avoiding collision of the feet and keeping the robot balanced to elude tilting.

The dynamics of the Scara robot are described by a differential equation

$$\boldsymbol{M}(\boldsymbol{q})\ddot{\boldsymbol{q}} + \boldsymbol{B}(\boldsymbol{q},\dot{\boldsymbol{q}})\dot{\boldsymbol{q}} + \boldsymbol{k}(\boldsymbol{q}) = \boldsymbol{\tau}, \tag{4.5}$$

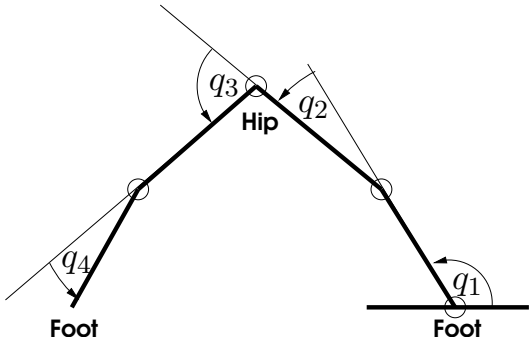

Figure 4.3: Scara with 4 DoF – Initial Configuration for Simulation.

where $\boldsymbol{M}$ is the mass matrix, $\boldsymbol{B}$ the matrix for Coriolis and centrifugal forces and $\boldsymbol{k}$ the vector of gravitational forces. The motor torques $\boldsymbol{\tau}$ are obtained from a PD position control loop

$$\boldsymbol{\tau} = \boldsymbol{K}_P(\boldsymbol{q}_d - \boldsymbol{q}) + \boldsymbol{K}_D(\dot{\boldsymbol{q}}_{\boldsymbol{d}} - \dot{\boldsymbol{q}}), \tag{4.6}$$

where the proportional gain $\boldsymbol{K}_P$ and the derivative gain $\boldsymbol{K}_D$ are matrices in diagonal form, and each element is positive. This choice of gains represents independant PD controllers for each joint. The joint angle $\boldsymbol{q}_d(t)$ is the desired trajectory in joint space. For the simulation all link masses and the link lengths are equally set to "1". Friction is neglected.

Jacobi Compensation is now used to move the swing foot outwards, to a new desired foot position $\boldsymbol{x}_{d,\text{foot}}$, while a constant reference trajectory $\boldsymbol{q}_t$ is assumed.

The input velocity $\dot{\boldsymbol{x}}_c$ of the Jacobi Compensation shown in Fig. 4.2 is computed from the actual Cartesian foot position $\boldsymbol{x}_{a,\text{foot}}$ and the desired position $\boldsymbol{x}_{d,\text{foot}}$ as

$$\dot{\boldsymbol{x}}_c = \boldsymbol{\Gamma}_P\,(\boldsymbol{x}_{a,\text{foot}} - \boldsymbol{x}_{d,\text{foot}}) + \boldsymbol{\Gamma}_D \frac{\mathrm{d}}{\mathrm{d}t}(\boldsymbol{x}_{a,\text{foot}} - \boldsymbol{x}_{d,\text{foot}}), \tag{4.7}$$

where $\boldsymbol{\Gamma}_P$ and $\boldsymbol{\Gamma}_D$ again are constant diagonal matices with positive entries.

In this example the Jacobian evaluates to

$$\boldsymbol{J}_{\text{foot}} = \begin{bmatrix} \frac{\partial \boldsymbol{x}_{c,\text{foot}}}{\partial q_1} & \dots & \frac{\partial \boldsymbol{x}_{c,\text{foot}}}{\partial q_4} \end{bmatrix} \quad \in \mathbb{R}^{2\times 4}. \tag{4.8}$$

Applying the method described in Sec. 4.2 yields the simulation result – concerning initial and calculated final posture – presented in Fig. 4.4(a). The performance of the method for "outward movement of the foot" is satisfying, i. e. settling is fast and stable and the desired position is reached as can be seen in Fig. 4.4(b).

The next task to be investigated is moving the hip over the supporting area. In analogy to the previous simulation a Jacobian

$$\boldsymbol{J}_{\text{hip}} = \begin{bmatrix} \frac{\partial \boldsymbol{x}_{c,\text{hip}}}{\partial q_1} & \dots & \frac{\partial \boldsymbol{x}_{c,\text{hip}}}{\partial q_4} \end{bmatrix} \quad \in \mathbb{R}^{2\times 4} \tag{4.9}$$

is set up and the hip is commanded to move to the right; the result is shown in Fig. 4.4(a) as a dash-dotted plot.

Although the hip joint performs the desired motion, the entailed displacement of the left foot is unintended in practical biped application. One possible solution for fixing the foot in Cartesian position is using the concatenated Jacobian

$$\boldsymbol{J}_{\text{foot,hip}} = \begin{bmatrix} \frac{\partial \boldsymbol{x}_{c,\text{foot}}}{\partial q_1} & \dots & \frac{\partial \boldsymbol{x}_{c,\text{foot}}}{\partial q_4} \\ \frac{\partial \boldsymbol{x}_{c,\text{hip}}}{\partial q_1} & \dots & \frac{\partial \boldsymbol{x}_{c,\text{hip}}}{\partial q_4} \end{bmatrix} \quad \in \mathbb{R}^{4\times 4}, \tag{4.10}$$

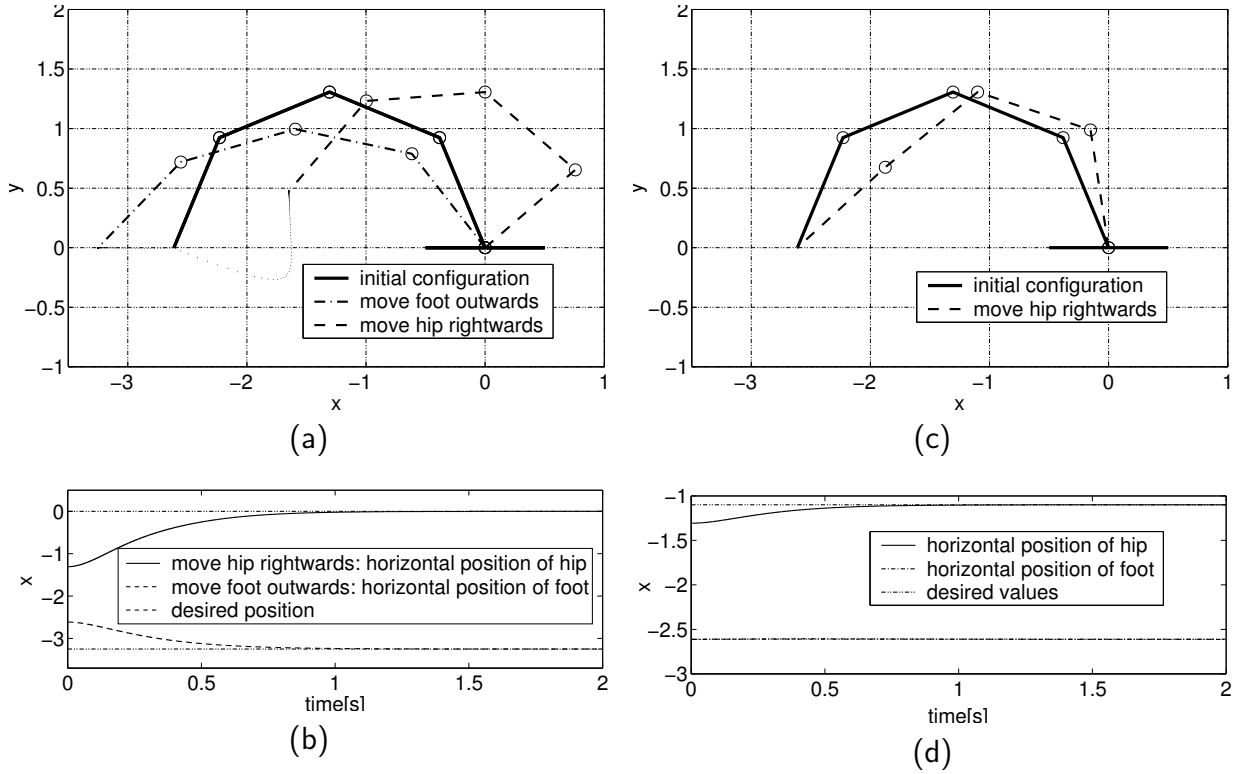

Figure 4.4: Jacobi Compensation simulations. (a) Initial and final configuration for "move foot outwards" and for "move hip rightwards". (b) Associated hip/foot trajectories over time. (c) Initial and final configuration for "move hip but keep in rest foot". (d) Associated hip/foot trajectories over time.

hence both points of the robot can be moved independently within kinematic limits. Using $\boldsymbol{J}_{\text{foot,hip}}$ and commanding a hip motion while the foot velocity is commanded zero yields the desired behavior. Note, that $\boldsymbol{J}_{\text{foot,hip}}$ being are square matrix is uniquely invertible, and the pseudoinverse $\boldsymbol{J}^{\#}_{\text{foot,hip}}$ can be replaced by an ordinary inverse $\boldsymbol{J}^{-1}_{\text{foot,hip}}$.

However, there is a geometrical conflict between the two goals hip movement over supporting area and foot in rest, i. e. it is never possible to reach both goals at the same time. This geometric conflict is reflected in a loss of rank of the Jacobian. To avoid singularity of $\boldsymbol{J}_{\text{foot,hip}}$ care has to be taken in choosing the desired Cartesian positions of hip and foot, involving kinematic considerations. The result of simulation is depicted in Fig. 4.4(c) and (d): the desired motion of the hip in Cartesian x-direction has to be reduced with respect to the experiment using $\boldsymbol{J}_{\text{hip}}$, allowing the left foot to remain at a constant position.

With this understanding of Jacobi Compensation its stability properties are now investigated.

4.4 Stability Analysis

In this section, the stability of a Jacobi-compensated system is investigated [126]. For a first analysis, Sec. 4.4.1 gives a qualitative examination of the system dynamics to understand their properties. The stability of the system is then proved based on Lyapunov's theorem in Sec. 4.4.2.

4.4.1 Qualitative Analysis of System Dynamics

The analysis discussed in this section is based on the data of the humanoid robot presented in App. A and [30, 128]. The considered cascaded control architecture shown in Fig. 4.5 consists of a joint-level PD position control and the overlaid Jacobi Compensation.

As can be seen, the Jacobi Compensation closes a feedback loop with the pseudoinverse Jacobian $\boldsymbol{J}^{\#}(\boldsymbol{q}_a(t))$ being a nonlinear function of the actual joint configuration $\boldsymbol{q}_a(t)$. In the following, perfect trajectory following will be assumed and $\boldsymbol{q}_a(t)$ is replaced by $\boldsymbol{q}_t(t)$; thus, $\boldsymbol{J}^{\#}(\boldsymbol{q}_t(t))$ will be evaluated along a given trajectory $\boldsymbol{q}_t(t)$.

The trajectory $\boldsymbol{q}_t(t)$ consists of a single step that lasts 6 s. During the initial double support phase, taking 3 s, the robot shifts its center of mass over the supporting foot. In the following single support phase, the robot moves the swing foot forward and ends in a configuration symmetric to the original one.

Various measures are introduced that help to understand the evolution of the Jacobian properties. Without loss of generality $\boldsymbol{J}^{\#}(\boldsymbol{q}_t(t)) \in \mathbb{R}^{n\times m}$, $n > m$, is assumed to have full rank m – otherwise the robot is in a singular configuration which has to be avoided.

Singular Value Decomposition

For understanding the system dynamics, the Singular Value Decomposition (SVD)

$$\boldsymbol{J}^{\#}(\boldsymbol{q}_t(t)) = \boldsymbol{U}(t)\boldsymbol{\Sigma}(t)\boldsymbol{V}^T(t) \tag{4.11}$$

of the pseudoinverse Jacobian $\boldsymbol{J}^{\#}$ is investigated. As $\boldsymbol{J}^{\#} \in \mathbb{R}^{n\times m}$, is a non-square matrix, and $\boldsymbol{\Sigma}$ is required to have the same size as $\boldsymbol{J}^{\#}$, the matrix $\boldsymbol{\Sigma} = \begin{bmatrix}\text{diag}(\sigma_i) & \boldsymbol{0}\end{bmatrix}^T$ contains the singular values σ_i sorted in diagonal form ($\mathbb{R}^{m\times m}$) in decreasing order and is supplemented by a zero-matrix $\boldsymbol{0} \in \mathbb{R}^{(n-m)\times m}$. The matrices $\boldsymbol{U} \in \mathbb{R}^{n\times n}$ and $\boldsymbol{V} \in \mathbb{R}^{m\times m}$ are composed of orthonormal bases.

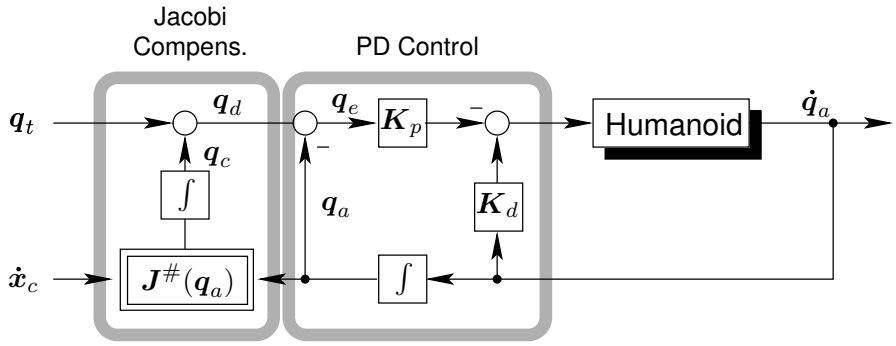

Figure 4.5: Control scheme.

Writing (4.11) elementwise as

$$\boldsymbol{J}^{\#}\boldsymbol{v}_i = \sigma_i \boldsymbol{u}_i, \tag{4.12}$$

where $\boldsymbol{v}_i$ and $\boldsymbol{u}_i$ represent the i-th column vector of $\boldsymbol{V}$ and $\boldsymbol{U}$ respectively, suggests that the singular value σ_i can be interpreted as the gain of the Jacobian in coordinate direction $\boldsymbol{u}_i$ [75]. As the σ_i vary with the actual working point, the Jacobian can be badly conditioned for certain joint configurations, i. e. have rather different gains in different directions of motion. That means that small changes on the correction term $\dot{\boldsymbol{x}}_c$ in some directions lead to large motions in joint space while other directions have little effect.

Apart from the singular values $\boldsymbol{\Sigma}$ also the principal transformation axes $\boldsymbol{U}$ rotate depending on $\boldsymbol{q}_t$. Therefore the Jacobi output $\dot{\boldsymbol{q}}_c$ can vary even with a constant correction term $\dot{\boldsymbol{x}}_c$ as the joint configuration follows a trajectory.

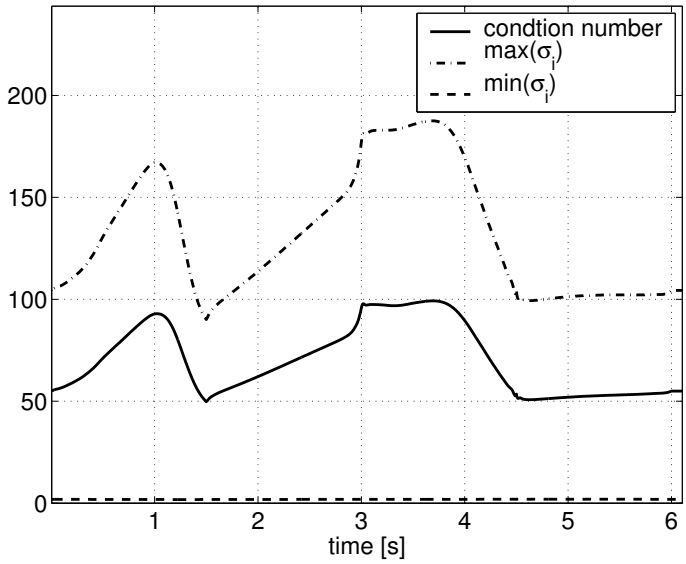

Figure 4.6: Minimum and maximum singular value and the corresponding condition number along the trajectory.

This is illustrated in Fig. 4.6, where the minimum singular value σ_m and maximum singular value σ_1 of $\boldsymbol{J}^{\#}(\boldsymbol{q}_t(t))$ along a given walking trajectory $\boldsymbol{q}_t(t)$ are shown.

Condition number

Furthermore the condition number (see [86])

$$\kappa = \frac{\max_i(\sigma_i)}{\min_i(\sigma_i)} = \frac{\sigma_1}{\sigma_m} \tag{4.13}$$

of $\boldsymbol{J}^{\#}$ at each time step is shown. This condition number κ is commonly used to rate the dexterity in a workspace and should be $\kappa = 1$ for a workspace with equal manipulability in all directions.

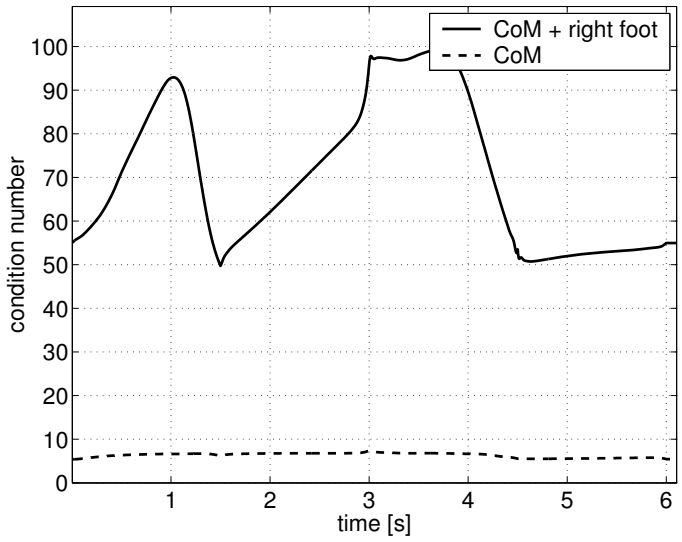

Figure 4.7: Condition numbers for Jacobians modifying the CoM and both, CoM and position of the right foot.

With growing size of the Jacobian, more degrees of freedom of the robot are bound by the correction motion and the imposed constraints. Therefore the conditioning of the Jacobian generally becomes worse for larger matrices. Fig. 4.7 shows the condition number for the Jacobian $\boldsymbol{J}_{\mathrm{CoM}} \in \mathbb{R}^{12\times 3}$ adjusting the attitude of the center of mass (CoM) (dashed line) and that of another Jacobian $\boldsymbol{J}_{\mathrm{CoM,foot}} \in \mathbb{R}^{12\times 6}$ manipulating both, the CoM and the position of the swing foot (solid line).

Time Evolution of Jacobian

In order to obtain a measure for the changes in the Jacobians at two consecutive sample times, $\boldsymbol{J}^{\#}$ has been computed along the trajectory $\boldsymbol{q}_t(t)$ at the constant sample time $T = 4\,\mathrm{ms}$. The changes of the Jacobians at time $t = t^*$ with respect to the previous sample $t = t^* - T$ are expressed in the difference matrix

$$\Delta\boldsymbol{J}(t^*) = \boldsymbol{J}^{\#}(\boldsymbol{q}_t(t^*)) - \boldsymbol{J}^{\#}(\boldsymbol{q}_t(t^* - T)).$$

Hence, difference measure

$$\Delta(t^*) = \sum_{i=1}^{m}\sum_{j=1}^{n} |\Delta J_{i,j}(t^*)| \tag{4.14}$$

being the sum of the absolute value of all elements of the difference matrix between two sample times quantifies the difference between two consecutive Jacobians. Fig. 4.8 shows the evolution of Δ along the trajectory $\boldsymbol{q}_t(t)$. Comparing this plot with the condition number of the CoM-Jacobian in Fig. 4.7 confirms the fact, that a badly conditioned Jacobian $\boldsymbol{J}^{\#}$ yields high velocities in joint space.

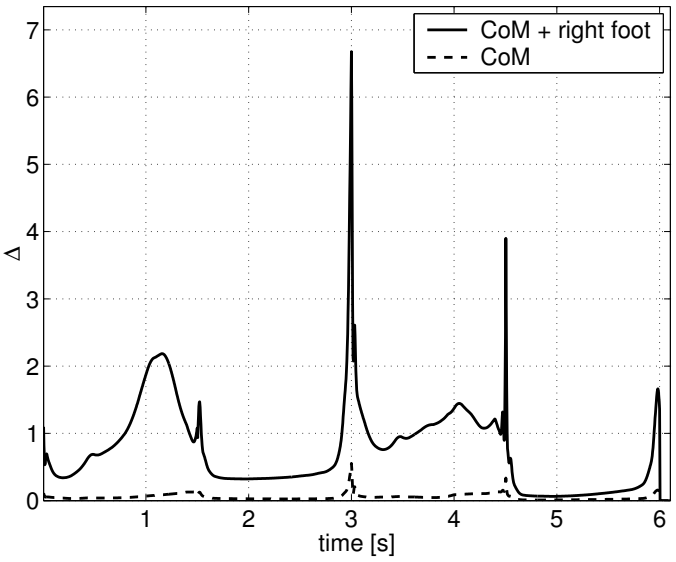

Figure 4.8: Evolution of the difference measure Δ defined in (4.14).

Therefore investigations on the stability of Jacobi compensation are of interest.

4.4.2 Lyapunov Stability of Jacobi Compensation

The dynamic behavior of the humanoid robot follows the differential equation

$$\boldsymbol{M}(\boldsymbol{q})\ddot{\boldsymbol{q}} + \boldsymbol{B}(\boldsymbol{q}, \dot{\boldsymbol{q}})\dot{\boldsymbol{q}} + \boldsymbol{k}(\boldsymbol{q}) = \boldsymbol{\tau}, \tag{4.15}$$

where $\boldsymbol{\tau}$ is the torque applied to the robot.

This stability analysis is based on Lyapunov's theorem:

Definition 4.6: *Lyapunov stability [87].*

A system is (locally) stable, if a (locally) positive definite function (Lyapunov function) $V(\boldsymbol{x}, t)$ can be found with the following properties:

- $V(\boldsymbol{0}, t) = 0$ and $V(\boldsymbol{x}, t) > 0 \; \forall t > 0$
- $\dot{V}(\boldsymbol{x}, t) < 0, \; \forall t > 0$

■

As suggested in [93], a candidate Lyapunov function

$$V = \frac{1}{2}\dot{\boldsymbol{q}}_e^T \boldsymbol{M}\dot{\boldsymbol{q}}_e + \frac{1}{2}\boldsymbol{q}_e^T \boldsymbol{K}_p \boldsymbol{q}_e \tag{4.16}$$

is chosen, with the control error

$$\begin{aligned}\boldsymbol{q}_e &= \boldsymbol{q}_t - \boldsymbol{q}_a + \int \boldsymbol{J}^{\#}\dot{\boldsymbol{x}}_c \,\mathrm{d}t \\ &= \boldsymbol{q}_t - \boldsymbol{q}_a + \boldsymbol{q}_c.\end{aligned}$$

As the matrix $\boldsymbol{M}$ and the proportional gain $\boldsymbol{K}_p$ of the control law shown in Fig. 4.5 are positive definite, (4.16) is a valid candidate Lyapunov function where the first term represents the kinetic energy and the second term is a generalized potential energy stored in the system.

The time derivative

$$\dot{V} = \frac{1}{2}\frac{\mathrm{d}}{\mathrm{d}t}\dot{\boldsymbol{q}}_e^T \boldsymbol{M}\dot{\boldsymbol{q}}_e + \dot{\boldsymbol{q}}_e^T \boldsymbol{K}_p \boldsymbol{q}_e \tag{4.17}$$

of the Lyapunov function contains in its first term the rate of change of kinetic energy which – according to mechanics – is equal to the power provided by external forces. Hence (4.17) can be written as

$$\dot{V} = \dot{\boldsymbol{q}}_e^T(\boldsymbol{\tau} - \boldsymbol{g}) + \dot{\boldsymbol{q}}_e^T \boldsymbol{K}_P \boldsymbol{q}_e, \tag{4.18}$$

$\boldsymbol{g}$ is the acceleration of gravity. The torque $\boldsymbol{\tau}$ is obtained from the control law

$$\boldsymbol{\tau} = -\boldsymbol{K}_p \boldsymbol{q}_e + \boldsymbol{K}_d \dot{\boldsymbol{q}}_a + \boldsymbol{g}. \tag{4.19}$$

Inserting (4.19) into (4.18) yields

$$\begin{aligned}\dot{V} &= \dot{\boldsymbol{q}}_e^T \boldsymbol{K}_d \dot{\boldsymbol{q}}_a \\ &= (\dot{\boldsymbol{q}}_t - \dot{\boldsymbol{q}}_a + \dot{\boldsymbol{q}}_c)^T \boldsymbol{K}_d \dot{\boldsymbol{q}}_a,\end{aligned} \tag{4.20}$$

which can can be interpreted as the energy dissipated by the damping gain $\boldsymbol{K}_d$ in the control law.

As Lyapunov's theorem requires the time derivative $\dot{V}$ of the Lyapunov function to be negative, the Jacobi Compensation is stable, if the dissipated energy is larger than the energy generated by the motion, thus

$$(\dot{\boldsymbol{q}}_t + \dot{\boldsymbol{q}}_c)^T \boldsymbol{K}_d \dot{\boldsymbol{q}}_a < \dot{\boldsymbol{q}}_a^T \boldsymbol{K}_d \dot{\boldsymbol{q}}_a \tag{4.21}$$

must hold.

A rough approximation is obtained by writing (4.21) element wise and requiring the inequality to hold for each element.

As $\boldsymbol{K}_p$ and $\boldsymbol{K}_d$ are the parameters of a PD control loop these matrices are often chosen in diagonal form thus describing separate PD controllers for each robot joint without coupling. With this assumption it is possible to write (4.21) element wise, where q_{ti}, q_{ci}, q_{ai} signify the i-th element of the vector $\boldsymbol{q}_t$, $\boldsymbol{q}_c$, $\boldsymbol{q}_a$ and k_{pi} and k_{di} represent the i-th diagonal element of $\boldsymbol{K}_p$ or $\boldsymbol{K}_d$ resp., i. e. the element in the i-th row and the i-th column. Hence, asking the inequality (4.21) to hold for each element separately

$$\begin{cases} \dot{q}_{ci} < \dot{q}_{ai} - \dot{q}_{ti} & \forall \dot{q}_{ai} > 0 \\ \dot{q}_{ci} > \dot{q}_{ai} - \dot{q}_{ti} & \forall \dot{q}_{ai} < 0. \end{cases} \tag{4.22}$$

gives a rough approximation representing a boundary for the velocity $\dot{\boldsymbol{q}}_c$ of the Jacobi compensation. Thus the control loop remains stable, if the posture of the robot is altered sufficiently slowly[1].

This result is in accordance with experimental experiences [94], where Jacobi Control generally showed stable behavior for smooth posture modifications with few constraints. For large Jacobians incorporating many constraints, the pseudoinverse may become badly conditioned, resulting in high joint velocities $\dot{\boldsymbol{q}}_c$. Hence large Jacobians often destabilize the system in certain joint configurations.

A solution to handle this problem of singularities is suggested in the following.

4.5 Singularity-Robust Inverse

When computing (4.4), the Moore-Penrose pseudoinverse

$$\boldsymbol{J}^{\#} = \boldsymbol{J}^T(\boldsymbol{J}\boldsymbol{J}^T)^{-1} \tag{4.23}$$

offers a least-squares solution for $\dot{\boldsymbol{q}}_c$ that fulfills

$$\min_{\dot{\boldsymbol{q}}_c} \|\dot{\boldsymbol{x}}_c - \boldsymbol{J}\dot{\boldsymbol{q}}_c\|_2. \tag{4.24}$$

As this solution generally is not unique, $\dot{\boldsymbol{q}}_c$ is chosen such that

$$\min_{\dot{\boldsymbol{q}}_c} \|\dot{\boldsymbol{q}}_c\|_2 \tag{4.25}$$

is satisfied, see [75]. The pseudoinverse hence solves a cascaded optimization problem minimizing the error rather than considering the feasibility of the motion. This results in badly conditioned pseudoinverses and thus high velocities as observed in Figs. 4.7 and 4.8.

To overcome this deficiency, Nakamura [75] proposed to minimize both properties simultaneously by solving

$$\min \left\| \begin{pmatrix} \dot{\boldsymbol{x}}_c - \boldsymbol{J}\dot{\boldsymbol{q}}_c \\ \dot{\boldsymbol{q}}_c \end{pmatrix} \right\|_{\boldsymbol{W}}, \tag{4.26}$$

where $\boldsymbol{W}$ is a weighting matrix of the norm $\|\boldsymbol{x}\|_{\boldsymbol{W}} = \sqrt{\boldsymbol{x}^T\boldsymbol{W}\boldsymbol{x}}$. Minimizing the error and the velocity simultaneously avoids velocity peeks as found by the hierarchical optimization structure of the pseudoinverse solution. Choosing $\boldsymbol{W}$ as the identity matrix $\boldsymbol{I}$, the solution for (4.26) is found by the *Singularity Robust (SR-) Inverse*

$$\boldsymbol{J}^*(\boldsymbol{q}_a) = \boldsymbol{J}^T(\boldsymbol{J}\boldsymbol{J}^T + k\boldsymbol{I})^{-1}, \tag{4.27}$$

see [75] for a detailed derivation. The scalar k is a weighting factor that influences the trade-off between exactness and feasibility of a motion. For $k \to 0$ the SR-Inverse $\boldsymbol{J}^*$ becomes identical to the pseudoinverse $\boldsymbol{J}^{\#}$, while larger k increase the weight of the velocity in the optimization (4.26) and hence produce inverses that are less sensitive to singularities at the cost of a larger error $||\dot{\boldsymbol{x}}_c - \boldsymbol{J}\dot{\boldsymbol{q}}_c||$.

Fig. 4.9 shows the influence of the weighting factor k on the condition number of the SR-Inverse along the same trajectory as in the previous experiments: for larger k the negative influence of singularities on the conditioning of the matrix is efficiently reduced.

[1] Unfortunately it is not possible to conclude from this result about general stability of Jacobi Compensation if condition (4.20) is not met, as Lyapunov's theorem cannot make negative statements on stability.

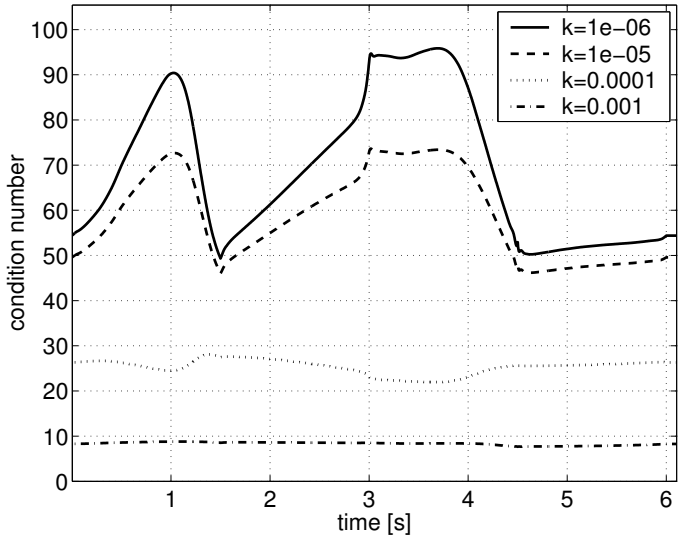

Figure 4.9: Condition numbers of SR-Inverses for different weighting factors k.

On the other hand increasing k also leads to a larger deviation of the actual motion $\hat{\dot{\boldsymbol{q}}}_c = \boldsymbol{J}^*(\boldsymbol{q}_a)\,\dot{\boldsymbol{x}}_c$ of the endeffector from the desired motion $\dot{\boldsymbol{q}}_c = \boldsymbol{J}^{\#}(\boldsymbol{q}_a)\,\dot{\boldsymbol{x}}_c$. To ensure small deviation of $\hat{\dot{\boldsymbol{q}}}_c$ from the desired path $\dot{\boldsymbol{q}}_c$, $\boldsymbol{J}\boldsymbol{J}^* \approx \boldsymbol{I}$ should hold. This property is evaluated in the error measure

$$\Gamma = \sum_{i=1}^{m}\sum_{j=1}^{m} |(\boldsymbol{J}\boldsymbol{J}^* - \boldsymbol{I})_{i,j}|, \tag{4.28}$$

which is the sum of all absolute values of the matrix $\boldsymbol{J}\boldsymbol{J}^* - \boldsymbol{I} \in \mathbb{R}^{m\times m}$. This error measure Γ should be small to ensure low divergence from the desired motion. The evolution of Γ for various k along the trajectory is shown in Fig. 4.10. Comparing Fig. 4.9 and Fig. 4.10 shows that by selecting the weighting factor k a tradeoff between accuracy and stability of the control loop is being made; these experiments suggest $k = 0.0001$ to be a reasonable tradeoff. Furthermore, the weighting factor k can be dynamically adapted as shown in [75].

The method of Jacobi Compensation is now investigated in hardware experiments.

4.6 Experimental Results

In the following, results of two experiments are described: In the first experiment, the trajectories generated according to [6] and App. A as solutions of optimal control problems are applied to the humanoid without modification as reference trajectories to local joint PD position controllers. The resulting walking performance is sometimes not stable due to modeling errors, gear backlash and other effects. To improve gait stability precalculated trajectories were modified manually by teaching in of Jacobi Compensation coordinates in a second experiment.

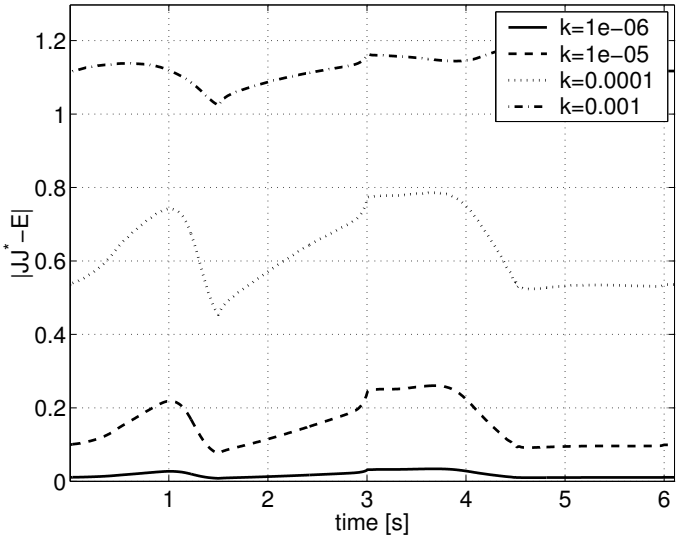

Figure 4.10: Error measure Γ defined in (4.28) along the gait trajectory.

4.6.1 Trajectory Following Using Precalculated Trajectories

Precalculated trajectories are applied to the humanoid as reference trajectories to joint level PD position controllers. Fig. 4.11 shows the measured data of the left knee. Since the knee joint supports a significant part of the robot total weight, the load in the other joints are similar or less than the knee load.

From Fig. 4.11(a) one can see, that the error of the commanded joint trajectory (dashed) and the measured position (solid) is quite small and does not exceed 0.025 rad for a complete stride. This validates the performance of the PD joint position control with a sampling rate of 250 Hz. The corresponding motor current (solid) and pulse-width-modulation (PWM) ratio (dashed) are shown in Fig. 4.11(b). This plot similarly displays that the knee joint of the robot operates well below its limits with currents of 3 A (below the maximum H-bridge amplifier current of 4 A) and the PWM ratio always less than 50%.

Despite small errors in trajectory following in joint space, the robot gait is slightly tottering, i. e. the center of mass is not shifted sufficiently far over the supporting foot. Hence, the robot tilts towards the swing foot which draggles on the ground. One cause may be attributed to unmodeled backlash in the gears and other effects such as link flexibilities. In an attempt to alleviate the errors in the torso posture, a teach-in Jacobi Compensation (cf. Sec. 4.2) phase is introduced as follows.

4.6.2 Teach-in Compensation

In experiments with precalculated trajectories it turned out that the CoM is not shifted sufficiently far over the supporting leg due to modeling errors. Together with consequences of the unmodeled dynamics, this results in tilting of the robot towards the swing leg as soon as the swing leg lifts off the ground. To improve stability, a teach-in phase has been set up where the robot reproduces the precalculated trajectories and stops every 2 seconds for manual trajectory adaption. The operator modifies $\Delta \boldsymbol{x}_c$ and Jacobi Compensation is applied for calculation of the appropriate joint space variation $\Delta \boldsymbol{q}$ or a joint level offset $\Delta \boldsymbol{q}$ is set by keyboard commands to achieve a statically stable trajectory point. These

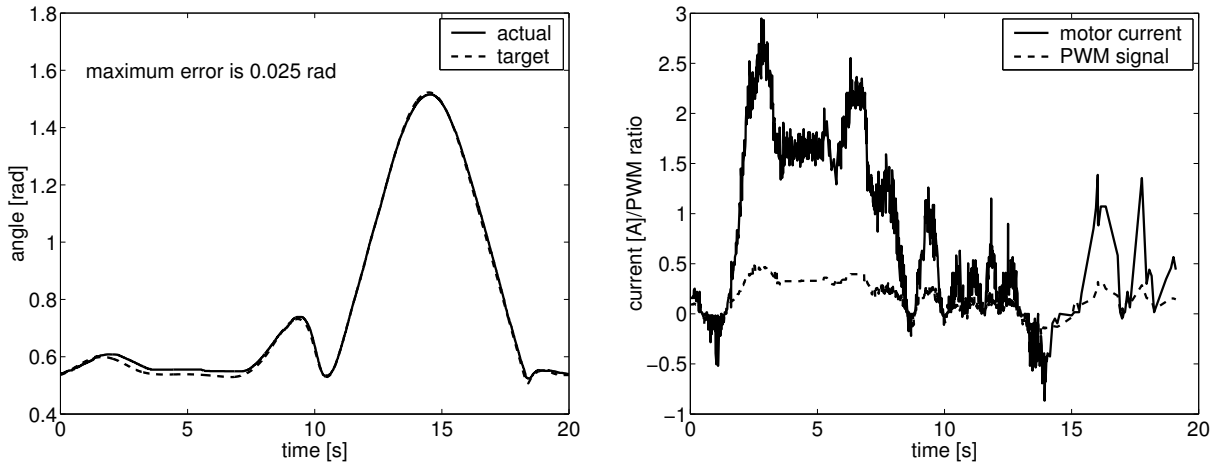

Figure 4.11: Humanoid. Experiments with trajectory following control using precalculated trajectories. a) Control error for knee joint of left leg for one step sequence. b) Motor current and PWM ratio.

trained modifications of the precalculated trajectory are then linearly interpolated and superimposed with $\boldsymbol{q}_t$ during normal operation. The improvement of walking behavior in particular stability was significant as a result from this manual teach-in compensation method.

As the robot now has to support its complete weight by the knee, the control error is higher than before, the maximum error is 0.042 rad. Furthermore, the joint now reaches its maximum load capabilities with the motor current saturating and the PWM ratio being close to 100%. This is not surprising, as the robot has been designed for fast locomotion where the required motor torque is smaller than the torque necessary for statically balancing on one leg.

The effect of the compensation is shown in Fig. 4.12 where the target trajectory and the modified trajectories of the left ankle joint are presented. Note that the joint positions could only be measured at the actuator, therefore the real joint configuration differs from the measured one by the backlash and link elasticities. Hence the measured trajectory in Fig. 4.12 diverges from the target trajectory, although the real configuration is closer to the desired one.

The compensation mainly affects the support phase, where the robot has to be balanced on the left leg and hence small errors in the joint angle degrade static stability. Fig. 4.13 shows snapshots of some stages in a walking sequence.

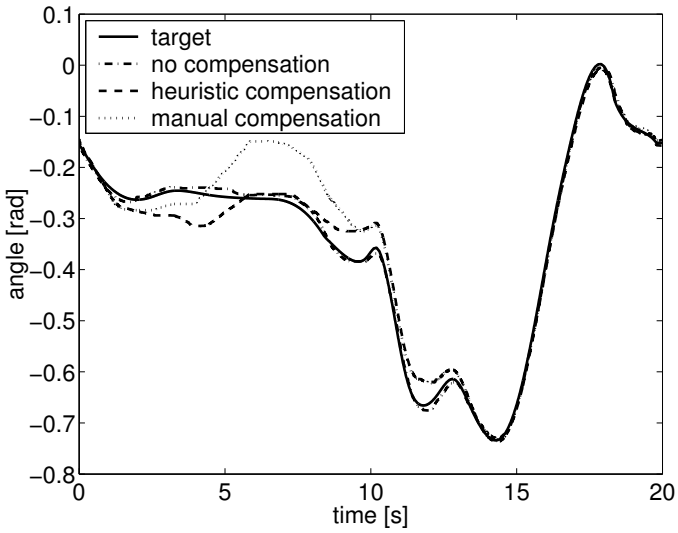

Figure 4.12: Humanoid. Comparison of target trajectory, controlled trajectory without compensation and controlled trajectory with manual compensation of knee joint of left leg.

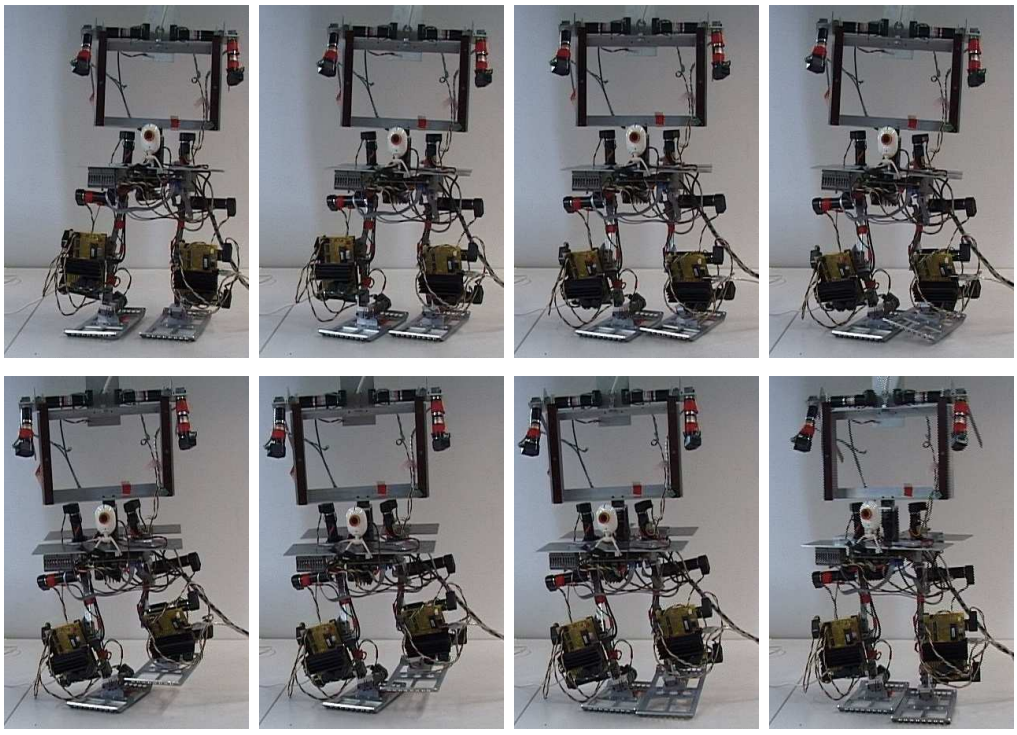

Figure 4.13: Humanoid. Step sequence with manual compensation, snapshots taken every 0.86 s.

4.7 Summary

When using precalculated trajectories for humanoid walking, it is often desirable to interfere with with the planned motion. One reason is to adapt the trajectories to situation slightly differing from the assumptions during motion generation, e. g. shallow slopes or external distrubances such as wind. Another possible modification is to compensate errors in trajectory following due to control errors, joint backlash, or link flexibilities.

A novel method termed *Jacobi Compensation* has been presented which allows modification of precalculated trajectories online during the robot gait. It is possible to shift parts of the robot in given Cartesian directions of selected task coordinates thereby altering the posture of the humanoid to improve e. g. stability.

Using Jacobians to alter humanoids trajectories by moving dedicated parts of the robot has not been reported yet and is considered novel. The possibility of adapting existing trajectories to slightly different situations is also new.

Dynamics properties of the closed feedback loop containing the pseudoinverse Jacobian have been investigated. Using Lyapunov's theorem it has been shown that the system with Jacobi Compensation feedback is stable for moderate posture modifications. To prevent the Jacobi Compensation feedback loop from generating high velocities in the vicinity of singularities, the Singularity-Robust Inverse has been suggested as replacement for the Moore-Penrose pseudoinverse.

Implementations of this method have been demonstrated in simulations with a simple but illustrative setup. Furthermore applicability has been proven in hardware experiments with a humanoid walking robot with promising results.

5 Walking Control of Humanoid Theta

The humanoid robot Theta, developed at the University of Tokyo, features – amongst other innovative design ideas – a special knee joint construction allowing to switch between an actuated and a free swinging mode. Smooth walking motion however can only be achieved based on a carefully designed controller ensuring fast switching between the modes while avoiding jerky motions. Therefore, a nonlinear, time optimal, hybrid controller for the knee joint is developed and a walking controller based on the inverted pendulum approach is implemented.

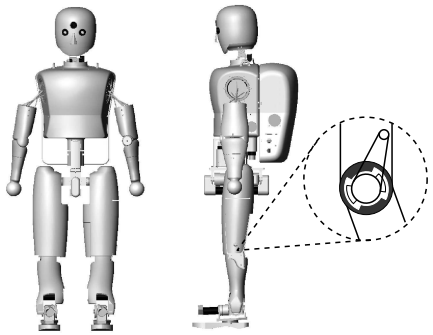

5.1 Problem Description

Although current humanoid robots [32, 48, 52, 78, 132] are mechanically and from the control point of view very sophisticated, their gait often lacks the appealing charm of smooth and dynamic human motion. However, natural behavior seems to be crucial for achieving general acceptance of robots in public environments [112].

Humanoid motion is different from that of humans in mainly two accounts: On the one hand, the human body is highly complex and thus disposes of a large motility significantly exceeding the 12 degrees of freedom commonly found in the legs of humanoid robots. On the other hand, humans exploit the natural dynamics of their extremities, hence walking motion requires little force input from the muscles.

McGeer [68, 69] presented very impressive experiments with passive walking machines showing stable walking behavior. Even more surprisingly, he demonstrated that – by shaping natural dynamics of a passive walking machine – smooth and human-like walking is obtained.

One main focus of the humanoid robot UT-Theta, developed at the Nakamura & Yamane Lab. of the University of Tokyo [79, 80], see Fig. 5.1, is to achieve human-like motion. Two innovative design ideas mechanically support these efforts: due to a double spherical hip joint, the motility of the robot is significantly increased without employing additional joints. A knee mechanism with backlash clutch for switching between active and passive mode of operation allows free swinging motions for the lower legs.

As the knee joint in each contact situation only allows unilateral transmission of forces, conventional control techniques cannot be applied because of its highly nonlinear characteristics. A special knee controller is required that has to fulfill strong requirements: If the

direction of actuation is reversed, the clutch has to traverse the backlash gap; switching times between the directions of actuation must be minimized to keep the nonactuated phase of the knee short. Nevertheless, high control accuracy is required, as the contact necessary for transmitting forces from the knee to the shank must be established smoothly to avoid impact that might result in a position overshoot.

A hybrid, nonlinear, time optimal knee controller [130] meeting these requirements is presented. This knee controller is crucial for successfully implementing the walking controller, as it relies on precise control of the foot landing position.

Regarding the walking control theory a great variety of approaches has been proposed as discussed in Sec. 2.3. One of the main difficulties lies in the great dynamical complexity of a humanoid robot. Many works on biped locomotion follow the general idea of reducing the complexity of the problem by adopting a simplified system, which approximates the dynamics of the real robot.

The approach presented here follows the inverted pendulum concept with a non instantaneous double support phase, following the ideas illustrated in [138], in order to improve stability. An equilibrium controller using force sensors in the feet is also implemented, together with a posture estimator based only on kinematic and force data, without the need for costly and noisy gyroscopes and accelerometers [139].

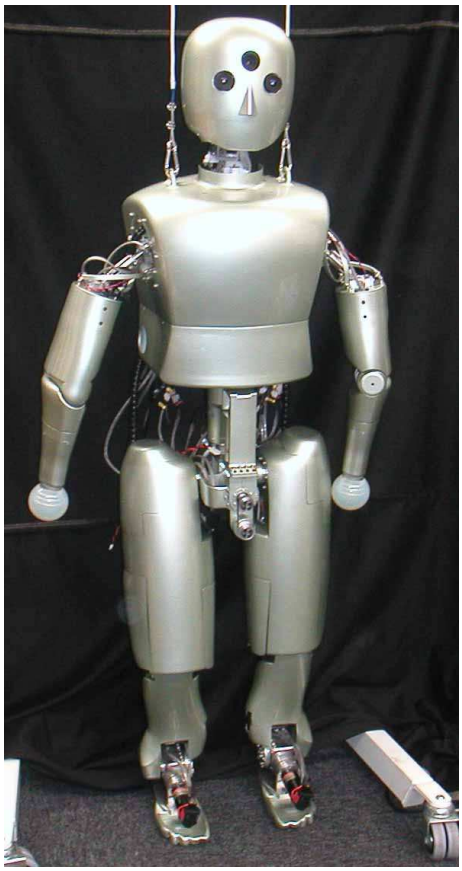

Figure 5.1: Humanoid robot UT-Theta.

This chapter starts with a detailed description in Sec. 5.2 of the particularities in the mechanical design of the humanoid UT-Theta. While Sec. 5.3 deals with the low level control of the knee joints, a description of the high level walking generator and control is presented in Sec. 5.4, together with some experimental results.

5.2 Mechanical Design of Humanoid Theta

Towards the goal of enhancing the walking abilities of humanoid robots, not only the control must be improved but also the mechanical properties of the system need to be refined. The humanoid walking robot UT-Theta [76, 79], see Fig. 5.1, which has been designed and built at the Department of Mechano-Informatics at the University of Tokyo, implements several new design concepts. Theta, made of magnesium alloy, is 160 cm tall with a total weight of 47 kg and has 6 Degrees of Freedom (DoF) in each leg, the arms dispose of 4 DoF each. The head being equipped with 3 cameras can be turned about 3 axes. The robot is completely autonomous with on board batteries and computation power.

Main focus for the design were a joint allocation maximizing the whole body mobility – which is achieved by *double spherical hip joints* – and a joint transmission design for the knee allowing to switch between drive and free mode, called the *backlash clutch*.

5.2.1 Double Spherical Hip Joints

Conventional hip joints as shown in Fig. 5.2 impose an important restriction on the whole body motility of robot: if the upper body is inclined in the lateral plane, one of the knees must be bent. This is an important restriction towards the goal of achieving elegant, human-like motion for a humanoid robot, as hip and trunk motion are strongly coupled.

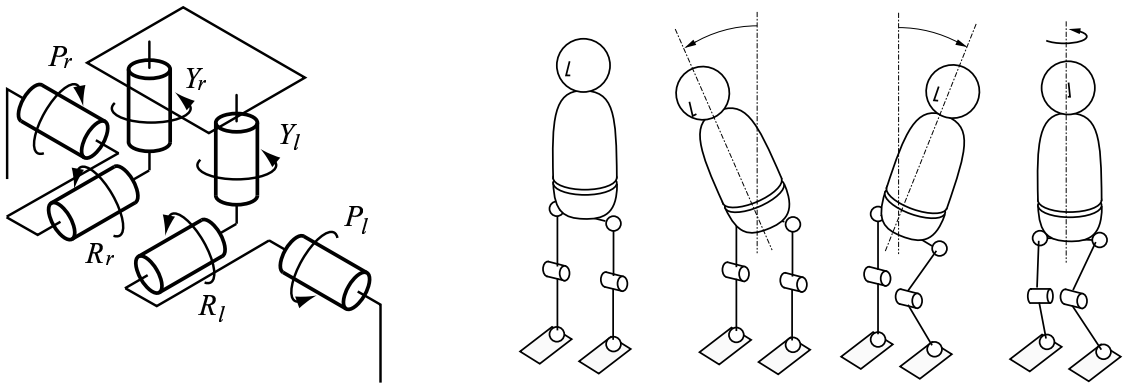

Figure 5.2: Conventional hip joints: lateral and rotatory upper body motion requires knee joint activity.

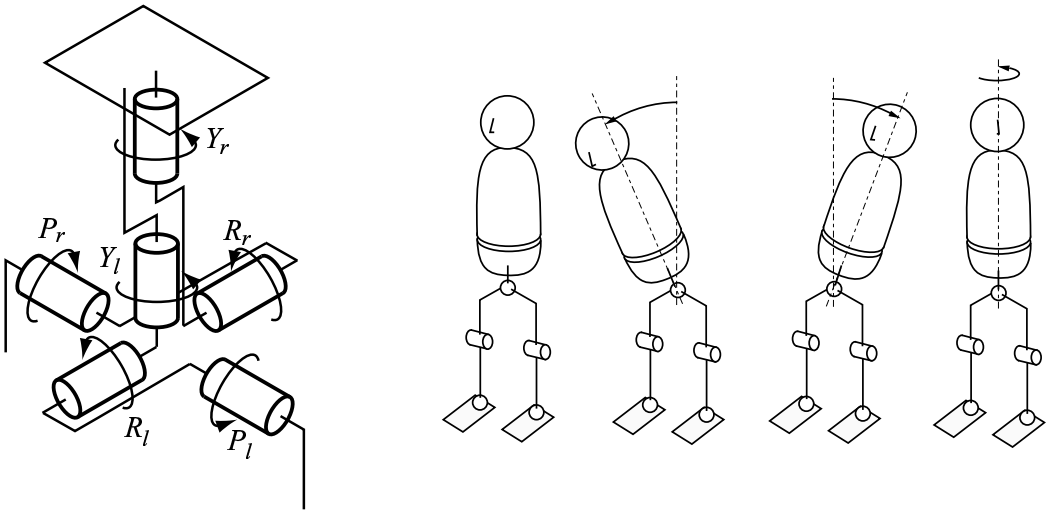

Figure 5.3: Double spherical hip joints: full manipulability of the upper body not depending on leg motion.

To overcome this deficiency, double spherical hip joints have been developed, where all 6 rotational axes of both hip joints intersect in one point, see Fig. 5.3. Due to the hip joints, the upper body can be inclined independently of the leg motion in any direction.

Another particularity of UT-Theta is the special knee construction.

5.2.2 Backlash Clutch

Experiments by McGeer [68, 69] have shown that the natural dynamics of passive walking machines can produce stable walking patterns. Furthermore the walking motion looked very natural and human-like. Inspired by these results a special knee joint has been developed allowing to switch between passive swinging and an actuated mode. Thus UT-Theta can be seen as a first attempt to bridge between passive walking machines and humanoid robots.

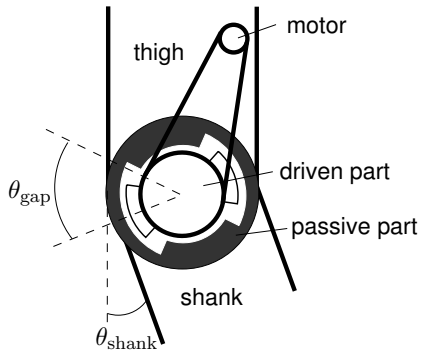

Figure 5.4: Principle of the backlash clutch.

The knee joint shown in Fig. 5.4 basically consists of two parts: The "passive part" is ring-shaped with two notches at opposite sides. These notches can host the tappets of the disk-shaped driven part. The tappets of the driven part being smaller than the notches allow it to rotate by some degrees within this backlash gap. While the passive part is attached to the shank, the driven part is not fixed to any other component of the robot and actuated by a motor. If the driven part is in the middle of the backlash gap, its rotation angle θ_{drive} is defined to be identical to the rotation angle θ_{shank} of the shank and thus of the passive part. With the backlash gap having an angle $2\,\theta_{\text{gap}} \approx 10°$, the tappets of the driven part are in contact with the passive part, if $\theta_{\text{drive}} = \theta_{\text{shank}} \pm \theta_{\text{gap}}$ holds.

With this knee joint construction the shank can be actuated by getting the driven part in contact situation and transmitting the torque of the motor to the shank. On the other hand, if the driven part is placed in the middle of the backlash gap, the shank is not actuated and can move freely according to its natural dynamics. However, switching between active and passive mode imposes a delicate control problem.

5.3 Control of the Knee Backlash Clutch

Due to the mechanical design of the backlash clutch discussed in Sec. 5.2.2, it is impossible to quickly invert the direction of actuation, as the contact between the driven and the passive part only allows force transmission in one direction. To invert the direction of shank acceleration, the driven part of the clutch must traverse the backlash gap and get into the corresponding contact situation.

Due to this unilateral interaction at the knee joint, the motion planning algorithm must select the appropriate direction of force propagation for a given walking situation, i. e. flexion or extension of the knee. From practical considerations for motion planning, the following qualitative behavior of the knee controller seems desirable:

- If a new knee mode (flexion or extension) is selected, the driven part must establish the corresponding contact situation as quickly as possible (*transition mode*) while avoiding hard collision of the driven and the passive part, as an impact might result in an immediate loss of contact again and accelerate the shank unintendedly.

- When the desired contact situation is established, the position of the shank must be adjusted to the commanded angle (*contact mode*). It is important that this adjustment motion is very smooth as abrupt velocity changes can lead to a loss of contact due to the inertia of the shank.

- If the shank in extension mode is extended – or in flexion mode is inclined – further than commanded, the driven part should not interact any further with the shank, thus allowing free motion of the shank (*free mode*).

In the following, the control strategy for each of these modes is discussed.

5.3.1 Transition Mode

The purpose of the transition mode is to establish contact between the driven and the passive part of the knee in minimum time. Furthermore, contact impact must be avoided to prevent further acceleration of the shank.

The qualitative description leads to the following mathematical constraints: When the transition mode is initiated at $t = t_0$, the initial position and velocity of the shank ($\theta_{\text{shank}}(t_0)$, $\dot{\theta}_{\text{shank}}(t_0)$) and of the driven part ($\theta_{\text{drive}}(t_0)$, $\dot{\theta}_{\text{drive}}(t_0)$) are arbitrary. Contact between the driven and the passive part at the final time t_f of the switching period is achieved, if $\theta_{\text{drive}}(t_f) = \theta_{\text{shank}}(t_f) \pm \theta_{\text{gap}}$ holds. In order to achieve a smooth contact without impact, both parts must have the same velocity $\dot{\theta}_{\text{drive}}(t_f) = \dot{\theta}_{\text{shank}}(t_f)$.

These constraints can be simplified by introducing the coordinate transformation $q(t) = \theta_{\text{shank}} - \theta_{\text{drive}}(t) \pm \theta_{\text{gap}}$. Hence the initial condition becomes $q(t_0) \neq 0$, with an arbitrary velocity $\dot{q}(t_0)$ and the final condition is formulated as $q(t_f) = 0$, $\dot{q}(t_f) = 0$, i. e. the goal of the transition mode controller is to transfer an arbitrary initial state $\begin{bmatrix} q(t_0) & \dot{q}(t_0) \end{bmatrix}^T$ to the origin of the q-$\dot{q}$-plane in minimum time t_f.

Time optimal control generally is achieved by bang-bang-controllers [81]. This means that the driven part must be accelerated with the maximum possible acceleration and then decelerated as hard as possible. This must be achieved with only one switch and without overshoot of the target position.

To find the appropriate switching point, a simplified version of the principle of *Invariance Control* [62–64] is used. The key idea is to define a region in state space where the control goal is achieved. The system is allowed to evolve freely within this region. If the region has its maximum size, leaving it implies that the control goal is violated. Hence, if the system state hits the boundary of the region, a control input must be set such that the system state does not leave the region, thus controlling the region invariant, constituting the name *Invariance Region*.

Applying this principle to the knee control problem, the control goal is reaching the origin of the q-$\dot{q}$-plane without position overshoot and the boundary of the Invariance Region is characterized by all points in q-$\dot{q}$-space, where braking with maximum deceleration moves the system state directly to the origin of state space. Inside the Invariance Region, the clutch is accelerated. When hitting the boundary, hard braking will keep the system state on the boundary.

The boundaries of this region are determined from physics. The motion of the driven part of the clutch is described by

$$q(t) = q(t_0) + \frac{\dot{q}(t_0) - \dot{q}(t)}{2} t. \tag{5.1}$$

Solving the relation $\dot{q}(t) = \dot{q}(t_0) + at$ for the time t and inserting this into (5.1) yields

$$q(t) = q(t_0) + \frac{\dot{q}(t_0) - \dot{q}(t)}{2} \frac{\dot{q}(t) - \dot{q}(t_0)}{a}. \tag{5.2}$$

Substituting the control goal $q(t_f) = 0$, $\dot{q}(t_f) = 0$ in (5.2) and assuming the maximum deceleration $-a = a_{\text{max,brake}}$, the equation

$$q(t_0) = \frac{1}{2a_{\text{max,brake}}}\dot{q}(t_0)^2 \tag{5.3}$$

is obtained, describing the boundary of the invariance region as shown in Fig. 5.5. The system state $\begin{bmatrix} q(t_0) & \dot{q}(t_0) \end{bmatrix}$ are points in state space, where the system state can reach the origin by applying $a_{\text{max,break}}$ without position overshoot, i. e. without change of sign of q.

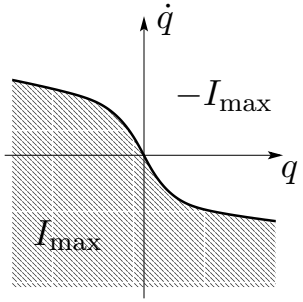

Figure 5.5: Switching surface in q-$\dot{q}$-space.

In order to ensure contact to be established in optimal time, maximum positive acceleration $a_{\text{max,accel}}$ is applied until the boundary is reached.

The maximum acceleration and deceleration result from applying the maximum permissible positive or negative current to the motor. Note that the maximum deceleration is significantly higher than the maximum acceleration due to the effects of friction and back-EMF, i. e. additional voltage induced by the braking process.

As q is a relative coordinate depending on the angle θ_{drive} and θ_{shank} of the driven part and of the shank, the maximum deceleration $a_{\text{max,brake}} = \ddot{\theta}_{\text{drive,max,brake}} - \ddot{\theta}_{\text{shank}}(t)$ also depends on the current acceleration $\ddot{\theta}_{\text{shank}}(t)$ of the shank.

The driven part not being in contact with the passive part and assuming free swinging, the only acceleration acting on the shank is the earth acceleration. The earth acceleration being much lower than the maximum deceleration $\ddot{\theta}_{\text{drive,max,brake}}$ of the driven part, this effect can be neglected in practical implementation and $a_{\text{max,brake}} = \ddot{\theta}_{\text{drive,max,brake}} = \text{const}$ can be assumed.

A problem arises from late detection of the boundary due to discrete sampling. In time discrete implementations of the controller, the invariance condition (5.3) is only checked with the sampling time T, therefore the exact instant of crossing the boundary generally cannot be detected. Hence, even if the invariance condition at time $t = t_k$ is met, it might be violated at the next sample $t = t_k + T = t_{k+1}$. Thus, the controller starts braking too late and the control goal cannot be made without position overshoot.

To cope with this problem, an upper bound $\begin{bmatrix} \overline{q}_{k+1} & \dot{\overline{q}}_{k+1} \end{bmatrix}^T$ for the joint state is predicted at time $t = t_k$ by assuming acceleration of the joint with $a_{\text{max,accel}}$. With this assumption, the joint position

$$\overline{q}_{k+1} = q_k + \dot{q}_k T + \frac{a_{\text{max,accel}} T^2}{2} \tag{5.4}$$

is obtained. Using time discrete computation for the acceleration

$$\dot{q}_k = \frac{q_k - q_{k-1}}{T},$$

Equation (5.4) becomes

$$\overline{q}_{k+1} = 2q_k - q_{k-1} + \frac{1}{2}a_{\text{max,accel}} T^2.$$

Furthermore the corresponding upper bound

$$\dot{\overline{q}}_{k+1} = \frac{q_k - q_{k-1}}{T} + a_{\text{max,accel}} T$$

for the velocity is calculated.

Using this upper bound to verify the invariance condition (5.3), it will not be violated and contact is established without impact.

Once contact situation is established, the shank angle must be adjusted to the commanded position.

5.3.2 Contact Mode

In contact situation, a PD position controller is used to adjust the reference position θ_{ref} at the driven part of the backlash clutch. To account for the backlash gap θ_{gap}, the commanded angle θ_{cmd} must be modified according to

$$\theta_{\text{ref}} = \theta_{\text{cmd}} \pm \theta_{\text{gap}},$$

where the choice of sign for the modification depends on the desired contact situation, i. e. extension or flexion.

One difficulty arises from the fact that at the instant when contact is established, the real position usually does not exactly match the position calculated by the motion planner; a reason for that is the motion of the shank while the knee is in transition mode. Therefore instantaneously adjusting θ_{cmd} results in a jump of the shank position. This high acceleration mostly leads to a loss of contact at the clutch and a position overshoot. The unintended reaction force on the robot can even disbalance the biped.

To overcome this problem, the controller determines at the instant $t = t_c$ of contact the difference $\Delta\theta_0 = \theta_{\text{drive}}(t_c) - \theta_{\text{cmd}} \pm \theta_{\text{gap}}$ between the current position of the driven part and the commanded angle. Further on a correction term $\Delta\theta(t - t_c) = \Delta\theta_0\, s(t - t_c)$ is added to the commanded angle θ_{cmd}, thus compensating the initial error and avoiding steps in the commanded trajectory. The function $s(t)$ is a cubic spline with the properties $s(0) = \Delta\theta_0$, $\dot{s}(0) = 0$, $s(t_f) = 0$ and $\dot{s}(t_f) = 0$, see Fig. 5.6. Depending on the walking situation, the desired duration $t_f - t_c$ for reducing the position error compensation varies; therefore the final time t_f is set by the motion planner.

The advantage of this approach compared to lowpass filtering is that the bandwidth of the controller is not affected thus still allowing to follow fast commanded trajectories.

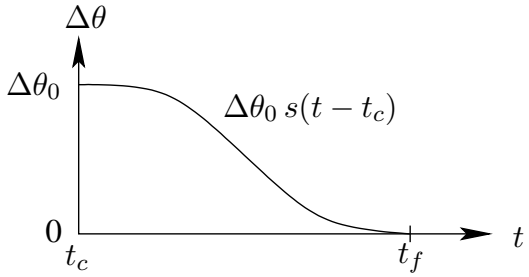

Figure 5.6: Position error compensation by spline function.

Walking experiments with the robot showed, that – due to the intricate mechanical knee construction and thereby resulting flexibilities – the control error between commanded angle θ_{cmd} and the adjusted angle θ_{shank} is larger than the average control error in the other

joints. To reduce the stationary control error, a compensation controller with integrative behavior has been implemented. This controller computes a compensation angle

$$\theta_{\text{comp}} = \int \text{sat}\big(k(\theta_{\text{cmd}} - \theta_{\text{shank}}),\ \delta_{\max}\big)\mathrm{d}t,$$

with the gain k and the saturation function

$$\text{sat}(x, \delta_{\max}) = \begin{cases} \delta_{\max} & \text{if } x > \delta_{\max} \\ x & \text{if } -\delta_{\max} \le x \le \delta_{\max} \\ -\delta_{\max} & \text{if } x < -\delta_{\max} \end{cases}.$$

The saturation function is used to limit the integration rate and hence the velocity of the correction motion.

The complete control loop in contact mode is shown in Fig. 5.7

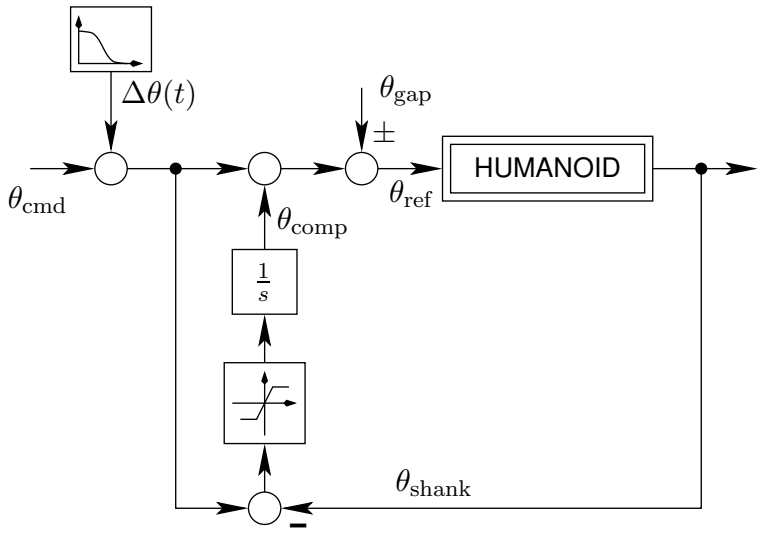

Figure 5.7: Control loop in contact mode.

5.3.3 Free Mode

If the shank is either bent more than commanded in flexion mode or in extension mode is stretched further than desired, the knee drive should not interact with the shank. Hence the driven part remains at the commanded position, or – if $\theta_{\text{shank}} > \theta_{\text{cmd}} \pm \theta_{\text{gap}}$ – in the middle of the backlash gap.

The performance of the knee controller is experimentally investigated in the following section.

5.3.4 Experimental Evaluation of the Knee Control

A first experiment looks into the performance of the the switching controller as described in Sec. 5.3.1.

The driven part of the backlash clutch travels from one contact situation to the opposite as shown in Fig. 5.8. The highlighted area marks the time, where the Invariance Controller is active. In repeated experiments the switching time never exceeded 50 ms. Plotting the system state during switching in the q-$\dot{q}$-plane (Fig. 5.9) clearly shows that the maximum deceleration $a_{\max,\text{brake}}$ of the driven part is much higher than the maximum acceleration $a_{\max,\text{accel}}$. The spike with positive velocity during braking occurs because the value for the maximum deceleration $a_{\max,\text{brake}}$ in (5.3) is chosen slightly lower than the real physical value. This is necessary as a safety margin to allow for disturbances such as changes in friction due to warming of the gear.

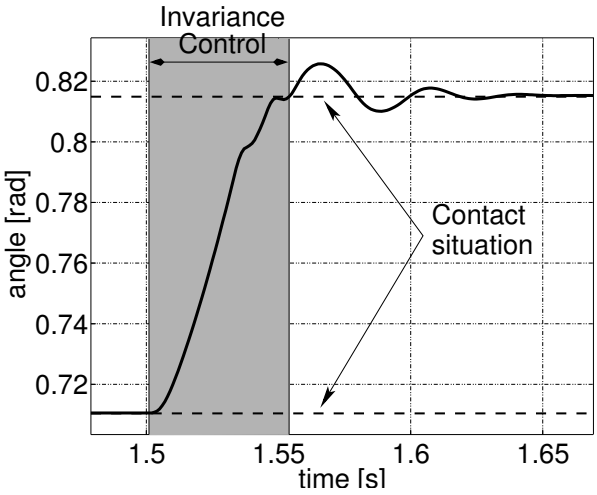

Figure 5.8: Hardware experiment: Switching from one contact situation to the other in time domain.

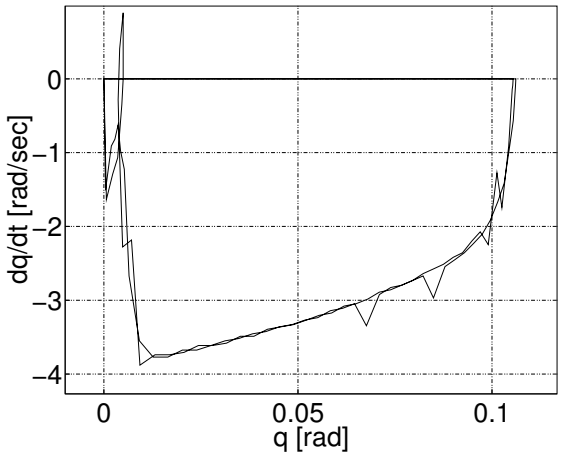

Figure 5.9: Hardware experiment: Switching contact situations in state domain.

The behavior of the controller in contact mode described in Sec. 5.3.2 can be seen in Fig. 5.10. Initially the knee is in free mode and the driven part follows the shank motion. At approx. $t = 0.3\,\text{s}$ the knee is switched into extension mode, hence the driven part of the backlash clutch gets into contact. At this instant, there is a large difference between the actual position of the shank and the commanded angle. This difference is reduced slowly using the spline function $s(t)$, in this case the reduction time has been set to 0.4 s. In the following the controller adjusts the shank position to the commanded angle using the integrating compensation controller. At approx. $t = 1.2\,\text{s}$ the shank is manually extended further than the commanded angle and the driven part of the backlash clutch now follows the shank angle thus allowing free motion. If the shank position is reduced to the commanded angle, the position controller becomes active again.

In order to evaluate the performance of the controller, an experiment has been implemented using the extension and flexion mode of the controller as a position controller. In this experiment, rather than switching into free mode if the shank is extended or bent further than commanded, the controller switches to the opposite mode, i. e. if the shank is bent more than commanded, the controller switches to extension mode and vice versa. Using this position controller, the shank is commanded a sine trajectory with increasing frequency about its free hanging position, thus gravity has little dampening effect. In this experiment, smooth switching with low impact is very important, as a large impact would result in an overshoot and thus cause the controller mode to switch back. From the result

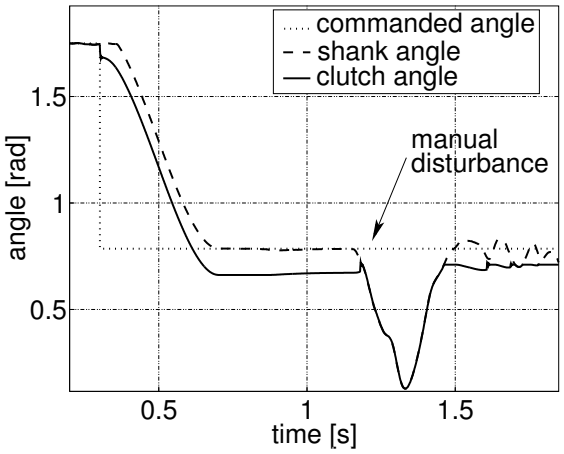

Figure 5.10: Hardware experiment: Switching from free mode to extension mode and manually stretching the shank further than commanded.

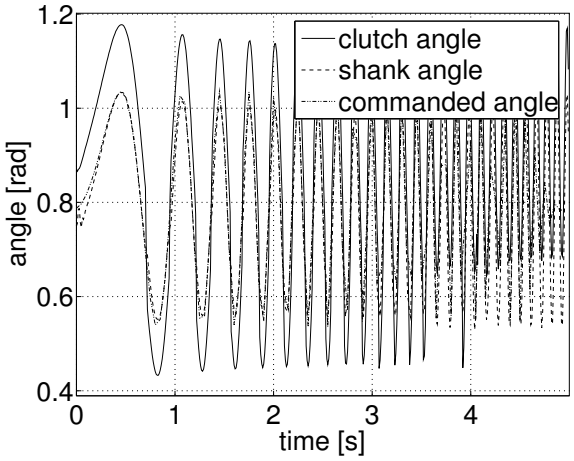

Figure 5.11: Hardware experiment: Swinging motion with increasing frequency using a position controller.

presented in Fig. 5.11 it can be seen that the controller works stable over a very large frequency domain.

5.4 Walking Control Exploiting Zero Dynamics

The walking controller employed here is based on the Inverted Pendulum approach first presented by Kajita et al. [43–46]. In this method, the complex tilting dynamics of the humanoid are approximated by the simple dynamics of an inverted pendulum.

In this method, the robot is not controlled during the single support phase, i. e. as soon as the swing foot lifts off the ground, the robot moves as imposed by the system state during lift off. Hence, to control the walking motion, the system state at lift off must be chosen such that the body motion during single support evolves in the desired way; the appropriate lift off state is established during double support phase. The lateral velocity must be chosen high enough to allow a sufficiently long single support pahse, but must not exceed the threshold where the robot starts tilting to the oposite side. The walking speed is reflected by the sagital velocity. The required lift off state is computed from a simplified model, assuming the robot dynamics similar to those of an inverted pendulum.

Hence, in a first step, the equations of motion of the linear inverted pendulum constituting the robot model are derived.

5.4.1 Inverted Pendulum Dynamics

The dynamics of the inverted pendulum describe the robot in the single support phase; consequently the base of the pendulum is located in the support foot as shown in Fig. 5.12. In this work the passive approach [43] is adopted, hence there is no torque at the base of the pendulum. The acting force $\boldsymbol{F}$ is exerted on the mass m and directed parallel to the rod of the pendulum as illustrated in Fig. 5.12.

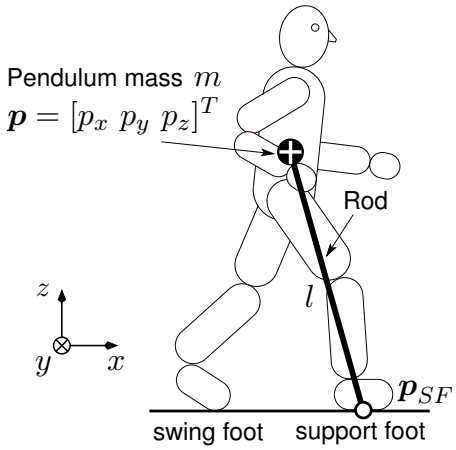

Figure 5.12: Inverted pendulum approximation.

Applying D'Alembert's principle the system dynamics are

$$m\ddot{p}_x = F\frac{p_x}{l}, \tag{5.5}$$

$$m\ddot{p}_y = F\frac{p_y}{l}, \tag{5.6}$$

$$m\ddot{p}_z = F\frac{p_z}{l} - mg, \tag{5.7}$$

where $F = |\boldsymbol{F}|$ is the magnitude of the force, $\boldsymbol{p}$ is the position vector of mass m and l is the length of the pendulum rod.

This model is simplified by an additional assumption: during the human walking process, the height of the hip slightly oscillates around a constant value, therefore the z-coordinate p_z of mass m is assumed constant [43], i. e. $\ddot{p}_z = 0$. This is achieved according to (5.7) by setting

$$F = \frac{mgl}{p_z}, \tag{5.8}$$

which corresponds to an input-output linearization [41]. Substituting (5.8) back into (5.5) and (5.6), the dynamics become

$$\ddot{p}_x = \gamma^2 p_x \tag{5.9}$$

$$\ddot{p}_y = \gamma^2 p_y \tag{5.10}$$

where $\gamma = \sqrt{\frac{g}{p_z}}$ is constant. Equations (5.9)–(5.10) represent the zero dynamics of the system if (5.8) is applied and are solved analytically to

$$p_x(t) = C_1 e^{-\gamma t} + C_2 e^{\gamma t} + p_{SF,x} \tag{5.11}$$

$$p_y(t) = C_3 e^{-\gamma t} + C_4 e^{\gamma t} + p_{SF,y} \tag{5.12}$$

where $\boldsymbol{p}_{SF}$ is the position of the support foot, and the constants

$$\begin{aligned} C_1 &= \frac{\gamma\big(p_x(0) - p_{SF,x}\big) - \dot{p}_x(0)}{2\gamma} & C_2 &= \frac{\gamma\big(p_x(0) - p_{SF,x}\big) + \dot{p}_x(0)}{2\gamma} \\ C_3 &= \frac{\gamma\big(p_y(0) - p_{SF,y}\big) - \dot{p}_y(0)}{2\gamma} & C_4 &= \frac{\gamma\big(p_y(0) - p_{SF,y}\big) + \dot{p}_y(0)}{2\gamma} \end{aligned} \tag{5.13}$$

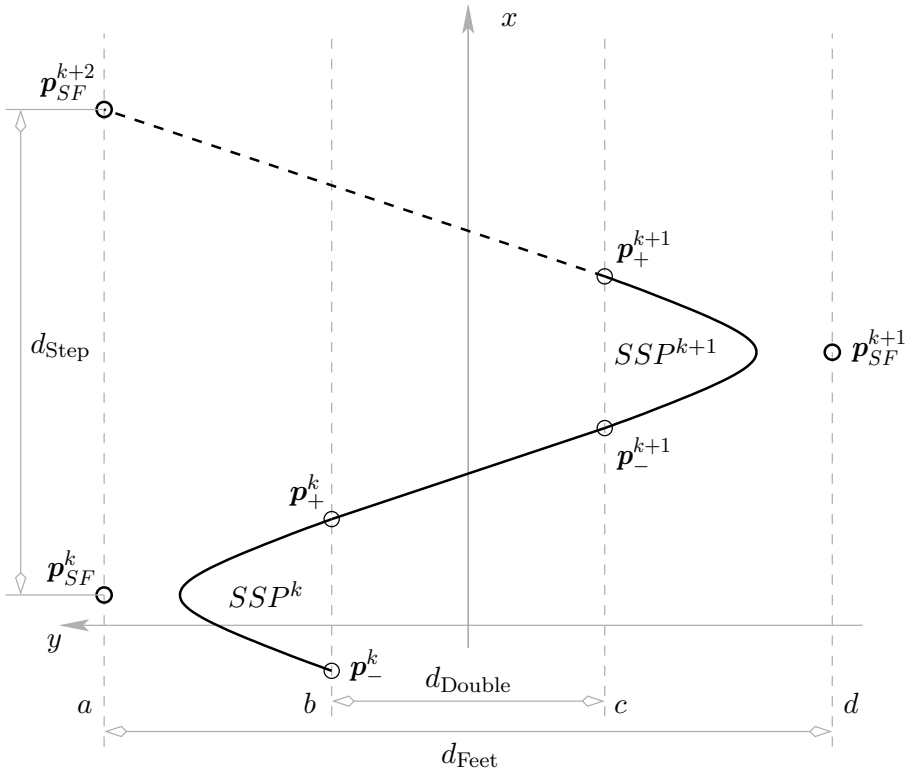

Figure 5.13: Scheme of the double and single support phases.

only depend on the initial conditions of the pendulum.

When the robot is in the double support phase two forces can be applied to the mass of the pendulum. This fact allows to influence the horizontal force F_h within certain limits, which is exploited to control the motion of the robot.

5.4.2 Walking Pattern Generator

The walking pattern generator and control is now described, referring to Fig. 5.13. In this approach the walking reference trajectory is a set of successive reference positions for the support feet. For a straight forward walking the feet travel on two parallel lines, line a and d. Here the support feet are indicated by $\boldsymbol{p}_{SFL}^{i}$ and $\boldsymbol{p}_{SFR}^{i}$ for the left and right foot respectively, the superscript i denotes the consecutive number of the single support phase. The bold line marks the trajectory of the pendulum mass projected to the ground (GCoM).

While the GCoM is between lines b and c, the robot is in double support phase. The aim of this phase is to accelerate the system – using the horizontal force F_h – such that the desired initial system for the single support phase is reached. If the GCoM reaches lines b or c, the swing foot lifts off the ground and the single support phase is initiated. During the single support phase, the system is not actuated and evolves according to its passive dynamics. The swing foot is controlled such that it touches the ground when the GCoM reaches lines b or c again and the next double support phase is initiated.

Double Support

The duration of the single support phase is determined by the initial velocity of the pendulum. The initial velocity must be chosen such that the GCoM $p_y(t)$ does not cross the traveling lines a or d of the support foot, which would make the robot tilt.

The higher the initial velocity, the closer the pendulum will get to lines a or d, and the longer it will take to go back to line c. The limit condition is when the pendulum reaches line d, in an infinite time, i. e.

$$\lim_{t\to\infty} p_y(t) = p_{SF,y}, \text{ thus } \lim_{t\to\infty} \dot{p}_y(t) = 0. \tag{5.14}$$

According to (5.12), this can only be true if $C_4 = 0$ holds, which yields an upper limit

$$\overline{\dot{p}}_y(0) = -\gamma\,(p_y(0) - p_{SF,y}). \tag{5.15}$$

for the initial lateral velocity. Any value smaller than $\overline{\dot{p}}_y(0)$ will produce a finite time for the single support duration, that can be calculated with the formula

$$T_f = \frac{1}{\gamma} \ln\left(\frac{p_{\text{land},y} - p_{SF,y} \pm \sqrt{(p_{SF,y} - p_{\text{land},y})^2 - 4\,C_3C_4}}{2\,C_4}\right), \tag{5.16}$$

where $p_{\text{land},y}$ is the y-coordinate of the desired foot landing point. Here, the desired velocity

$$\dot{p}_y = k\gamma p_y \qquad k \in]0,1[\tag{5.17}$$

is chosen as a constant fraction k of the critical one.

With this data it is now possible to plan the double support phase so that it brings the pendulum to the boundary b or c of the double support region with the desired final velocity.

Single Support

The trajectory of the pendulum mass during the single support phase SSP^k depends only on the initial system state in $\boldsymbol{p}_-^k$ and the location $\boldsymbol{p}_{SF}^k$ of the pendulum base, i. e. the support foot. These parameters are fixed for the current SSP^k, hence the trajectory cannot be altered. However, the landing position $\boldsymbol{p}_{SF}^{k+1}$ of the swing foot – being the support foot during the following SSP^{k+1} – represents an important design parameter to be chosen during the current SSP^k.

Note that the y-coordinates $\boldsymbol{p}_{SF,y}$ of the support feet are restricted by the premise that the feet travel along lines a and d. Therefore, only the x-coordinate $p_{SF,x}^{k+1}$ remains to be determined. This is done by imposing an additional constraint on the system state at the end $\boldsymbol{p}_+^{k+1}$ of the following single support phase SSP^{k+1}. In order to ensure smooth motion, the pendulum in $\boldsymbol{p}_+^{k+1}$ must be tangential to the line connecting $\boldsymbol{p}_+^{k+1}$ and the desired location $\boldsymbol{p}_{SF}^{k+2}$ for the next support foot. This condition can be analytically expressed by

$$\frac{\dot{p}_{+,x}^{k+1}}{\dot{p}_{+,y}^{k+1}} = \frac{p_{SF,x}^{k+2} - p_{+,x}^{k+1}}{p_{SF,y}^{k+2} - p_{+,y}^{k+1}} \tag{5.18}$$

In (5.18) $p_{+,y}^{k+1}$ and $p_{SF,y}^{k+2}$ are known since these variables are restricted to lines a/d and b/c respectively. Hence, the duration T_f of SSP^{k+1} is calculated according to (5.16) and the corresponding final velocity $\dot{p}_{+,y}^{k+1}$ follows (5.17).

The sagittal position and velocity

$$\begin{aligned} p_{+,x}^{k+1} &= C_1^{k+1} e^{-\gamma T_f} + C_2^{k+1} e^{\gamma T_f} + p_{SF,x}^{k+1} \\ \dot{p}_{+,x}^{k+1} &= -\gamma C_1^{k+1} e^{-\gamma T_f} + \gamma C_2^{k+1} e^{\gamma T_f} \end{aligned} \tag{5.19}$$

at the instant of foot landing are computed following (5.11), with C_1 and C_2 being a function of $\boldsymbol{p}_{-}^{k+1}$, $\dot{\boldsymbol{p}}_{-}^{k+1}$ and p_{SF}^{k+1}. By substituting (5.19) in equation (5.18) and solving for

$$p_{SF,x}^{k+1} = \frac{2\,\gamma\,\alpha_1\,p_{SF,x}^{k+2} + \dot{p}_{-,x}^{k+1}(\alpha_2 - \alpha_3) - p_{-,x}^{k+1}\,\gamma(\alpha_2 + \alpha_3)}{\gamma(2\alpha_1 - \alpha_2 - \alpha_3)}, \tag{5.20}$$

with

$$\begin{aligned} \alpha_1 &= \frac{\dot{p}_{+,y}^{k+1}}{p_{SF,y}^{k+2} - p_{+,y}^{k+1}} \\ \alpha_2 &= (\alpha_1 - \gamma) e^{-\gamma T_f} \\ \alpha_3 &= (\alpha_1 + \gamma) e^{\gamma T_f}, \end{aligned}$$

an equation fot the sagittal foot landing position is obtained.

This gives the solution for the final point of the swing foot trajectory. The single support phase is now completely defined, and can be executed.

5.4.3 Implementation on UT-Theta

In the 3D-Linear Inverted Pendulum Method, the mass of the robot is assumed to be concentrated in one point, the CoM. In practice, the position of the CoM depends on the joint angles of the robot links. Calculating the exact CoM each sampling interval takes a relevant portion of the available computing resources, and complicates the implementation of the walking controller. Therefore the CoM is considered to remain in a fixed position relative to the main body of the robot, an assumption justified by the fact that the main body, the head and the arms amount to more than 70% of the total robot mass. The arms are not actuated during the experiment and the upper body is controlled to remain in an upright position. Furthermore the motion range of the legs is limited, hence the error caused by this assumption can be treated as a disturbance, which the walking control is able to correct. As a consequence the walking controller algorithm is computationally lighter, and can be executed in real time.

In order to estimate the posture of the robot and therefrom derive the state of the inverted pendulum, the absolute orientation of the body of the robot is needed. As data from the robot gyroscopes and accelerometers proved not to be sufficiently reliable, a technique based on joint kinematics was adopted: if flat contact of the support foot sole with the ground is verified, the orientation of the foot sole with respect to the world is known, assuming a horizontal floor. Using direct kinematics, it is thus possible to obtain the posture of the robot relative to the world. Since the robot is equipped with 6-axis force sensors in each foot it is possible to ensure flat foot contact by limiting admissible ranges for foot torques.

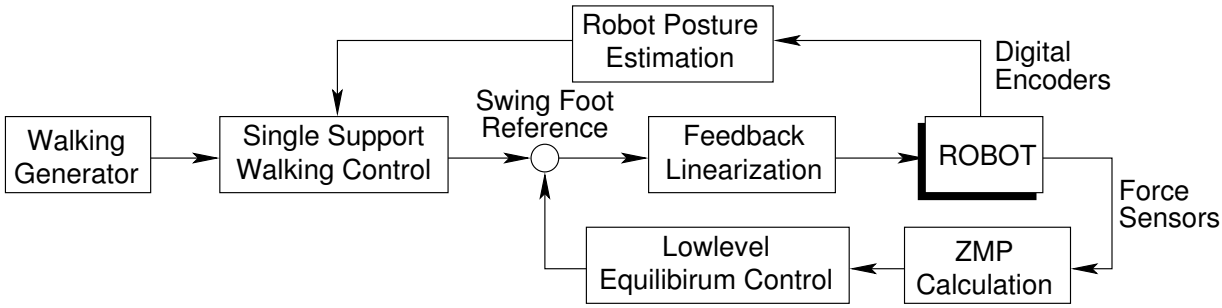

Figure 5.14: Scheme of the single support control including the equilibrium control using the ZMP data

The initial assumption of zero torques at the base, i. e. the ideal position $\boldsymbol{p}_{\mathrm{ZMP}}^{\mathrm{ideal}}$ of the ZMP is always in the center of the foot, permits to use the position error

$$\boldsymbol{p}_{\mathrm{ZMP}}^{\mathrm{err}} = \boldsymbol{p}_{\mathrm{ZMP}}^{\mathrm{real}} - \boldsymbol{p}_{\mathrm{ZMP}}^{\mathrm{ideal}} = \boldsymbol{p}_{\mathrm{ZMP}}^{\mathrm{real}} \tag{5.21}$$

between the real $\boldsymbol{p}_{\mathrm{ZMP}}^{\mathrm{real}}$ and the ideal position as an indicator if the robot is disbalanced. The objective is to correct the motion of the robot so that the ZMP goes back to the center of the foot and the $\boldsymbol{p}_{\mathrm{ZMP}}^{\mathrm{err}}$ to zero. In agreement with the approach followed so far the swing foot trajectory is modified to restore the equilibrium when the robot switches to the double support phase. This is achieved by the control heuristic

$$p_{\mathrm{SwingFoot},x} = p_{\mathrm{SwingFoot},x}^{\mathrm{des}} + p_{\mathrm{ZMP},x}^{\mathrm{err}}, \tag{5.22}$$

that performed well in experiments.

The complete control scheme of the implementation is shown in Fig. 5.14.

Due to the particular type of knee joint mounted on UT-Theta the walking control had to be carefully aligned with the knee control. When the robot is in the double support phase both knees are in extension mode, since the weight of the robot is sustained by both legs. The knee is switched to the flexion mode when the corresponding foot must be lifted from the ground, the knee torque in this situation has to change sign. The knee is kept in the flexion mode throughout the whole swing phase, and then put back to extension mode when an impact force is detected by the swing foot force sensor. Different impact experiments have indicated that the passive mechanism contributes to reduce the impact forces, because at the touchdown the knee mechanism is in free mode for approximately 50 ms, the time necessary for the control to switch the knee state. In this passive mode the natural motion of the knee tends to absorb part of the impact energy.

Regarding the swing phase it must be noted that the contact condition in the knee during our experiments is maintained because the inertial accelerations in the leg are smaller than the gravitational forces. For higher walking speeds this condition might not be verified, so a more complex swing phase controller should be adopted, and different knee modes, such as the free swing mode, should be used.

5.4.4 Experimental Results

The proposed walking pattern generator and control presented so far was implemented on the humanoid robot UT-Theta. Some problems were encountered during the impact

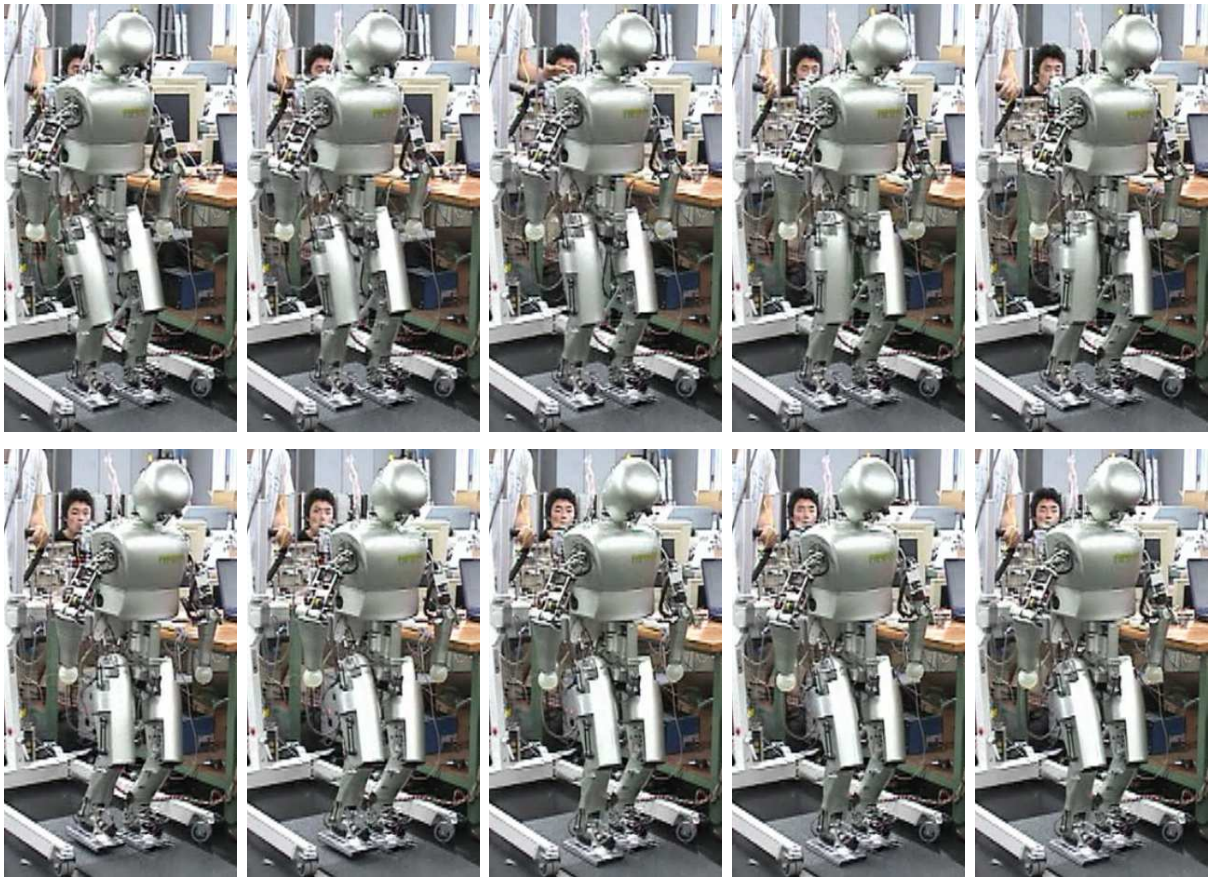

Figure 5.15: Stroboscopic sequence of a complete step, snapshots are taken every 0.2 s.

phase, because of the performance of the low level joint controllers and the presence of some mechanical backlash on certain joints. Relatively high joint oscillations, that needed some time to be absorbed, were also observed. This fact lead to the introduction of an absorption phase between the end of a single support and the beginning of the double support. This phase has a fixed time duration of 3 seconds, but current on-going work is aimed at reducing the time duration of this phase and eventually eliminate it. After this additional phase was introduced the robot could walk without falling for an arbitrary number of steps. The robot was commanded to execute 12 steps, with $d_{\text{Step}} = 0.12\,\text{m}$, $d_{\text{Feet}} = 0.1\,\text{m}$, $d_{\text{Double}} = 0.06\,\text{m}$. A picture sequence of one complete cycle, made up of the double support, single support and impact phase can be observed in Fig. 5.15, where each picture was taken at a $t = 0.12\,\text{s}$ interval.

In the upper row of images the robot is in double support phase and transfers the weight from the left to the right foot. In the lower row the robot executes the single support phase, bringing forward the swing foot (left foot) and then switch again to the double support phase.

5.5 Summary

A walking control strategy based on the inverted pendulum approach has been implemented on the humanoid robot UT-Theta, which has been developed at the University of Tokyo. The inverted pendulum approach avoids many problems arrising from the high dynamical complexity of humanoid robots by approximating the dynamics of the robot by those of an inverted pendulum. During the single support phase, the robot is not controlled and moves ballistically, similar to an inverted pendulum; the motion is only determined by the system state during lift-off of the swing foot. The control task is to reach the desired lift-off state by performing appropriate motions during the double support phase.

In the experimental section, a method for estimating the body posture is illustrated, based on kinematic information coming from the joint encoders. This information is used for an equilibrium control based solely on foot force sensor data is proposed, hence gyroscopes or accelerometers are not needed.

A major mechanical speciality of UT-Theta is knee joint construction allowing to switch between an actuated and a free swinging mode. This is achieved by actuating a disk with tappets rotating inside a ring with notches, which is connected to the shank. As the notches are larger than the tappets, the actuated disk can move freely within this backlash gap and drive the shank in either direction or allow free swinging.

However, discontinuities due to collision impact between the notches and tappets leads to jerky motion and can even destabilize the robot. Thus impacts must be avoided. Another difficulty is inversing the direction of actuation, at the clutch has to traverse the backlash gap. In this case, switching times must be minimized to keep the unactuated phase of the knee short.

As the knee joint shows highly nonlinear characteristics due to its hybrid character, conventional control techniques exhibit a poor control performance. To fulfill the requirements, a nonlinear, time optimal, hybrid controller for the knee joint has been developed, which is based on the principle of Invariance Control. Walking experiments with UT-Theta proved the knee controller crucial for successfull walking: impactless transitions in extremely short time are essential to handle quick load inversion in the knee joint at the instant of foot landing. Furthermore the controller proved very robust with respect to parameter distrubances. The successfull application of a hybrid joint offers new chances to exploit passive dynamics in humanoid robots thus increasing their efficiency.

6 Conclusions and Future Directions

6.1 Concluding Remarks

The thesis led through the development process of humanoid robots from the initial hardware design to humanoid walking control. At each step – design, posture adaptation, and control – new ideas and concepts have been introduced and validated in hardware experiments.

The first step towards humanoid biped walking is a thorough hardware design with respect to the specific requirements of the robot. Special consideration must be given to the selection of an appropriate motor-gear-combination, as oversized motors increase the weight of the robot and generally have a higher power consumption. Due to the excess weight, the walking performance is deteriorated, as only lower accelerations can be achieved.

In an attempt to generalize the design process, a systematic method has been proposed that allows to determine the actuation requirements of a robot and select an appropriate – i. e. in the case of a humanoid biped minimum weight – motor-gear-combination from the manufacturers offerings. Using a detailed dynamic model of the robot, gait trajectories for a target velocity are computed by solving an optimal control problem, minimizing e. g. the energy consumption during the step. From these gait trajectories, the requirements on the actuators for maximum torque and velocity are obtained. Although the actuator selection process has been exemplarily introduced for humanoid robots, this method is generic and can be applied to any type of robot.

Based on the motor selection process, a humanoid biped prototype has been built. In contrast to most humanoid robot projects, this small-size autonomous humanoid walking machine uses off-the-shelf components wherever possible, especially commercially available high performance DC motors. The biped is intended for fast, dynamic walking at a speed of 0.5 m/s corresponding to approx. 3 steps per second for 70 cm tall robots. Thus, the dynamic behavior is extremely important. The actuator selection method proved very useful and efficient during the design of the robot. The humanoid is a prototype and feasibility study towards a future small size walking robot, which is easily maintainable and conceived as a general platform to implement and test intelligent control systems and novel concepts in applied artificial intelligence.

These high target velocities impose significant demands on the walking controller. Two basic types of biped walking controllers – offline and online trajectory generation – have been implemented in the scope of this thesis.

The first approach is to generate gait trajectories offline and replay them on the robot. This method allows to consider special "aesthetic" criteria like smoothness and energy efficiency during the planning process. Similar to the actuator selection process, gait trajectories have been computed by solving an optimal control problem incorporating the side conditions as constraints to an optimal control problem. Thus, the step is optimized over an entire walking cycle rather than static optimizations for posture snapshots as in

most existing approaches. Convergence of this type of problems being very sensitive to initial values, which generally have to be tuned manually, they currently cannot be solved online. Hence, trajectories must be calculated offline and stored in a database.

One disadvantage of precalculated trajectories is that the robot is unable to accomplish motions for which trajectories are not available. Therefore a huge database of step primitives generally is necessary. In an effort to reduce the size of the required database and to increase the possible field of application of the robot it is therefore desirable to modify trajectories online such that they can be applied to slightly different situations than they have originally been computed for. One of the key challenges is sensor-based online modification of computed trajectories to improve walking stability and performance. A novel *Jacobi Compensation* method has been proposed that allows to move parts of the body in selected task coordinate directions using Jacobian matrices and thus alter the posture of the robot. The use of Jacobians for arbitrary posture manipulation and trajectory adaptation has not been reported yet. Experiments showed that the method increases the motion diversity and thus the versatility of the robot significantly.

Another walking control strategy has been implemented on the humanoid robot UT-Theta, developed at the University of Tokyo. One of the main difficulties lies in the great dynamical complexity of a humanoid robot. Many works on biped locomotion follow the general idea of reducing the complexity of the problem by adopting a simplified system, which could approximate the dynamics of the real robot.

The approach presented here follows the inverted pendulum concept, with the characteristic of a non instantaneous double support phase, in order to improve stability. In this approach the complex dynamics of a humanoid robot are approximated by the much simpler dynamics of a linear inverted pendulum. During the single support phase, the robot is not controlled and moves ballistically, similar to an inverted pendulum; the motion is only determined by the system state during lift-off of the swing foot. The control task is to reach the desired lift-off state by performing appropriate motions during the double support phase.

UT-Theta is equipped with a special knee joint construction allowing to switch between an actuated and a free swinging mode. This is achieved by actuating a disk with tappets rotating inside a ring with notches, which is connected to the shank. As the notches are larger than the tappets, the actuated disk can move freely within this backlash gap and drive the shank in either direction or allow free swinging.

Smooth walking motion however can only be achieved if discontinuities due to collision impact between the notches and tappets are avoided while guaranteeing short switching times. As the knee joint in contact situation only allows unilateral transmission of forces, conventional control techniques cannot be applied because of its highly nonlinear characteristics. If directions of actuation are reversed, the clutch has to traverse a backlash gap; switching times between the directions of actuation must be minimized to keep the not actuated phase of the knee short. Nevertheless, high control accuracy is required, as the contact necessary for transmitting forces from the knee to the shank must be established smoothly to avoid impact that might result in a position overshoot. To fulfill the requirements, a nonlinear, time optimal, hybrid controller for the knee joint has been developed, which is based on the principle of Invariance Control. Walking experiments with UT-Theta proved the knee controller crucial for successfull walking: impactless transitions in extremely short time are essential to handle quick load inversion in the knee joint at the instant of foot landing. Furthermore the controller proved very robust with respect to

parameter disturbances. The successfull application of a hybrid joint offers new chances to exploit passive dynamics in humanoid robots thus increasing their efficiency.

6.2 Outlook

The research presented in this dissertation is the basis for future developments in humanoid robotics. The first step directly emerging from the presented work is to construct a small size humanoid biped robot. This robot is dedicated to serve as an open platform to implement new control methods, where the robot is perceived as a hybrid system and thus is capable of incorporating different ground contact situations in the motion pattern, like rolling about the toes during pre-swing phase or landing on the heel. It is expected that the hybrid approach significantly increases walking performance and is essential for robot jogging and running; experimental results and case studies corroborate these assumptions.

With respect to future acting of the robot in a human environment, special care has to be taken of the human-robot-interaction. Currently however, humanoids are only able to act in dedicated environments that have been explicitly designed with respect to their abilities. Hence, it is important to realize a dynamic perception system allowing the robot to act in dynamically changing environments without endangering humans. This requires on the one hand high speed stereo camera systems to keep track of the changes in the environment and on the other hand sophisticated algorithms to extract and predict motions of a multitude of objects simultaneously. Furthermore, an improved object classification is needed together with an information abstraction layer and a context dependent filter, selecting relevant information and discarding obsolete data.

This information abstraction and selection process is closely linked with task oriented action and autonomous behavior selection. In order to provide a real helper and partner to a human, the robot must be capable to accept general orders and perform the assigned task autonomously without supervision or repeated instructions for single motions. Hence the capability is required to split the global task situation dependent into several necessary subtasks and decide on a suitable action sequence to accomplish the task.

Such problem formulations also rise very interesting questions about prerequisites for these abilities. It is conceivable that implementation of this kind of abilities requires qualities that so far are not attributed to machines, like emotions, arousal or elementary drives, as these traits significantly influence the importance of perceptions and constitute an order for executing tasks. Such links between worlds that seem irreconcilable on first sight, like technically inspired robotics and life sciences, medicine and psychology are a major future challenge and account for the fascination of robotics.

A Mechanical Construction of the Humanoid Prototype

This appendix discusses the design concept and system development of a small and relatively fast walking, autonomous humanoid robot with 17 degrees of freedom (DoF). The selection of motor size and gear ratios is based on numerical optimization as described in Chapter 3. Here, the mechanical realization of the robot is presented including investigations on the achievable performance of a decentralized, microcontroller-based control architecture.

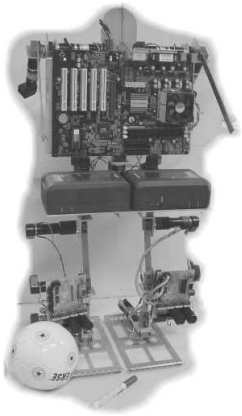

A.1 Problem Description

In this chapter, the design and mechanical realization of a new, small size and fast, autonomous humanoid walking machine are presented. The design concept is kinematically similar to PINO [135] and the Sony dream robot 3DR [55] but uses off-the-shelf, high performance DC motors. The key focus is to create an autonomous humanoid robot for fast, dynamic walking.

One self-imposed demand for the design is to keep the mechanical construction as simple, cheap, and lightweight as possible. Therefore, the robot should consist only of a small number of identical mechatronic modules linked together. Considering cost, the hardware design is based on commercially available components whenever possible. With no small, lightweight, and inexpensive motion control board commercially available at the time of conception, a microcontroller based board integrating a complete control loop has been developed. Reference and measured signals are exchanged with the central PC via the USB bus.

The selection of motors and gears as a first step of robot design has been presented in Chapter 3. It is based on fitting the most appropriate motors and gears to the generated minimal energy trajectories subject to power constraints balancing between system weight and motor power. The optimizations are performed for a walking speed of $> 0.5\,\mathrm{m/s}$. As the total height of the robot is 70–80 cm, this velocity requires roughly 3–4 steps per second.

The chapter discusses the hardware design and the software environment in Sec. A.2 and gives in Sec. A.3 a brief description of the performance of a self developed motion control board.

A.2 Hardware Design and Software Environment

The humanoid geometry is largely imposed by the RoboCup rules [107] and the proportions of its natural model [116]. Therefore the main parameters to decide for during the conceiving phase are the height – and thus weight – and the number of joints.

The decision on the height and weight are based on the criterion of keeping the humanoid manageable by a single operator. Otherwise, the robot should be easy to service, which contradicts an extensive miniaturization, as the machine easily gets cramped and parts become increasingly difficult to reach. As a compromise, a size of 70–80 cm has been chosen resulting in a weight of approx. 15 kg.

The robot is conceived as a three dimensional walker. Therefore, 12 DoF are required in the legs to allow the robot to walk around curves [92]. In fast biped walking, the swinging of the legs generates a significant moment about the vertical axis of the robot thus resulting in a twisting motion. As a means of counterbalancing this moment, the arms – having significant weight at their disposal, as two batteries are attached to them – each dispose of two degrees of freedom. Together with a further joint about the vertical axis in the navel area, also intended for vertical moment absorption, the humanoid features a total of 17 DoF, as can be seen in Fig. A.1.

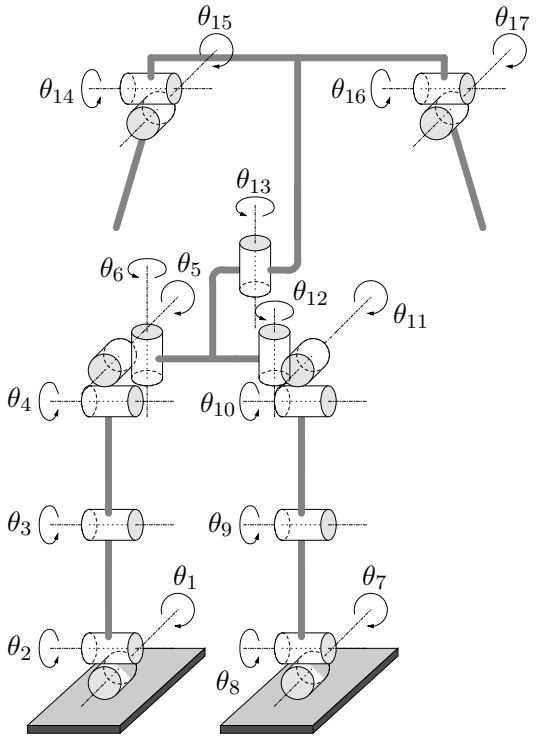

Figure A.1: Kinematic structure of the prototype robot.

For simplicity of design, one important aim is to assemble the robot from as many identical modules as possible. Therefore all joints are variations of the elementary joint shown in Fig. A.2: The shaft of the motor-gear-unit is fixed to an L-shaped base plate. Attached to the axis of the motor is a lever arm whose far end is connected to the base plate of the next joint. Though this lightweight construction spares additional bearings the motor axis is still sufficiently stable to support the exerted load. For the links between

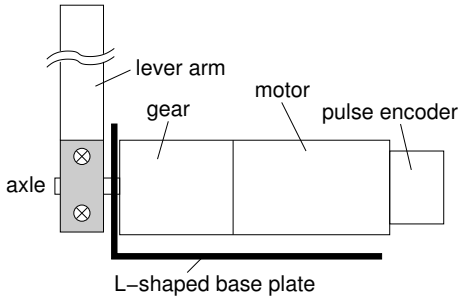

Figure A.2: Schematic of a joint.

the motors ordinary steel with a rectangular profile of $3 \times 15\,\mathrm{mm}^2$ is used. This slightly flexible construction is chosen to incorporate an additional mechanical shock absorption mechanism damping the impact of the feet hitting the ground. Joints requiring more than one DoF, like the ankle or the hip, are realized by two or more sequential motors with orthogonally oriented axes of rotation, see Fig. A.3.

The mechanical robot construction arising from linking these elementary modules is shown in Figs. A.4 and A.5. The robot carries three batteries as power supply, two of them visible on the picture at the height of the hips and below the navel joint. The third battery is located symmetrically behind the hips together with an ATX power supply for the main PC which covers the upper body. The chosen Sony BP-L90A batteries provide a capacity of 90 Wh each, thus allowing for approximately 45 min autonomous walking.

The motors are accessed using the microcontroller board shown in Figs. A.3 and A.5. The core of the board is a Motorola MC68HC908BD48 8 bit microcontroller including 3 USB endpoints, a 6 channel A/D converter and a 16 channel pulse-width modulator (PWM). The PWM signals are amplified by a National LMD18200 mosfet H-bridge, hence a motor load of up to 3 A at 55 V is admissible. The actual position of a motor is determined by evaluating the signals of pulse encoders attached to each motor using US Digital LS7266 quadrature decoders. Each board – weighing 170 g – can control 4 motors, hence representing a lightweight motion control solution.

With these components position PD control loops are implemented on the microcontroller. The A/D converters on the microcontroller are wired to sense the motor current which also allows to drive the motors with current control. The motion control boards are linked with the main PC on the robot via an USB connection. Through this link, new control inputs are delivered to the board retrieving the measured values at the same transfer stage.

For a main computer carried along by the robot a full size ATX mainboard is used. Being similar in weight compared to most full sized single board computers with equivalent computational power, a full size computer can be tolerated. The PC is equipped with an Athlon 1300 MHz CPU providing enough computational power for motion control and additional tasks such as object recognition using a camera system.

This controller board significantly decreases the size and weight of the necessary electronics. Furthermore the cabling is much easier to handle due to the decentralized architecture as only USB connections and power supply have to be wired throughout the robot.

To obtain a graphical interface to the robot and the motion control boards, a MATLAB S-function has been implemented allowing to drive the robot from within the SIMULINK

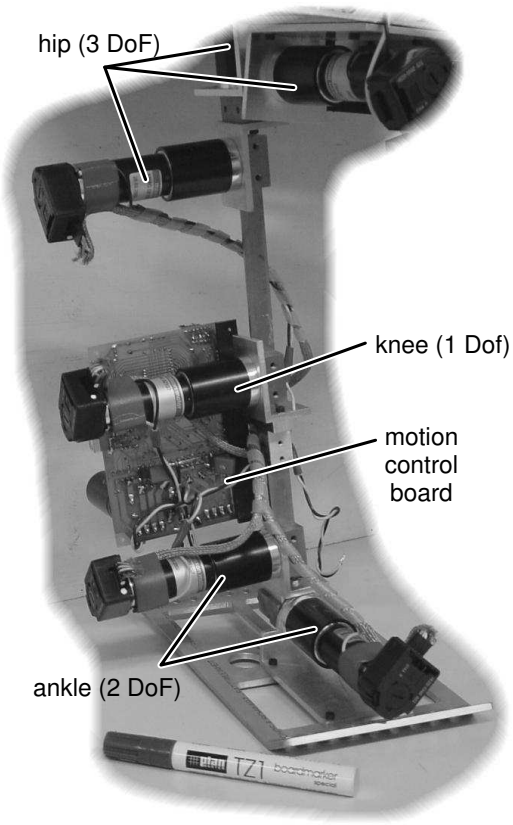

Figure A.3: Left leg rear view.

simulation environment. Experiments showed, that this rapid prototyping environment handles well the soft realtime constraints for the outer control loop without the need for a hard realtime environment as presented in [124, 125]. This may be attributable to the efficient task scheduling capabilities of the Linux kernel.

Based on this rapid control prototyping framework, future experiments can easily be implemented. Performance achievable with the decentralized solution using the microcontroller with USB connection to the PC is discussed in the following.

A.3 Performance of the Motion Control Board

In a first step, the performance of the microcontroller is investigated. One important aspect is the maximally achievable sampling rate for the control loop.

In order to obtain a sufficient minimal angle resolution, a 16 bit representation is used to index a 360° workspace, making computation time consuming on an 8 bit microcontroller. With the implemented PD position control loop for four motors, the time required for reading the actual position of the motors from the external pulse decoders, computing and applying a new control signal is 1300 μs. The USB communication requires another 240 μs computation time on the microcontroller. However, due to restrictions in the USB protocol in control transfer mode, packets may only be sent every 4 ms, hence an overall sampling rate for the position control loop of 250 Hz is achieved.

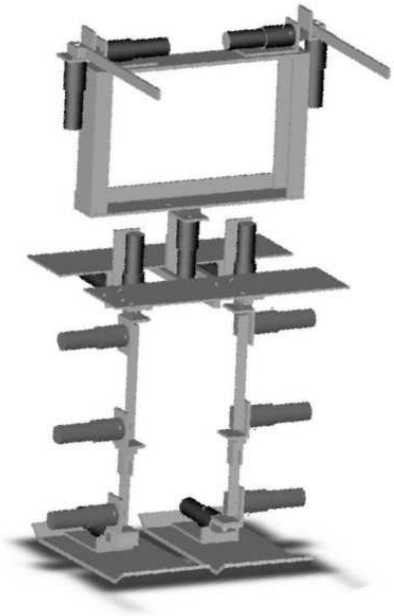

Figure A.4: CAD drawing of the robot.

The reference signal which is provided through the USB bus also can be delivered at the same rate. The PC has to send a set of four reference signals to the board and receives the latest four measured signals in return. Measurements of communication timing with two microcontroller boards attached have shown a mean communication time of 4.00 ms per board with a variance of 0.0084 $(\text{ms})^2$. This low jitter can be attributed to the efficient task scheduling mechanism of the Linux kernel, hence offering acceptable soft realtime capabilities on a machine with low system load. Implementing the data exchange with each board in separate threads, all boards can be provided with reference signals simultaneously, i. e. the communication times are not cumulative.

To test the trajectory tracking capabilities of the PD controller running at 250 Hz, one step has been executed with the robot and the performance of the ankle and the knee joint of the support leg are monitored, as shown in Fig. A.7. These joints have been chosen, as they have to support a particularly high weight, and hence show the highest control errors. However, during the experiments, the control error never exceeded 0.019 rad; this is considered sufficiently accurate for humanoid walking.

Furthermore, the PWM ratios during the step, shown in Fig. A.7 never exceed 0.4, hence the motion control boards are not working at their limit yet and have the potential to accommodate for disturbances.

Summarizing the results for the microcontroller board, a local control loop at 250 Hz can be implemented including the exchange of reference signal and measured values with a PC via USB. These rates are sufficient for motion control and prove the choice of USB for data exchange suitable for the desired purpose.

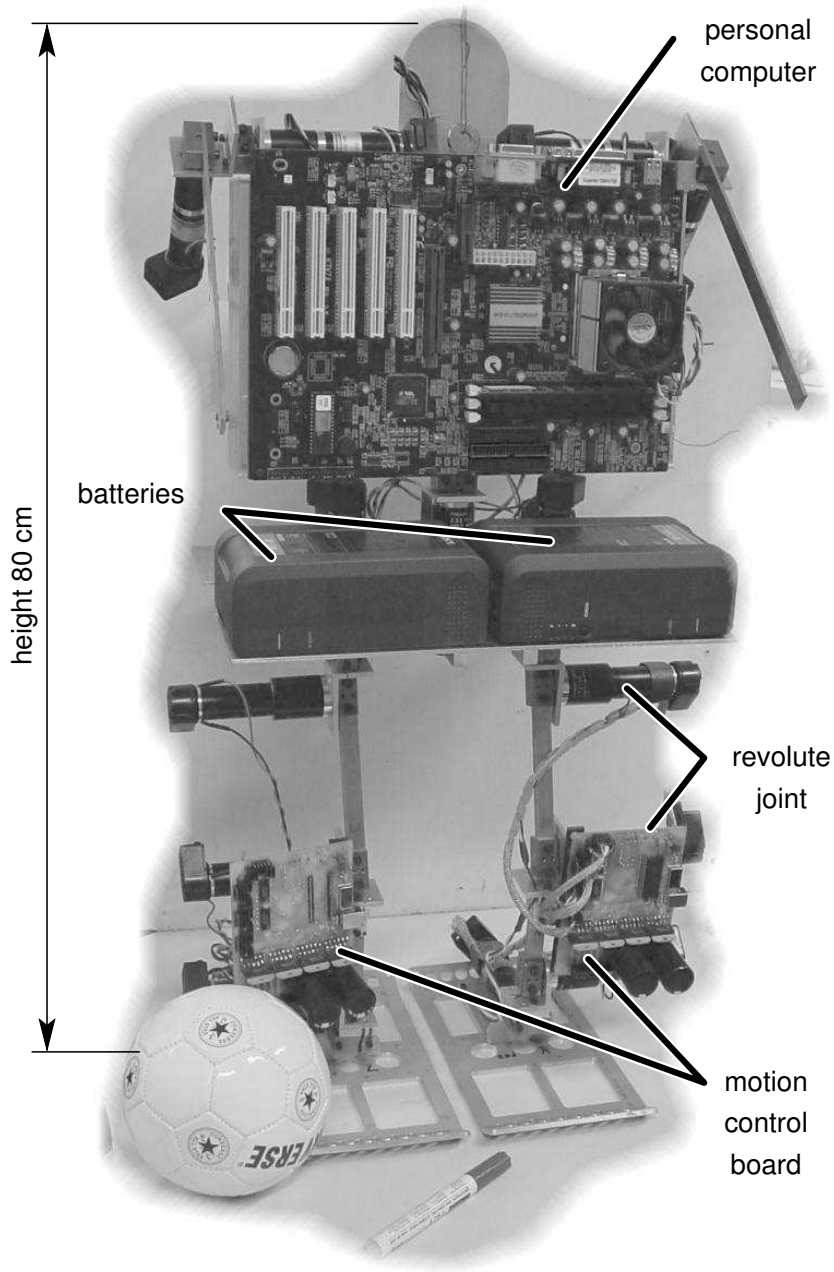

Figure A.5: Mechanical realization of the robot.

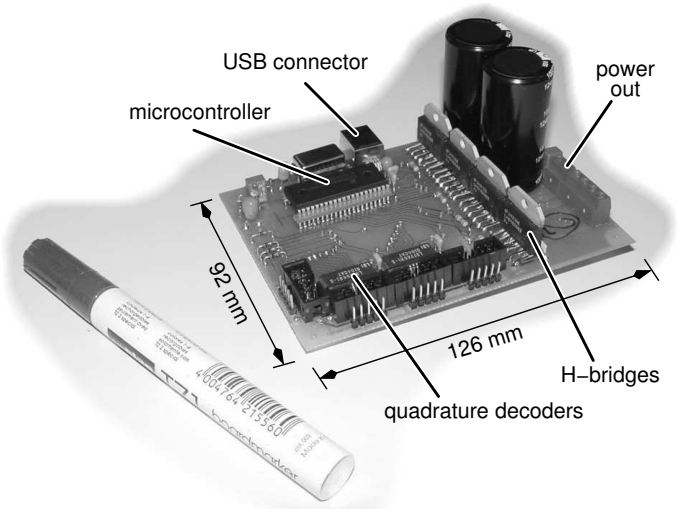

Figure A.6: Microcontroller board used to drive up to four motors.

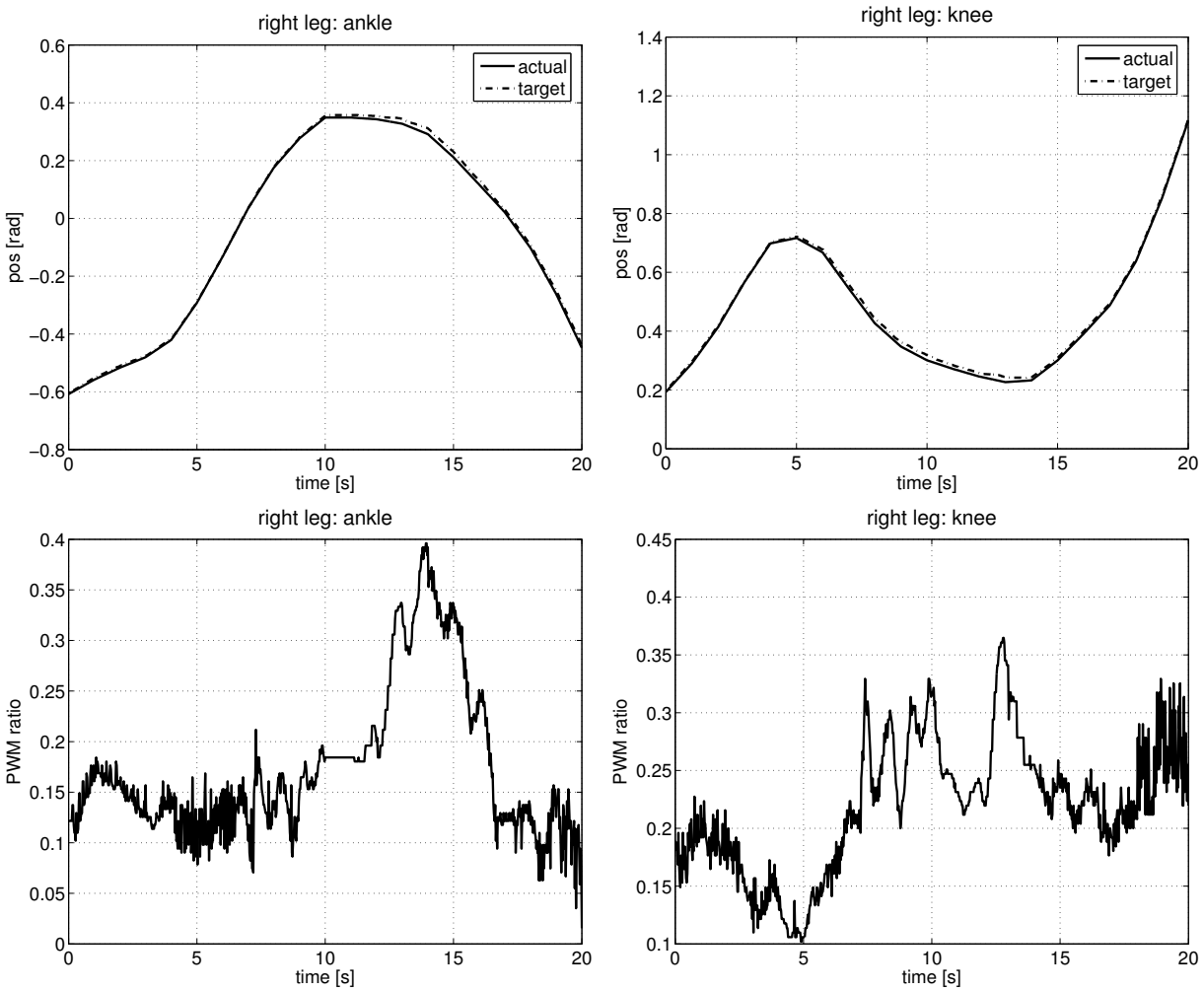

Figure A.7: Trajectory following (top) during a step for the support foot ankle (left) and knee (right). The lower plots show the corresponding PWM ratios.

A.4 Summary

In this chapter the hardware design of a new, autonomous walking robot with 17 DoF has been presented. The design is optimized for high speed walking with up to 3 steps per second, or equivalently about 0.5 m/s. Another constraint for the design was easy manufacturability, hence the robot is composed of as many identical mechatronic modules as possible.

The hardware realization of the afore discussed biped robot has been described in detail including a newly developed USB motion control board. First experiments validating this motion control board show accurate trajectory tracking capabilities proving the concept of a microcontroller communicating with a PC through USB suitable for control applications. This is regarded as crucial for the success of the biped walking project, as the motion control board solution represents a lightweight interface between the PC and the robot hardware. Due to this microcontroller solution a dedicated realtime environment on the PC proved not to be necessary. Performance of the motors so far are in line with theoretical considerations on the choice of a motor-gear-combination.

B Gait Trajectory Generation

One way of achieving humanoid biped walking is to offline calculate suitable gait trajectories and replay them on the robot. This chapter presents a method to generate such trajectories by solving an optimal control problem. Many constraints, such as energy efficiency or smoothness can be incorporated, thus allowing for dynamic and human-like motions.

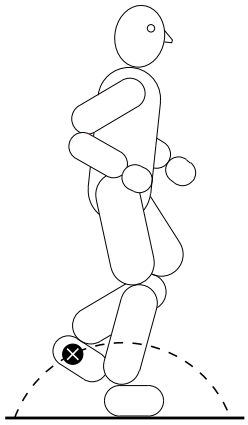

B.1 Problem Description

Currently two different strategies are being followed in research to achieve biped locomotion: Gait trajectories are either computed online according to the actual intention and perception data of the robot [38, 42, 45, 47, 104, 104, 134], or a large set of trajectories is computed offline [5, 14, 30, 127, 128] and the robot selects one of these precalculated trajectories according to the situation [60].

As suitable gait trajectories for a biped robot are subject to many constraints and the gait is required to fulfill some "aesthetic" criteria [35], like smoothness, energy efficiency and effectiveness, online generation of gait trajectories requires recursive optimization of the trajectory and cannot be computed by evaluating distinct equations. Therefore such computations generally are far from possible to be executed online with current computer power. Hence, many research groups focus on offline generation of trajectories which are modified only to achieve balance control [36].

Gait generation is divided into several tasks: One needs to set up the biped dynamics to be able to simulate the gait of the biped, and the inverse kinematics are needed to compute the location of parts of the robot given a certain link configuration. With these information, the motion of the robot is simulated with the joint torque as control input. From the walking data an objective function, the "cost" of the trajectory is computed which then is subject to further optimization.

B.2 Modeling

The dynamical model is that of a rigid, multibody system experiencing contact forces:

$$\begin{aligned} \ddot{\boldsymbol{q}} &= \boldsymbol{M}(\boldsymbol{q})^{-1}\Big(\boldsymbol{B}\,\boldsymbol{u} - \boldsymbol{C}(\boldsymbol{q},\dot{\boldsymbol{q}}) - \boldsymbol{G}(\boldsymbol{q}) + \boldsymbol{J}_c(\boldsymbol{q})^T \boldsymbol{f}_c\Big) \\ \boldsymbol{0} &= \boldsymbol{g}_c(\boldsymbol{q}) \end{aligned} \tag{B.1}$$

where $\boldsymbol{M}$ is the positive-definite mass-inertia matrix, $\boldsymbol{C}$ is the Coriolis and centrifugal force vector, $\boldsymbol{G}$ the gravitational force vector, $\boldsymbol{q}$ the generalized coordinates, and $\boldsymbol{u}(t)$ are the control inputs mapped with the constant matrix $\boldsymbol{B}$ to the actively controlled joints. The constraint Jacobian $\boldsymbol{J}_c = \frac{\partial \boldsymbol{g}_c}{\partial \boldsymbol{q}}$ is obtained from the holonomic ground contact constraints $\boldsymbol{g}_c$, and $\boldsymbol{f}_c$ is the ground contact force. These equations are evaluated using recursive, multibody algorithms which are arguably the most efficient numeric approach for calculating such high-dimensional dynamics [29].

Based on this kinematic model, gait trajectories are computed by solving an optimal control problem.

B.3 Optimized Walk of a Biped

Gait trajectories for the biped are found by solving an optimal control problem. This is done by minimizing a cost function $\boldsymbol{J}$, e. g. $\boldsymbol{J} = \int \boldsymbol{q}^T \boldsymbol{q}\,\mathrm{d}t$ subject to the system dynamics (B.1) and a number of constraints.

Constraints

The optimization constraints for gait generation [2] ensure the physical feasibility of the resulting motion. These constraints consider a *complete* gait cycle in $[0, t_f]$.

- *Periodic gait constraints*

  To ensure repeatability of a step, the system must be in the same state at the end $t = t_f$ of the gait cycle as it was in the beginning $t = 0$. The left side approach $\lim_{\varepsilon>0,\varepsilon\to 0} t_f - \varepsilon$ of the end t_f of the gait cycle is expressed by t_f^-.

  1. Periodicity of continuous state $\boldsymbol{x} = \begin{bmatrix}\boldsymbol{q} & \dot{\boldsymbol{q}}\end{bmatrix}^T$

     $$\boldsymbol{x}(t_f^-) = \boldsymbol{x}(0) \tag{B.2}$$

  2. Periodicity of ground contact forces $\boldsymbol{f}_c$:

     $$\boldsymbol{f}_c(t_f^+) = \boldsymbol{f}_c(0) \tag{B.3}$$

- *Exterior environmental constraints*

  These constraints avoid violation of physical laws when the robot is interacting with its environment.

  1. Kinematic constraints on the height (z-coordinate) of the swing leg tips.
     The foot tip must be above the ground during swing phase. The foot height $h_{\text{foot},z}$ is calculated from a forward kinematics function $f_{\text{fkin}}(\cdot)$ of the joint angles $\boldsymbol{q}$:

     $$h_{\text{foot},z} = f_{\text{fkin}}(\boldsymbol{q}(t)) \geq 0. \tag{B.4}$$

2. Ground contact forces lie within the friction cone and unilateral contact constraints are not violated. In the case of point contact, ground linear forces $\boldsymbol{F}_R = [F_{R,x}F_{R,y}F_{R,z}]^T$ must satisfy

$$\sqrt{F_{R,x}^2 + F_{R,y}^2} \leq \mu_R F_{R,z}, \quad F_{R,z} \geq 0 \tag{B.5}$$

with friction coefficient μ_R. In the case of multiple contact, such as a foot lying flat on the ground, the rotational contact force vector $\boldsymbol{F}_T = [F_{T,x}F_{T,y}F_{T,z}]^T$ is additionally constrained

$$|F_{T,x}| \leq 0.5\, F_z l_{y,\text{foot}}, \quad |F_{T,y}| \leq 0.5\, F_{T,z} l_{x,\text{foot}}, \quad |F_{T,z}| \leq \mu_T F_z \tag{B.6}$$

where μ_T is a friction coefficient, and $l_{x,\text{foot}}$ and $l_{y,\text{foot}}$ are the length and width of the foot.

- *Interior modeling constraints*

These constraints guarantee the validity of the dynamical model at discontinous points. Discontinuities occur especially when the swing foot collides with the ground and the optimization has to switch between different dynamical models to account for changes in the dynamical properties due to a new contact situation.

1. Jump conditions in the system velocities due to inelastic collisions of the legs with the ground. If the exterior constraint (B.4) is violated, a collision occurs. The resulting instantaneous jump in the state velocities at the k-th such collision event is

$$\dot{q}(t_{S,k}^+) = \sigma(\boldsymbol{q}(t_{S,k}^-), \dot{\boldsymbol{q}}(t_{S,k}^-)) \tag{B.7}$$

where $\boldsymbol{q}(t_{S,k}^-)$ and $\boldsymbol{q}(t_{S,k}^+)$ indicate the values of $\boldsymbol{q}$ just before and after the collision event respectively. The function $\sigma(\cdot)$ calculates the jump in the state velocities resulting from the point of collision instantaneously reaching a zero velocity.

2. Magnitude bounds on states, controls and control rates:

$$\begin{array}{ll} L_{\boldsymbol{q}} \leq \boldsymbol{q} \leq U_{\boldsymbol{q}} & L_{\dot{\boldsymbol{q}}} \leq \dot{\boldsymbol{q}} \leq U_{\dot{\boldsymbol{q}}} \\ L_{\boldsymbol{u}} \leq \boldsymbol{u} \leq U_{\boldsymbol{u}} & L_{\dot{\boldsymbol{u}}} \leq \dot{\boldsymbol{u}} \leq U_{\dot{\boldsymbol{u}}} \end{array} \tag{B.8}$$

$L_{(\cdot)}$ and $U_{(\cdot)}$ are constant vectors of length equal to their arguments.

3. Actuator torque-speed limitations. The applied torque at the actuated joint i is constrained by the characteristic line of the motor-gear train:

$$|u_i| \leq (\dot{q}_{\max,i} - |\dot{q}_i|)\frac{G_i^2 \eta_i}{s_i}, \tag{B.9}$$

where u_i is the applied torque at joint i, $\dot{q}_i$ and $\dot{q}_{max,i}$ are the joint i velocity and maximum absolute joint velocity respectively, G_i is the gear ration, η_i is the gear efficiency and s_i is the slope of the motor characteristic line.

Based on these constraints and the dynamical model, the biped gait can be optimized using different performance criteria.

Gait optimization

The question of optimality is subject to the demands the gait is supposed to fulfill. Hence in the following, three criteria are presented reflecting different aspects of gait quality.

Balance Performance 1: Average distance in the ground plane between the FRI and the ground projected center of mass GCoM normalized by the distance traveled d.

$$\boldsymbol{J}_{s1}(\boldsymbol{q}, \dot{\boldsymbol{q}}, \boldsymbol{u}) = \frac{1}{d} \int_0^{t_f} \|\mathrm{GCoM} - \mathrm{FRI}\|^2 \, \mathrm{d}t \tag{B.10}$$

This value alone is not sufficient to verify or design a dynamically balanced gait, yet it may be combined with additional dynamic measures of the system such as the angular momentum which can provide a stability assessment during gait optimization, simulation, and on-line control.

Efficiency is secondary in importance to balanced gait in legged systems, but it can also have a strong influence in the successful design of an autonomous biped. A challenge for systems with limited power supply is to combine energy conserving motion with a balanced gait. It has been witnessed in humans that steady-state forward walking approximates a minimum energy motion according to a dynamical model for the human body [85]. An attempt to reproduce smooth, natural motion should also take these factors into account.

Energy Performance 1: In legged systems where a high torque is generated by a large current in the motor, the primary form of energy loss is called the Joule thermal loss [50]. One may minimize the integral of this value over the gait:

$$\boldsymbol{J}_{e1}(\boldsymbol{u}) = \frac{1}{s} \int_0^{t_f} \sum_{i=1}^{N} R_i \left(\frac{u_i}{G_i K_i} \right)^2 \, \mathrm{d}t \tag{B.11}$$

where R_i, G_i, K_i, and u_i are the armature resistance, gear ratio, torque factor, and applied torque for link i respectively, while s is the step length or total distance traveled over one stride.

Energy Performance 2: Another efficiency cost criterion is the specific resistance ε as used in [25]. This measures the output power in relation to the mass moved and the velocity attained and is a dimensionless quantity. Its integral over the gait cycle is a normalized form of the kinetic energy

$$\boldsymbol{J}_{e2}[\dot{\boldsymbol{q}}, \boldsymbol{u}] = \int_0^{t_f} \frac{\sum_{i=1}^{N} |u_i \dot{q}_i|}{mgv} \mathrm{d}t \ , \tag{B.12}$$

where m is the mass of the system, $\dot{q}_i$ is the joint i angle velocity and v is the average forward velocity.

Working with those criteria, the Energy Performance $\boldsymbol{J}_{e1}$ turned out to produce smooth trajectories and show best convergence during the optimization process. However, combinations of these performance measures are generally needed to obtain the desired results.

B.4 Summary

Optimal control problems offer a possibility to consider "aesthetic" criteria like smoothness and energy efficiency during the planning process of humanoid gait trajectories. Side conditions can be described by constraints to the problem, where a cost function – assessing e. g. the energy consumption – is minimized. Thus, the step is optimized over an entire walking cycle rather than static optimizations for posture snapshots as in most existing approaches.

This type of problems currently cannot be solved online, as convergence of the optimization is very sensitive to initial values. Good starting values generally cannot be found automatically and thus have to be tuned manually. A solution is to calculate the trajectories offline and store them in a huge database; the robot selects the appropriate gait pattern online.

The gait trajectories generated with the method described in this chapter proved in hardware experiments very smooth. Although convergence of the problem is rather delicate, many constraints could be incorporated rendering the method very useful for obtaining suitable walking patterns.

Bibliography

[1] AIST. HRP-2. `http://www.kawada.co.jp/global/ams/hrp_2.html`, 1998–2002.

[2] T. Arakawa and T. Fukuda. Natural motion trajectory generation of biped locomotion robot using genetic algorithm through energy optimization. In *Proceedings of the International Conference on Systems, Man and Cybernetics*, pages 1495–1500, 1996.

[3] T. Arakawa and T. Fukuda. Natural motion generation of biped locomotion robot using hierarchical trajectory generation method consisting of GA, EP layers. In *Proceedings of the IEEE International Conference on Robotics and Automation*, pages 211–216, Albuquerque, New Mexico, USA, 1997.

[4] I. Asimov. *I, Robot*. Spectra, 1991.

[5] J.-M. Bourgeot, N. Cislo, and B. Espiau. Path-planning and tracking in a 3D comlex environment for an anthropomorphic biped robot. In *Proceedings of the IEEE/RSJ International Conference on Intelligent Robots and Systems IROS*, pages 2509–2514, Lausanne, Switzerland, October 2002.

[6] M. Buss, M. Hardt, J. Kiener, M. Sobotka, M. Stelzer, O. von Stryk, and **D. Wollherr**. Towards an autonomous, humanoid, and dynamically walking robot: Modelling, optimal trajectory planning, hardware architecture, and experiments. In *Proceedings of the IEEE/RAS International Conference on Humanoid Robots*, Karlsruhe, Germany, 2003.

[7] Cabinet Office Japan. Annual report on the aging society: 2004 (summary). `http://www8.cao.go.jp/kourei/english/annualreport/2004/04wp-e.html`, 2004.

[8] G. Capi, Y. Nasu, L. Barolli, M. Yamano, K. Mitobe, and K. Takeda. A neural network implementation of biped robot optimal gait during walking generated by genetic algorithm. In *Proceedings of the Mediterranean Conference on Control and Automation*, Dubrovnik, Croatia, 2001.

[9] S. Collins, A. Ruina, R. Tedrake, and M. Wisse. Efficient bipedal robots based on passive-dynamic walkers. *Science*, 307:1082–1085, February 2005.

[10] S. H. Collins, M. Wisse, and A. Ruina. A three-dimensional passive-dynamic walking robot with two legs and knees. *The International Journal of Robotics Research*, 20(7):607–615, July 2001.

[11] R. Cupec. *Scene Reconstruction and Free Space Representation for Biped Walking Robots*. PhD thesis, Institute of Automatic Control Engineering (LSR), Technische Universität München, München, Germany, *to be published*.

[12] A. Dasgupta and Y. Nakamura. Making feasible walking motion of humanoid robots from human motion capture data. In *Proceedings of the IEEE International Conference on Robotics and Automation*, pages 1044–1049, Detroit, Michigan, May 1999.

[13] J. Denk. *Optimierungsbasierte Berechnung von Schrittprimitiven und Schrittsequenzen für perzeptionsgeführte zweibeinige Roboter*. PhD thesis, Institute of Automatic Control Engineering (LSR), Technische Universität München, München, Germany, 2004.

[14] J. Denk and G. Schmidt. Synthesis of a walking primitive database for a humanoid robot using optimal control techniques. In *Proceedings of the IEEE/RAS International Conference on Humanoid Robots*, pages 319–326, Tokyo, Japan, 2001.

[15] K. Doya. Walking pattern learning robot. *Journal of the Robotics Society in Japan*, 8(3):117, 1990.

[16] The RoboCup Federation. `http://www.robocup.org`.

[17] Y. Fujimoto and A. Kawamura. Simulation of an autonomous biped walking robot including environmental force interaction. *IEEE Robotics and Automation Magazine*, 5(2):33–42, June 1998.

[18] Fujitsu Automation. HOAP. `http://www.automation.fujitsu.com/en/products/products12.html`.

[19] K. Fujiwara, F. Kanehiro, S. Kajita, and H. Hirukawa. Safe knee landing of a human-size humanoid robot while falling forward. In *Proceedings of the IEEE/RSJ International Conference on Intelligent Robots and Systems IROS*, pages 503–508, Sendai, Japan, 2004.

[20] T. Fukaushima, Y. Kuroki, and T. Ishida. Development of a new actuator for a small biped walking entertainment robot. In *Proceedings of the International Conference on Power Electronics, Machines and Drives*, pages 126–131, Edinburgh, UK, 2004.

[21] M. Gienger. *Entwurf und Realisierung einer zweibeinigen Laufmaschine*. PhD thesis, Institute for Applied Mechanics, Technische Universität München, München, Germany, 2004.

[22] M. Gienger, K. Löffler, and F. Pfeiffer. Walking control of a biped robot based on inertial measurement. In *Proceedings of the International Workshop on Humanoid and Human Friendly Robotics (IARP)*, pages 22–29, Tsukuba, Japan, 2002.

[23] A. Goswami. Foot rotation indicator (FRI) point: A new gait planning tool to evaluate postural stability of biped robots. In *Proceedings of the IEEE International Conference on Robotics and Automation*, pages 47–52, Detroit, Michigan, May 1999.

[24] A. Goswami. Postural stability of biped robots and the foot rotation indicator (FRI) point. *International Journal of Robotics Research*, 18(6):523–533, 1999.

[25] P. Gregorio, M. Ahmadi, and M. Buehler. Design, control, and energetics of an electrically actuated legged robot. *IEEE Transactions on Systems, Man, and Cybernetics – Part B*, 27(4):626–634, 1997.

[26] Y. Guan, K. Yokoi, N. E. Sian, and K. Tanie. Feasibility of humanoid robots stepping over obstacles. In *Proceedings of the IEEE/RSJ International Conference on Intelligent Robots and Systems IROS*, pages 130–135, Sendai, Japan, 2004.

[27] M. Hardt. *Multibody Dynamical Algorithms, Numerical Optimal Control, with Detailed Studies in the Control of Jet Engine Compressors and Biped Walking*. PhD thesis, Department of Electrical & Computer Engineering, University of Califonia, San Diego, San Diego, California, 1999.

[28] M. Hardt, J.W. Helton, and K. Kreutz-Delgado. Optimal biped walking with a complete dynamical model. In *Proceedings of the IEEE Conference on Decision and Control*, pages 2999–3004, Arizona, USA, 1999.

[29] M. Hardt and O. von Stryk. The role of motion dynamics in the design, control and stability of bipedal and quadrupedal robots. In *Proc. RoboCup 2002 International Symposium*, Fukuoka, Japan, 2002.

[30] M. Hardt, **D. Wollherr**, M. Buss, and O. von Stryk. Design of an autonomous fast-walking humanoid robot. In *Proceedings of the 5th International Conference on Climbing and Walking Robots*, pages 391–398, Paris, France, 2002.

[31] A. Helm, M. Hardt, O. von Stryk, and R. Höpler. Development of a toolbox for model-based real-time simulation and analysis of legged robots. In *Proceedings of the GAMM Conference*, Augsburg, Germany, March 2002.

[32] K. Hirai, M. Hirose, Y. Haikawa, and T. Takenaka. The development of Honda humanoid robot. In *Proceedings of the IEEE International Conference on Robotics and Automation*, pages 1321–1326, Leuven, Belgium, 1998.

[33] M. Hirose, Y. Haikawa, T. Takenaka, and K. Hirai. Development of humanoid robot ASIMO. In *IEEE/RSJ International Conference on Intelligent Robots and Systems (IROS) – Workshop 2*, Maui, Hawaii, 2001.

[34] Honda Motor Co. ASIMO. `http://world.honda.com/ASIMO/`, since 1986.

[35] Q. Huang, S. Kajita, N. Koyachi, K. Kaneko, K. Yokoi, T. Kotoku, H. Arai, K. Komoriya, and K. Tanie. Walking pattern and actuator specification for a biped robot. In *Proceedings of the IEEE/RSJ International Conference on Intelligent Robots and Systems IROS*, pages 1462–1468, Kyongju, Korea, 1999.

[36] Q. Huang, K. Kaneko, K. Yokoi, S. Kajita, T. Kotoku, N. Koyachi, H. Arai, N. Imamura, K. Komoriya, and K. Tanie. Balance control of a biped robot combining off-line pattern with real-time modification. In *Proceedings of the IEEE International Conference on Robotics and Automation*, pages 3346–3352, San Francisco, CA, April 2000.

[37] M. Inaba, T. Igarashi, S. Kagami, and H. Inoue. A 35 DOF humanoid that can coordinate arms and legs in standing up, reaching and grasping an object. In *Proceedings of the IEEE/RSJ International Conference on Intelligent Robots and Systems IROS*, pages 29–36, Osaka, Japan, 1996.

[38] M. Inaba, F. Kanehiro, S. Kagami, and H. Inoue. Two-armed bipedal robot that can walk, roll over and stand up. In *Proceedings of the IEEE/RSJ International Conference on Intelligent Robots and Systems IROS*, pages 297–302, 1995.

[39] H. Inoue and H. Hirukawa. Explorations of humanoid robot applications. In *Proceedings of the IEEE/RAS International Conference on Humanoid Robots*, pages 497–499, Tokyo, Japan, 2001.

[40] T. Ishida, Y. Kuroki, and J. Yamaguchi. Mechanical system of a small biped entertainment robot. In *Proceedings of the IEEE/RSJ International Conference on Intelligent Robots and Systems IROS*, pages 1129–1134, Las Vegas, NV, USA, 2003.

[41] A. Isidori. *Nonlinear Control Systems*. Springer Verlag, Berlin, 1995.

[42] S. Kajita, F. Kanehiro, K. Kaneko, K. Fujiwara, K. Yokoi, and H. Hirukawa. A real-time pattern generator for biped walking. In *Proceedings of the IEEE International Conference on Robotics and Automation*, pages 31–37, Washington, DC, 2002.

[43] S. Kajita, F. Kanehiro, K. Kaneko, K. Yokoi, and H. Hirukawa. The 3D linear inverted pendulum mode: A simple modeling for a biped walking pattern generation. In *Proceedings of the IEEE/RSJ International Conference on Intelligent Robots and Systems IROS*, pages 239–246, Lausanne, Switzerland, 2001.

[44] S. Kajita, O. Matsumoto, and M. Saigo. Real-time 3D walking pattern generation for a biped robot with telescopic legs. In *Proceedings of the IEEE International Conference on Robotics and Automation*, pages 2299–2306, Seoul, Korea, 2001.

[45] S. Kajita and K. Tani. Study of dynamic biped locomotion on rugged terrain. In *Proceedings of the IEEE International Conference on Robotics and Automation*, pages 1405–1411, Sacramento, CA, USA, April 1991.

[46] S. Kajita and K. Tani. Experimental study of biped dynamic walking in the linear inverted pendulum mode. In *Proceedings of the IEEE International Conference on Robotics and Automation*, pages 2885–2891, Nagoya, Japan, 1995.

[47] S. Kajita, T. Yamaura, and A. Kobayashi. Dynamic walking control of a biped robot along a potential energy conserving orbit. *IEEE Transactions on Robotics and Automation*, 8(4):431–438, August 1992.

[48] K. Kaneko, F. Kanehiro, S. Kajita, H. Hirukawa, T. Kawasaki, M. Hirata, K. Akachi, and T. Isozumi. Humanoid robot HRP-2. In *Proceedings of the IEEE International Conference on Robotics and Automation*, pages 1083–1090, New Orleans, LA, USA, 2004.

[49] D. Katić and M. Vukobratović. Survey of intelligent control techniques for humanoid robots. *Journal of Intelligent and Robotic Systems*, 37:117–141, 2003.

[50] H. Kimura, I. Shimoyama, and H. Miura. Dynamics in the dynamic walk of a quadruped robot. *Journal on Advanced Robotics*, 4(3):283–301, 1990.

[51] Kitano Symbiotic Systems Project, ERATO, Japan Science and Technology Corp. PINO. `http://www.symbio.jst.go.jp/~yamasaki/`, since 1999.

[52] A. Konno, N. Kato, S. Shirata, T. Furuta, and M. Uchiyama. Development of a light-weight biped humanoid robot. In *Proceedings of the IEEE/RSJ International Conference on Intelligent Robots and Systems IROS*, pages 1565–1570, Takamatsu, Japan, 2000.

[53] A. L. Kun and W. T. Miller. Control of variable-speed gaits for a biped robot. *IEEE Robotics and Automation Magazine*, pages 19–29, September 1999.

[54] Y. Kuroki, B. Blank, T. Mikami, P. Mayeux, A. Miyamoto, R. Playter, K. Nagasaka, M. Raibert, M. Nagano, and J. Yamaguchi. Motion creating system for a small biped entertainment robot. In *Proceedings of the IEEE/RSJ International Conference on Intelligent Robots and Systems IROS*, pages 1394–1399, Las Vegas, NV, USA, 2003.

[55] Y. Kuroki, T. Ishida, and J. Yamaguchi. A small biped entertainment robot SDR-3X. In *IEEE/RSJ International Conference on Intelligent Robots and Systems (IROS) – Workshop 2*, Maui, Hawaii, 2001.

[56] J. Laci, H. Hooshang, and C. Bradley. A control strategy for adaptive bipedal locomotion. In *Proceedings of the IEEE International Conference on Robotics and Automation*, pages 563–569, Minneapolis, Minnesota, 1996.

[57] K. Löffler, M. Gienger, and F. Pfeiffer. Sensor and control design of a dynamically stable biped robot. In *Proceedings of the IEEE International Conference on Robotics and Automation*, pages 484–490, Taipei, Taiwan, 2003.

[58] S. Lohmeier, K. Löffler, M. Gienger, H. Ulbrich, and F. Pfeiffer. Computer system and control of biped "johnnie". In *Proceedings of the IEEE International Conference on Robotics and Automation*, pages 4222–4227, New Orleans, LA, USA, 2004.

[59] O. Lorch. *Beiträge zur visuellen Führung zweibeiniger Laufroboter in einem strukturierten Szenario*. PhD thesis, Institute of Automatic Control Engineering (LSR), Technische Universität München, München, Germany, 2003.

[60] O. Lorch, A. Albert, J. Denk, M. Gerecke, R. Cupec, J. F. Seara, W. Gerth, and G. Schmidt. Experiments in vision-guided biped walking. In *Proceedings of the IEEE/RSJ International Conference on Intelligent Robots and Systems IROS*, pages 2484–2490, Lausanne, Switzerland, 2002.

[61] O. Lorch, J. Denk, J. F. Seara, M. Buss, and G. Schmidt. Coordination of perception and locomotion planning for goal-oriented walking. In *Proceedings of the International Conference on Climbing and Walking Robots*, pages 183–192, Madrid, Spanien, 2000.

[62] J. Mareczek. *Invarianzregelung einer Klasse unteraktuierter Systeme*. PhD thesis, Institute of Automatic Control Engineering, Technische Universität München, München, Germany, 2001.

[63] J. Mareczek, **D. Wollherr**, M. Buss, and G. Schmidt. Rollover avoidance for steerable vehicles by invariance control. In *Proceedings of the European Control Conference*, pages 3522–3527, Porto, Portugal, 2001.

[64] J. Mareczek, **D. Wollherr**, and M. Buss und G. Schmidt. Überschlagsvermeidung bei Kraftfahrzeugen durch Invarianzregelung. *at - Automatisierungstechnik*, 50(2):70–78, 2001.

[65] K. Matsuoka. Mechanisms of frequency and pattern control in the neural rhythm generators. *Biological Cybernetics*, 56:345–353, 1987.

[66] Maxon Motor AG, Sachseln, Switzerland. *Maxon Motor Product Catalogue*, 2005.

[67] T. McGeer. Powered flight, child's play, silly wheels and walking machines. In *Proceedings of the IEEE International Conference on Robotics and Automation*, pages 1592–1597, 1989.

[68] T. McGeer. Passive dynamic walking. *International Journal of Robotics Research*, 9(2):62–82, April 1990.

[69] T. McGeer. Passive walking with knees. In *Proceedings of the IEEE International Conference on Robotics and Automation*, pages 1640–1645, 1990.

[70] T. McGeer. Dynamics and control of bipedal locomotion. *Journal of Theoretical Biology*, 163:277–314, 1993.

[71] P. J. McKerrow. *Introduction to Robotics*. Addison-Wesley, Sydney, Australia, 1991.

[72] H. Miura and I. Shimoyama. Dynamic walk of a biped. *The International Journal of Robotics Research*, 3(2):60–74, 1984.

[73] H. Miwa, T. Okuchi, H. Takanobu, and A. Takanishi. Development of a new human-like head robot WE-4. In *Proceedings of the IEEE/RSJ International Conference on Intelligent Robots and Systems IROS*, pages 2443–2448, Lausanne, Switzerland, September 2002.

[74] T. Nagasaki, S. Kajita, K. Kaneko, K. Yokoi, and K. Tanie. A running experiment of humanoid biped. In *Proceedings of the IEEE/RSJ International Conference on Intelligent Robots and Systems IROS*, pages 136–141, Sendai, Japan, 2004.

[75] Y. Nakamura. *Advanced Robotics – Redundancy and Optimization*. Addison Wesley, Reading, Massachusetts, 1991.

[76] Y. Nakamura, M. Okada, T. Shinohara, T. Goto, and S. Ban. Mechanical challenges for further humanoid robot evolution. In *Proceedings of The Third IARP International Workshop on Humanoid and Human Friendly Robotics*, Tsukuba, Japan, 2002.

[77] Napoleon, S. Nakaura, and M. Sampei. Balance control analysis of humanoid robot based on ZMP feedback control. In *Proceedings of the IEEE/RSJ International Conference on Intelligent Robots and Systems IROS*, pages 2437–2442, Lausanne, Switzerland, 2002.

[78] K. Nishiwaki, T.Sugihara, S. Kagami, F. Kanehiro, M. Inaba, and H. Inoue. Design and development of research platform for perception action integration in humanoid robot: H6. In *Proceedings of the IEEE/RSJ International Conference on Intelligent Robots and Systems IROS*, pages 1559–1564, Takamatsu, Japan, 2000.

[79] M. Okada, T. Shinohara, T. Gotoh, S. Ban, and Y. Nakamura. Double spherical joint and backlash clutch for lower limbs of humanoids. In *Proceedings of the IEEE International Conference on Robotics and Automation*, pages 491–496, Taipei, Taiwan, 2003.

[80] M. Okada, T. Shinohara, T. Gotoh, S. Ban, and Y. Nakamura. Humanoid robot mechanisms for responsive mobility. In *Proceedings of the 2nd International Symposium on Adaptive Motion of Animals and Machines*, 2003.

[81] M. Papageorgiou. *Optimierung*. Oldenbourg Verlag, Munich, Germany, 1991.

[82] M. Raibert. *Legged Robots That Balance*. MIT Press Cambridge, 1986.

[83] M. Raibert, B. Brown, and M. Chepponis. Experiments in balance with a 3d one-legged hopping machine. *The International Journal of Robotics Research*, 3(2):75–92, 1984.

[84] M. Raibert, S. Tzafestas, and C. Tzfestas. Comparative simulation study of three control techniques applied to a biped robot. In *Proceedings of the IEEE International Conference on Systems, Man, and Cybernetics*, pages 494–502, Le Touquet, France, 1993.

[85] J. Rose and J.G. Gamble. *Human Walking*. Williams & Wilkins, Baltimore, 1994.

[86] J. K. Salisbury and J. T. Craig. Articulated hands: Force control and kinematic issues. *International Journal of Robotics Research*, 1(1):4–17, 1982.

[87] S. Sastry. *Nonlinear Systems – Analysis, Stability, and Control*. Springer-Verlag, New York, 1999.

[88] L. Sciavicco and B. Siciliano. *Modelling and Control of Robot Manipulators*. Springer-Verlag, Berlin, Heidelberg, New York, 2001.

[89] J. F. Seara. *Intelligent Gaze Control for Vision-Guided Humanoid Walking*. PhD thesis, Institute of Automatic Control Engineering (LSR), Technische Universität München, München, Germany, 2004.

[90] J. F. Seara, K. H. Strobl, E. Martín, and G. Schmidt. Task-oriented and situation-dependent gaze control for vision guided humanoid walking. In *Proceedings of the IEEE/RAS International Conference on Humanoid Robots*, Karlsruhe, Germany, 2003.

[91] C.-L. Shih. Ascending and descending stairs for a biped robot. *IEEE Transactions on Systems, Man, and Cybernetics – Part A: Systems and Humans*, 29(3):255–268, May 1999.

[92] F. R. Sias Jr. and Y. F. Zheng. How many degrees of freedom does a biped need? In *Proceedings of the IEEE/RSJ International Conference on Intelligent Robots and Systems IROS*, pages 297–302, 1990.

[93] J.-J. Slotine and W. Li. *Applied Nonlinear Control*. Prentice Hall, Englewood Cliffs, New Jersey, 1991.

[94] M. Sobotka, **D. Wollherr**, and M. Buss. A jacobian method for online modification of precalculated gait trajectories. In *Proceedings of the 6th International Conference on Climbing and Walking Robots*, pages 435–442, Catania, Italy, 2003.

[95] Sony Corp. Sony dream robot – QRIO. `http://www.sony.net/SonyInfo/QRIO/`.

[96] M. Spong. Passivity based control of the compass gait biped. In *Proceedings of the IFAC Triennial World Congress*, Beijing, China, 1999.

[97] M. Spong. The passivity paradigm in bipedal locomotion. In *Proceedings of the International Conference on Climbing and Walking Robots*, Madrid, Spain, 2004.

[98] M. Spong and F. Bullo. Controlled symmetries and passive walking. In *Proceedings of the IFAC Triennial World Congress*, Barcelona, Spain, 2002.

[99] T. Sugihara. *Mobility Enhancement control of Humanoid Robot Based on Reaction Force Manipulation via Whole Body Motion*. PhD thesis, Department of Mechano-Informatics, The University of Tokyo, Tokyo, Japan, 2004.

[100] T. Sugihara and Y. Nakamura. Whole-body cooperative balancing of humanoid robot using cog jacobian. In *Proceedings of the IEEE/RSJ International Conference on Intelligent Robots and Systems IROS*, pages 2575–2580, Lausanne, Switzerland, 2002.

[101] T. Sugihara and Y. Nakamura. Contact phase invariant control for humanoid robot based on variable impedant inverted pendulum model. In *Proceedings of the IEEE International Conference on Robotics and Automation*, pages 51–55, Taipei, Taiwan, 2003.

[102] T. Sugihara, Y. Nakamura, and H. Inoue. Realtime humanoid motion generation through ZMP manipulation based on inverted pendulum control. In *Proceedings of the IEEE International Conference on Robotics and Automation*, pages 1404–1409, Washington, DC, USA, 2002.

[103] G. Taga. Self-organized control of bipedal locomotion by neural oscillators in unpredictable environment. *Biological Cybernetics*, 65:147–159, 1991.

[104] K. Tani, K. Ikeda, T. Yano, S. Kajita, and O. Matsumoto. The concept of model free robotics for robots to act in uncertain environments. In *Proceedings of the IEEE/Tsukuba International Workshop on Advanced Robotics*, pages 85–90, Tsukuba, Japan, November 1993.

[105] Technische Universität München. Johnnie. `http://www.amm.mw.tu-muenchen.de`, 1998–2004.

[106] O. Tezuka. *Astro Boy*. Dark Horse Manga, Milwaukie, OR, USA, 2002.

[107] The RoboCup Federation. *RoboCup Humanoid League 2002 Rule*. `http://www.robocup.org/regulations/humanoid/rule_humanoid.htm`, 2002.

[108] The University of Queensland. Guroo. `http://www.itee.uq.edu.au/~damien/GuRoo/`, since 2001.

[109] The University of Tokyo. H6. `http://www.jsk.t.u-tokyo.ac.jp/research/h6/H6_H7.html`, since 2000.

[110] The University of Tokyo. UT-μ:mighty. `http://www.ynl.t.u-tokyo.ac.jp/research/miu/miu.html`, since 2002.

[111] The University of Tokyo. UT-Theta. `http://www.ynl.t.u-tokyo.ac.jp/research/theta/theta.html`, since 2001.

[112] S. Thrun, J. Schulte, and C. Rosenberg. Interaction with mobile robots in public places. *IEEE Journal on Intelligent Systems*, pages 7–11, July/August 2000.

[113] Toyota Motor Corp. Partner Robots. `http://www.toyota.co.jp/en/special/robot/`.

[114] University of Hannover. BARt-UH. `http://www.biped.irt.uni-hannover.de`, 1999.

[115] K. Čapek. *R.U.R. – Rossum's Universal Robots*. Dover Publications, 2001.

[116] M. Vitruvius Pollio. *De Architectura Libri Decem (Ten Books on Architecture), Book III*, chapter 3 (Classification of Temples). not bequeathed, presumably 33–14 B.C.

[117] O. von Stryk. *User's Guide for DIRCOL: A Direct Collocation Method for the Numerical Solution of Optimal Control Problems*. Lehrstuhl für Höhere Mathematik und Numerische Mathematik, Technische Universität, München, 2.1 edition, 1999.

[118] M. Vukobratović, B. Borovac, and D. Ŝurdilović. Zero-moment point – proper interpretation and new applications. In *Proceedings of the IEEE/RAS International Conference on Humanoid Robots*, pages 237–244, Tokyo, Japan, 2001.

[119] M. Vukobratović and D. Juriĉiĉ. Contribution to the synthesis of biped gait. *IEEE Transactions on Bio-Medical Engineering*, BME-16(1):1–6, January 1969.

[120] M. Vukobratović and J. Stepanenko. On the stability of anthropomorphic systems. *Mathematical Biosciences*, 15:1–37, 1972.

[121] M. Vukobratović and J. Stepanenko. Mathematical models of gerneral anthropomorphic systems. *Mathematical Biosciences*, 17:191–242, 1973.

[122] Waseda University. Wabian. `http://www.shirai.info.waseda.ac.jp/humanoid/`, 1992–2000.

[123] E. R. Westervelt, J. W. Grizzle, and D. E. Koditschek. Hybrid zero dynamics of planar biped walkers. *IEEE Transactions on Automatic Control*, 48(1):42–56, January 2003.

[124] **D. Wollherr** and M. Buss. Cost oriented VR-simulation environment for computer aided control design. In *Proceedings of the 6th IFAC Symposium on Cost Oriented Automation*, pages 59–64, Berlin, Germany, 2001.

[125] **D. Wollherr** and M. Buss. Cost oriented virtual reality and realtime control system architecture. *Robotica*, 21(3):289–294, 2003.

[126] **D. Wollherr** and M. Buss. Posture modification for biped humanoid robots based on jacobian method. In *Proceedings of the IEEE/RSJ International Conference on Intelligent Robots and Systems IROS*, pages 124–129, Sendai, Japan, 2004.

[127] **D. Wollherr**, M. Buss, M. Hardt, and O. von Stryk. Research and development towards an autonomous biped walking robot. In *Proceedings of the IEEE/ASME International Conference on Advanced Intelligent Mechatronics AIM2003*, pages 968–973, Kobe, Japan, 2003.

[128] **D. Wollherr**, M. Hardt, M. Buss, and O. von Stryk. Actuator selection and hardware realization of a small and fast-moving, autonomous humanoid robot. In *Proceedings of the IEEE/RSJ International Conference on Intelligent Robots and Systems IROS*, pages 2491–2496, Lausanne, Switzerland, 2002.

[129] **D. Wollherr**, M. Hardt, M. Buss, and O. von Stryk. Development and control of autonomous, biped locomotion using efficient modeling, simulation, and optimization techniques. In *Proceedings of the IEEE International Conference on Robotics and Automation*, pages 1356–1361, Taipei, Taiwan, 2003.

[130] **D. Wollherr**, F. Zonfrilli, and Y. Nakamura. Active-passive knee control for the humanoid UT-Theta. In *Proceedings of the International Conference on Advanced Robotics*, Seattle, Washington, USA, 2005, *to appear*.

[131] J. Yamaguchi, S. Inoue, D. Nishino, and A. Takanishi. Develpment of a bipedal humanoid robot having antagonistic driven joints and three DoF trunk. In *Proceedings of the IEEE/RSJ International Conference on Intelligent Robots and Systems IROS*, pages 96–101, Victoria, Canada, 1998.

[132] J. Yamaguchi, E. Soga, S. Inoue, and A. Takanishi. Development of a bipedal humanoid robot - control method of whole body cooperative dynamic biped walking. In *Proceedings of the IEEE International Conference on Robotics and Automation*, pages 368–374, Detroit, MI, USA, 1999.

[133] K. Yamane and Y. Nakamura. Dynamics filter – concept and implementation of online motion generator for human figures. In *Proceedings of the IEEE International Conference on Robotics and Automation*, pages 688–694, San Francisco, CA, 2000.

[134] F. Yamasaki, K. Endo, M. Asada, and H. Kitano. A control method for humanoid biped walking with limited torque. In A. Birk, S. Coradeschi, and S. Tadokoro, editors, *RoboCup 2001*, pages 60–70. Springer Verlag, Berlin Heidelberg, 2002.

[135] F. Yamasaki, T. Miyashita, T. Matsui, and H. Kitano. PINO the humanoid: A basic architecture. In *4th International RoboCup Symposium*, Melbourne, Australia, 2000.

[136] M. Yamataka, H. Nakanishi, K. Yamabuchi, and A. Nakamura. Development of a small animal-type biped robot and its walking control system. In *Proceedings of the IEEE/RAS International Conference on Humanoid Robots*, pages 197–204, Tokyo, Japan, November 2001.

[137] Y. F. Zheng, J. Shen, and F. R. Sias Jr. A motion control scheme for a biped robot to climb sloping surfaces. In *Proceedings of the IEEE International Conference on Robotics and Automation*, volume 2, pages 814–816, 1988.

[138] F. Zonfrilli, G. Oriolo, and D. Nardi. A biped locomotion strategy for the quadruped robot Sony ERS-210. In *Proceedings of the IEEE International Conference on Robotics and Automation*, pages 2768–2774, Washington DC, USA, 2002.

[139] F. Zonfrilli, **D. Wollherr**, and Y. Nakamura. Walking control of the humanoid UT-Theta. In *Proceedings of the International Conference on Advanced Robotics*, Seattle, Washington, USA, 2005, *to appear*.